POLISH ACADEMY OF SCIENCES – WROCŁAW BRANCH

WROCŁAW UNIVERSITY OF TECHNOLOGY

ISSN 1644-9665
INDEX 375667

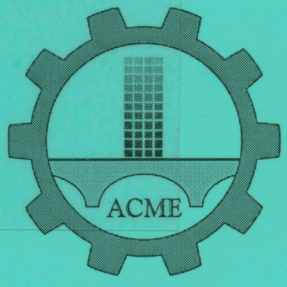

ARCHIVES OF CIVIL AND MECHANICAL ENGINEERING

Quarterly
Vol. IV, No. 1

WROCŁAW 2004

ADVISORY COMMITTEE

EDITORIAL BOARD

[1] The Faculty of Civil Engineering, Wrocław University of Technology
Wybrzeże Wyspiańskiego 27, 50-370 Wrocław, Poland
Tel. +48 71 320 22 46, Fax. +48 71 320 35 45, Email: mosty@pwr.wroc.pl

[2] The Faculty of Mechanical Engineering, Wrocław University of Technology
ul. Łukasiewicza 3/5, 50-371 Wrocław, Poland
Tel. +48 71 320 21 73, Fax. +48 71 320 34 22, Email: gronosta@itma.pwr.wroc.pl

POLISH ACADEMY OF SCIENCES – WROCŁAW BRANCH
WROCŁAW UNIVERSITY OF TECHNOLOGY

ARCHIVES OF CIVIL AND MECHANICAL ENGINEERING

Quarterly
Vol. IV, No. 1

WROCŁAW 2004

EDITOR IN CHIEF

JERZY GRONOSTAJSKI

EDITORIAL LAYOUT AND PROOF-READING

EWA SOBESTO, SEBASTIAN ŁAWRUSEWICZ

SECRETARY

TERESA RYGLOWSKA

Publisher: Committee of Civil and Mechanical Engineering
of Polish Academy of Sciences – Wrocław Branch,
Faculty of Civil Engineering and Faculty of Mechanical Engineering
of Wrocław University of Technology

OFICYNA WYDAWNICZA POLITECHNIKI WROCŁAWSKIEJ
Wybrzeże Wyspiańskiego 27, 50-370 Wrocław

Drukarnia Oficyny Wydawniczej Politechniki Wrocławskiej. Zam. nr 234/2004.

Contents

A. GRONOWICZ, S. WUDARCZYK, Analysis of redundant trajectory generator's accuracy 5
Z. GRONOSTAJSKI, K. JAŚKIEWICZ, The behaviour of CuSi5 silicon bronze during deformation along the complex strain path 17
K. MYŚLECKI, Approximate fundamental solutions of equilibrium equations for thin plates on elastic foundation 31
J. BIEŃ, P. RAWA, Hybrid knowledge representation in BMS 41
M. PODWÓRNA, Determination of the design model for simulating vibrations of steel beam bridges under moving trains 57
CZ.MACHELSKI, W. ZIELICHOWSKI-HABER, Internal forces due to live loads in a bridge structure comprising a steel space frame and a concrete slab 71
W. LORENC, E. KUBICA, Nonlinear modelling of composite beams prestressed with external tendons 83

Spis treści

A. GRONOWICZ, S. WUDARCZYK, Analiza dokładności redundantnego generatora trajektorii 5
Z. GRONOSTAJSKI, K. JAŚKIEWICZ, Zachowanie się brązu krzemowego CuSi5 podczas odkształcania wzdłuż złożonej drogi 17
K. MYŚLECKI, Przybliżone rozwiązania podstawowe równań równowagi płyt cienkich na podłożu sprężystym 31
J. BIEŃ, P. RAWA, Hybrydowa reprezentacja wiedzy w systemach zarządzania mostami 41
M. PODWÓRNA, Wyznaczenie modelu projektowego do symulacji drgań belkowych mostów stalowych obciążonych przejeżdżającymi pociągami 57
CZ.MACHELSKI, W. ZIELICHOWSKI-HABER, Siły wewnętrzne od obciążeń zmiennych w mostowych strukturach prętowych zespolonych z płytą pomostową 71
W. LORENC, E. KUBICA, Nieliniowe modelowanie belek zespolonych sprężanych kablami zewnętrznymi 83

ARCHIVES OF CIVIL AND MECHANICAL ENGINEERING

Vol. IV 2004 No. 1

Analysis of redundant trajectory generator's accuracy

ANTONI GRONOWICZ, SŁAWOMIR WUDARCZYK
Institute of Machine Design and Operation, Wrocław University of Technology
Wybrzeże Wyspiańskiego 27, 50-370 Wrocław

A planar mechatronic system with three degrees of freedom (a link mechanism having a closed structure and controllable drives) can execute any trajectory. Owing to the third drive the workspace is increased, but at the same time the problem of selecting driving functions for the execution of a particular trajectory arises. This paper deals with the effect of drive setting accuracy on the deviations in the execution of workspace points. A possible way of optimising the deviation of trajectories is shown. The accuracy of an illustrative system's work is analysed.

Keywords: *kinematics, mechatronic system, path optimization, workspace*

1. Introduction

The demand for adjustable systems which would execute a whole range of trajectories on a given plane can be met by the systems with two degrees of freedom. Such systems can have a series, parallel or mixed structure [1]. Aplications involve considerable loads or high speeds resulting in strong body forces, and so parallel-structure systems are suitable.

The simplest parallel systems for executing trajectories are based on a pentagon – a system of five links joined by couples of revolute or sliding pairs. Such systems can execute any trajectory within the attainable workspace whose size and shape are determined by the dimensions of the links and the motion range of the driving links. The systems have two major limitations which reduce the range of their possible applications, i.e.

- the relatively small workspace in comparison with series systems,
- different point position deviations for different workspace points at the same drive setting deviations.

The limitations can be overcome by employing systems with three degrees of freedom. By introducing the third degree of freedom the size of the workspace increases considerably. Furthermore, a specified workspace point can be realized using different system configurations, and by selecting the most advantageous configuration one can improve the accuracy with which the trajectory is executed. But such a modification results in greater complexity of the system, i.e. in an additional controllable drive. Some examplary designs of such systems are shown in Figure 1. When making up the sets of kinematic schemes it was assumed that the drives are located as close to the

frame as possible and there are no more than three sliding pairs in the system. Each of the systems is characterized by different kinematic and dynamic properties.

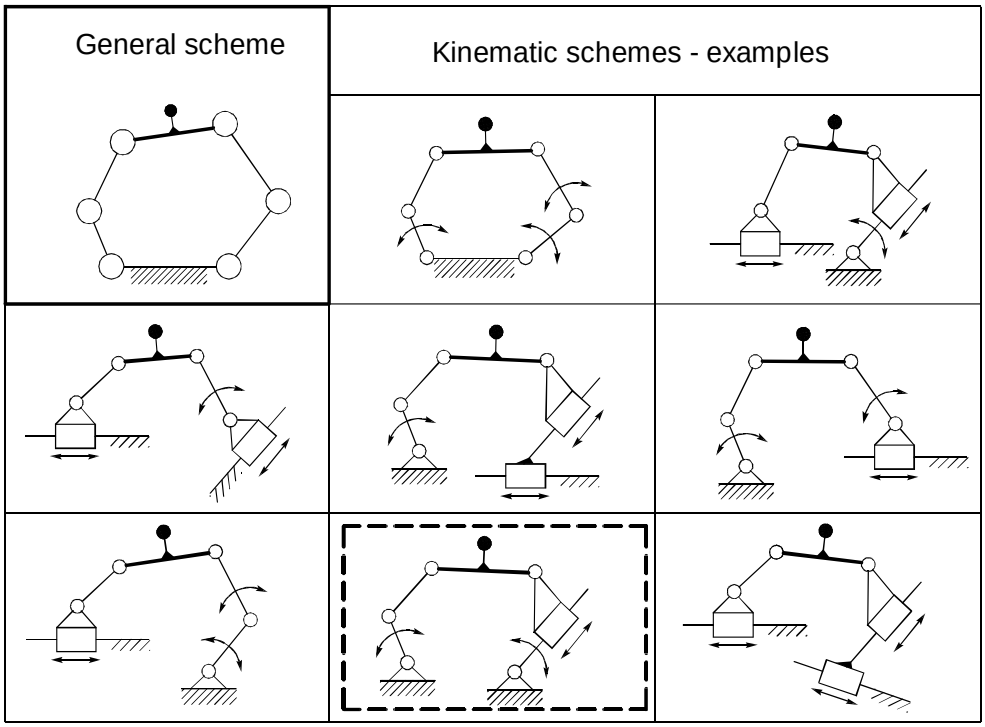

Fig. 1. Kinematic schemes of the systems with 3DOF for executing trajectories

In this paper, a system with three drives (shown in a frame in Figure 1) is analysed. A kinematic model is presented and then applied to the analysis of the workspace's shape and the effect of the particular system configurations on the accuracy of trajectory execution.

2. Description of system 4RTR

The system is shown in Figure 2. Point K of link 3 is to be moved along trajectory μ_K. This requires proper driving motions u_1, u_2 and u_3 effected, for example, by means of electric motors s_1 and s_2 coupled with harmonic drive for motions u_1 and u_2 or motor s_3 with a screw gear for u_3. In geometrical terms, we are dealing with pentagon $ABCDE$ whose sides AB and ED change their directions and the latter side can also change its length. It is apparent that the values of the coordinates of point K depend on the geometrical dimensions of the particular links and the values of motions u_i. The deviations of coordinates Δx_K, Δy_K of point K from the nominal values are due to such

factors as: clearance in the kinematic pairs, clearance in the gears and the flexibilities of system elements, but are mainly determined by the deviations of driving motions Δu_i. In many cases, deviations from assumed trajectory μ_K can disqualify a particular

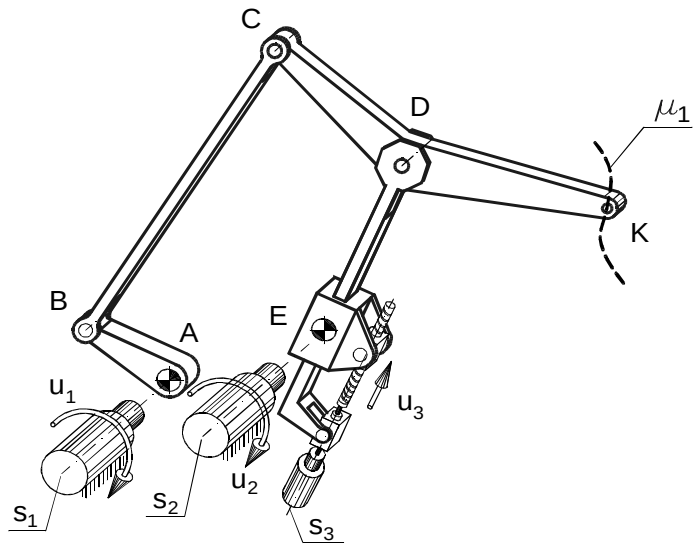

Fig. 2. Pictorial diagram of trajectory-executing system

system from a certain group of applications. They also ought to be taken into account when formulating requirements for the control system and the quality of the drives.

2.1. Kinematic relations

The absolute (Cartesian) coordinates' method, in which the *i*-th link is assigned a local system of coordinates $x_i\, y_i$, is used to describe the kinematics. The position of the *i*-th local system is equivalent to the position of the *i*-th link in global system $x_0\, y_0$. The motion of the *i*-th coordinate system is described by vector $\mathbf{q}_i$ whose components are:

$$\mathbf{q}_i = \begin{bmatrix} x_i & y_i & \theta_i \end{bmatrix}^T = \begin{bmatrix} \mathbf{r}_i^T & \theta_i \end{bmatrix}^T,$$

where:

x_i, y_i – the coordinates of the origin of the *i*-th local system in global system $x_0\, y_0$,

θ_i – the angle of orientation of the *i*-th local system relative to global system $x_0\, y_0$.

The motion of all the links of a system consisting of n movable links is described by vector $\mathbf{q}$

$$\mathbf{q} = \left[\mathbf{q}_1^T \quad \mathbf{q}_2^T \quad \dots \quad \mathbf{q}_n^T \right]^T . \tag{1}$$

In order to determine all the components of vector $\mathbf{q}$, an appropriate number of equations must be formulated. For this purpose equations of constraints, which follow from joining the links into kinematic pairs (equations $\mathbf{\Phi}^P$) and from driver motions (equations $\mathbf{\Phi}^C$), are used. As a result the following vector of algebraic equations [2] is obtained:

$$\mathbf{\Phi}(\mathbf{q},t) = \begin{bmatrix} \mathbf{\Phi}^P(\mathbf{q}) \\ \mathbf{\Phi}^C(\mathbf{q},t) \end{bmatrix} = 0 . \tag{2}$$

For the system considered (Figure 3) the variables of vector $\mathbf{\Phi}$ are:

- the vector of the dependent variables

$$\mathbf{q}_Z = [x_1 \; y_1 \quad x_2 \; y_2 \; \theta_2 \quad x_3 \; y_3 \; \theta_3 \quad x_4 \; y_4 \; \theta_4 \quad x_5 \; y_5 \;]^T ; \tag{3}$$

- the vector of the independent variables

$$\mathbf{q}_C = [u_1 \quad u_2 \quad u_3]^T , \text{ where } \mathrm{u}_1 = \theta_1,\ u_2 = \theta_5,\ u_3 = l, \tag{4}$$

which together form the vector

$$\mathbf{q} = \left[\mathbf{q}_Z^T \;\; \mathbf{q}_C^T \right]^T . \tag{5}$$

In the system considered (Figure 3), kinematic pairs of class 1 occur and each pair introduces two equations. For example, revolute pair A forces the overlapping of the axis of the frame (0) pin and that of the link (1) sleeve, which is tantamount to the equality of the ordinates and the abscissas of the pin's and the sleeve's centres, expressed in the global system bound up with frame 0. As a result the following equations are obtained:

$$x_1 = x_A + a_1 \cos\theta_1 ,$$
$$y_1 = y_A + a_1 \sin\theta_1 .$$

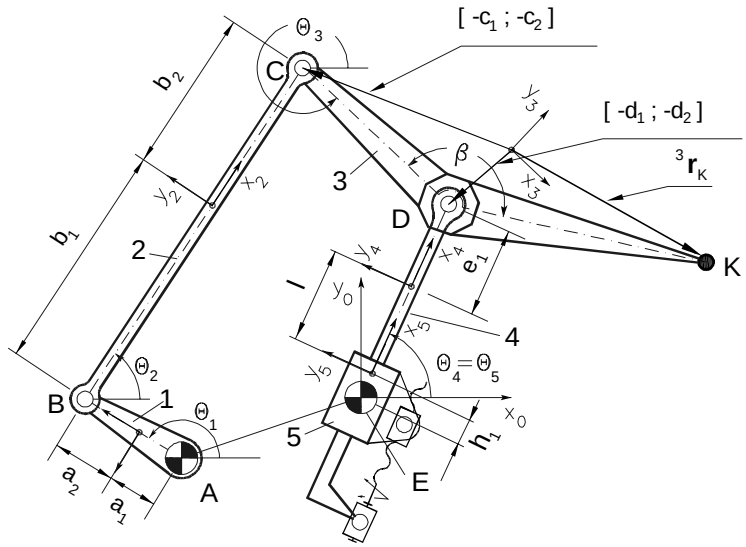

Fig. 3. Kinematic scheme of trajectory executing system with assumed coordinate systems

Leaving out the detailed derivations, the equations of constraints for the pairs (using the denotations shown in Figure 3) are presented in matrix (6):

$$\mathbf{\Phi}^{P} = \begin{bmatrix} x_1 - x_A - a_1\cos\theta_1 \\ y_1 - y_A - a_1\sin\theta_1 \\ x_1 - x_2 + a_2\cos\theta_1 + b_1\cos\theta_2 \\ y_1 - y_2 + a_2\sin\theta_1 + b_1\sin\theta_2 \\ x_2 - x_3 + b_2\cos\theta_2 + c_1\cos\theta_3 - c_2\sin\theta_3 \\ y_2 - y_3 + b_2\sin\theta_2 + c_1\sin\theta_3 + c_2\cos\theta_3 \\ x_3 - x_4 - d_1\cos\theta_3 + d_2\sin\theta_3 - e_1\cos\theta_4 \\ y_3 - y_4 - d_1\sin\theta_3 - d_2\cos\theta_3 - e_1\sin\theta_4 \\ -(x_4 - x_5)\cdot\sin\theta_5 + (y_4 - y_5)\cdot\cos\theta_5 \\ \theta_4 - \theta_5 \\ x_5 - h_1\cos\theta_5 \\ y_5 - h_1\sin\theta_5 \end{bmatrix} = 0. \tag{6}$$

To define the second group of equations $\mathbf{\Phi}^{C}$ of vector $\mathbf{\Phi}$ described by Equation (2) two different cases must be considered. The first one is a simple problem: the motion of the moving links is known and the motion of point *K* is determined. In the second

case, the motion of point K is known and the required motion of the moving links is determined.

In the simple problem, the drivers (Figure 3) are:

- the rotation of link 1 about the axis of pair A, which is described by angle $\theta_1 = u_1$;
- the rotation of link 5 (slide) about the axis of pair E described by angle $\theta_5 = u_2$;
- the variation in the distance of the origins of local systems $x_4\, y_4$ and $x_5\, y_5$ described by distance $l = u_3$.

Then for the known vector $\mathbf{q}_C$ we arrive at:

$$\mathbf{\Phi}^{C_1} = \begin{bmatrix} \Theta_1 - u_1 \\ \Theta_5 - u_2 \\ \sqrt{(x_4 - x_5)^2 + (y_4 - y_5)^2} - u_3 \end{bmatrix}. \tag{7}$$

In the inverse problem, the position of point K, prescribed by coordinates x_K, y_K in the global coordinate system, is known. Since a planar system with three degrees of freedom is considered, not only the position of point K, but also the value of one of the input motions in system of equations $\mathbf{\Phi}^{C_1}$ must be known. Ultimately, the following system of equations is obtained:

$$\mathbf{\Phi}^{C_2} = \begin{bmatrix} \mathbf{\Phi}^{C_1}(1,1) \text{ or } \mathbf{\Phi}^{C_1}(2,1) \text{ or } \mathbf{\Phi}^{C_1}(3,1) \\ x_3 + {}^3x_K \cos\theta_3 - {}^3y_K \sin\theta_3 - x_K(t) \\ y_3 + {}^3x_K \sin\theta_3 - {}^3y_K \cos\theta_3 - y_K(t) \end{bmatrix}, \tag{8}$$

where $\mathbf{\Phi}^{C_1}(i, 1)$ is one of the elements of vector (7).

Using Equations (6) and (7) or (8) one can determine the position of the system (vector $\mathbf{q}$) by solving (2). The analytical solution of the system of Equation (2) is complicated, but one can apply numerical methods, e.g. the Newton–Raphson method, or use ready-made procedures for solving systems of nonlinear equations.

2.2. Analysis of accuracy

If the variables that describe the system's configuration (vector $\mathbf{q}$) are known, one can determine the deviations (mainly due to the deviations in the setting of the drives [5]) of the executed trajectory's successive points K from their nominal values. For this purpose one must know the position vector $\mathbf{q}$ which can be determined by solving the system of equations (2). If separation (5) into dependent and independent variables describing the position of the system is used, the deviations will form this vector:

$$\delta \mathbf{q} = \left[\delta \mathbf{q}_Z^T \quad \delta \mathbf{q}_C^T \right]^T. \tag{9}$$

The components of vector

$$\delta \mathbf{q}_C = \left[\Delta u_1 \quad \Delta u_2 \quad \Delta u_3 \right]^T \tag{10}$$

are known and their values depend on the quality of the drives and that of the control system.

Set displacements – more precisely a variation of vector **q**, which for the defined position of the system is determined by differentiation over all the variables – are used for the analysis of the deviations [4]. Thus the following equation is used

$$\mathbf{\Phi}_q \delta \mathbf{q} = 0, \tag{11}$$

where

$$\mathbf{\Phi}_q = \frac{\partial \mathbf{\Phi}}{\partial \mathbf{q}}.$$

When the variables are separated, transformed Equation (11) can be written as follows:

$$\mathbf{\Phi}_{qZ} \, \delta \mathbf{q}_Z = -\mathbf{\Phi}_{qC} \, \delta \mathbf{q}_C. \tag{12}$$

The solution of Equation (12) yields dependent variable deviation vector $\delta \mathbf{q}_Z$.

The coordinates of point *K* are described by this equation:

$$\mathbf{r}_K = \mathbf{r}_3 + \mathbf{A}_3 \, {}^3\mathbf{r}_K, \tag{13}$$

where

$$\mathbf{A}_3 = \begin{bmatrix} \cos\theta_3 & -\sin\theta_3 \\ \sin\theta_3 & \cos\theta_3 \end{bmatrix}.$$

Taking into account the above, the deviations of point *K* are determined from the equation:

$$\delta \mathbf{r}_K = \delta \mathbf{r}_3 + \delta\theta_3 \, \mathbf{B}_3 \, {}^3\mathbf{r}_K, \tag{14}$$

where

$$\mathbf{B}_3 = \frac{\partial}{\partial \theta_3}\mathbf{A}_3 .$$

Using Equations (12) and (14) one can determine deviations $\delta\mathbf{r}_K$ of the coordinates of point K from the nominal positions if the values and signs of drive setting errors $\delta\mathbf{q}_C$ are known. Equation (14) can also be used to determine the maximum deviations of the executed trajectory from the prescribed one, but for this all the possible cases of the signs of deviations $\delta\mathbf{q}_C$ must be considered. If the most disadvantageous system of the signs is selected, one can determine the largest theoretically possible trajectory deviations $\delta\mathbf{r}_K$.

In order to make the analysis independent of drive setting deviations $\delta\mathbf{q}_C$, it is convenient to employ the method based on effect coefficients [3]. Then the deviations are determined from the equations:

$$\Delta x_{K\max} = \sum_{n=1}^{m} \left| w_{xn}\Delta u_n \right| \qquad \Delta y_{K\max} = \sum_{n=1}^{m} \left| w_{yn}\Delta u_n \right| \tag{15}$$

in which w_{xn} and w_{yn} are the coefficients representing the effect of the error in setting the n-th drive on deviations δx_K and δy_K of the coordinates of point K. The coefficients are determined from the formulas

$$w_{xn} = \frac{\delta x_K}{\delta u_n}, \qquad w_{yn} = \frac{\delta y_K}{\delta u_n}, \tag{16}$$

where δu_n is the deviation in setting the n-th drive.

The trajectory deviations determined from relations (15) are measured along the X-axis and Y-axis of global system. Effect coefficients (16) are determined on the basis of the components of vector $\delta\mathbf{q}_C$, but when calculating the effect due to error (δu_k) of drive k, the other two drives are immobilized by assuming $\delta u_i = \delta u_j = 0$ for i, $j \neq k$. It is useful to know the effect coefficients since their values are the function of only the system's dimensions and configuration, which makes the accuracy analysis independent of the actual values of the errors in setting the particular drives.

For trajectory executing systems it may be reasonable to use deviations measured in the direction normal (N) to the trajectory. Then the appropriate effect coefficients are calculated from this formula

$$w_{Nn} = \frac{\delta N_K}{\delta u_n}, \tag{17}$$

where:

$$\delta N_K = \delta x_K \cos(\alpha) + \delta y_K \sin(\alpha),$$

α – the angle of inclination of the normal to the trajectory in x_0, y_0.

The maximum deviation in the direction normal to the trajectory is determined from this formula

$$\Delta N_{K\max} = \sum_{1}^{m} \left| w_{Nn} \Delta u_n \right|. \tag{18}$$

3. Example of analysis

To design the basic dimensions of the system shown in scale in Figure 4 the method of synthesis developed in [5] was used. For prescribed rocker length *ED* the designed system's point *K* can cover only a part of the full workspace. Selected parts of the workspace which can be covered at particular rocker lengths are shown in Figure 4. The areas common for the fields determined for rocker lengths ED_i and ED_j can be covered by a rocker of the length $ED \in \langle ED_i, ED_j \rangle$. This means that the same point can be realized through different system configurations. Thus it is reasonable to ask about a criterion for selecting rocker length *ED* for the realization of a particular point of the workspace.

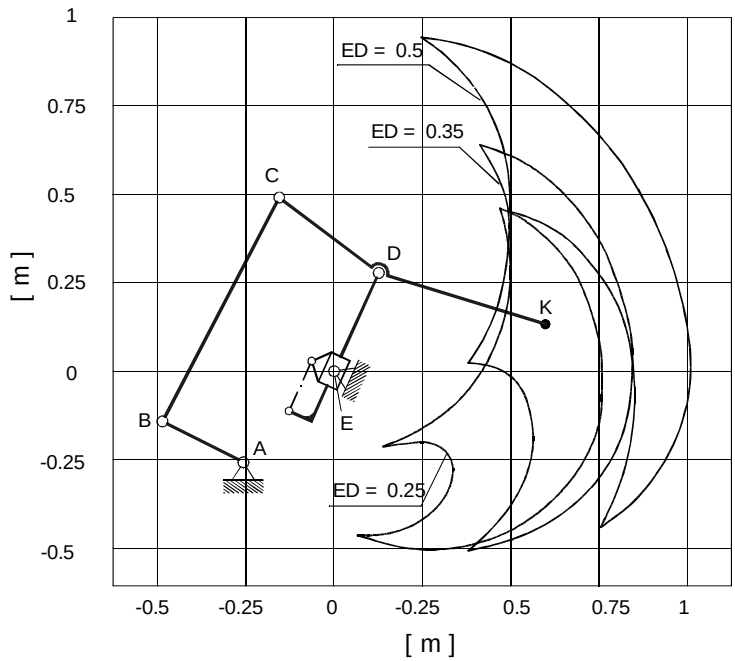

Fig. 4. Trajectory executing system with workspace covered (shown in scale)

For a trajectory generator its accuracy in the execution of a prescribed curve is important. In this regard, it is convenient to use effect coefficients. Then the minimization of the effect coefficients simultaneously along the axes x_0 and y_0 should be adopted as the criterion for selecting the most advantageous rocker length for the realized points. Here an objective function on which the multicriterial optimisation is to be based should be formulated. For a specified trajectory one can use the effect coefficients determined for the direction normal (N) to the trajectory whereby a clear-cut criterion can be applied.

In the considered case, to assess the accuracy of the system the following criterion was used:

$$F = \sqrt{\left(\sum w_{xn}\right)^2 + \left(\sum w_{yn}\right)^2} \rightarrow \min . \tag{19}$$

Having a system with specified dimensions (Figure 4), we began to determine the effect coefficients at selected points of the workspace.

The system configurations at the assumed points of the workspace (sets z_1, z_2, z_3 in Figure 6) were determined for successive (from the smallest to the largest) lengths of link ED (variable u_3) using relation (2). The pair constraint vector is expressed by Equation (6) and in accordance with (8) the equations of input motions are collected in the following vector:

$$\mathbf{\Phi}^{C_2} = \begin{bmatrix} \sqrt{(x_4 - x_5)^2 + (y_4 - y_5)^2} - u_3 \\ x_3 + {}^3x_K \cos\theta_3 - {}^3y_K \sin\theta_3 - x_K(t) \\ y_3 + {}^3x_K \sin\theta_3 - {}^3y_K \cos\theta_3 - y_K(t) \end{bmatrix}. \tag{20}$$

The analysis yields vector $\mathbf{q}$ (5) describing the configuration of the system, which serves as the basis for determining the effect coefficients (16) along the directions parallel to the axes of the global coordinate system. The determined values of effect coefficients w_{xn} and w_{yn} pertaining to each point of set z_3 for different values ED are represented as sides of a rectangle in Figure 5. Each of the sides is proportional to the value of the corresponding effect coefficient (the factor of proportionality is 30). The shaded rectangles correspond to the optimum rocker length ED determined for successive points K_i in accordance with adopted criterion (18). As shown in Figure 5, a different rocker length value corresponds to each of the shaded (optimal) fields. It is essential that this length should change stepwise for certain points located side by side.

In practice, when the motion of point K is executed in a continuous way, such a change is not possible and this means that the attainment of the theoretically possible minimum deviations at all the points of the trajectory is impracticable since it requires stopping point K and changing the ED value.

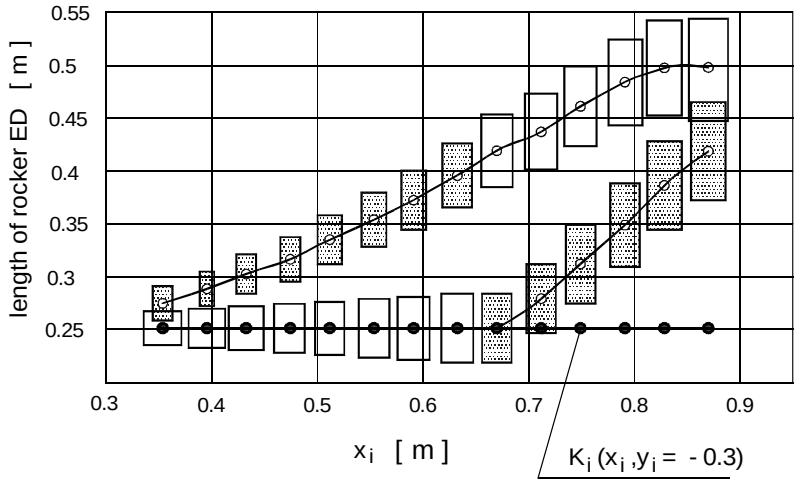

Fig. 5. Effect coefficients for selected points at different rocker lengths

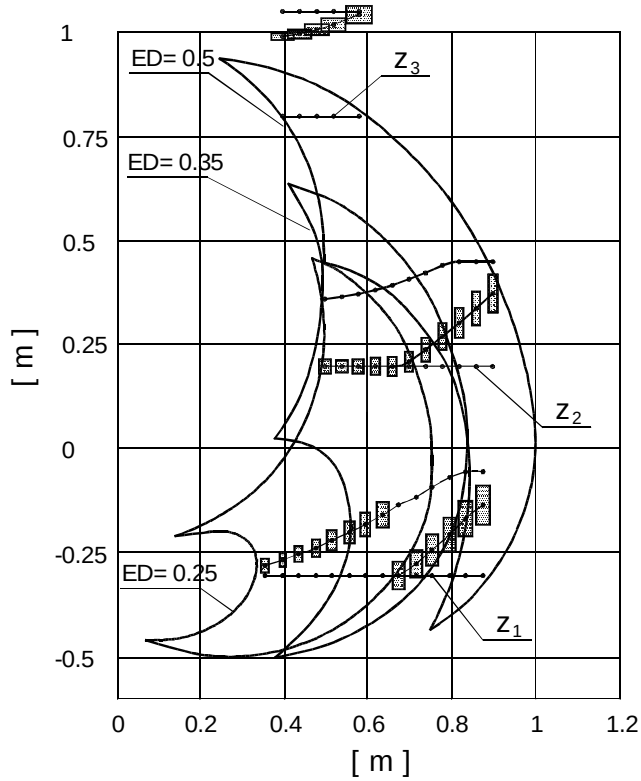

Fig. 6. Effect coefficients at selected workspace points

The effect coefficient relations for other workspace points are shown in Figure 6. For each workspace point there is an optimum rocker length which ensures the minimum, by adopted criterion (19), trajectory deviation.

As the analysis has shown the values of the effect coefficients at the particular workspace points differ considerably whereby different errors are made in their realization.

4. Conclusions

A methodology for analysing a redundant trajectory generator to minimize deviations represented by effect coefficients has been presented. The methodology makes it possible to answer the question, which is of major practical importance, whether for the known deviations of the drives a given system can meet the specified requirements. Whereas in the process of synthesis it supplies information about the quality of the drives and that of the control system.

The analysis has shown that in some cases it is necessary to adopt an additional optimisation criterion. The presented methodology can be helpful in the synthesis and analysis of similar kinematic systems.

References

[1] Gronowicz A.: *Foundations of Kinematic Systems Analysis* (in Polish), Wrocław University of Technology Publishing House, Wrocław, 2003.
[2] Haug E.J.: *Computer-Aided Kinematics and Dynamics of Mechanical Systems*, Allyn and Bacon, Boston, 1989.
[3] Miller S.: *Kinematic Systems* (in Polish), WNT, Warsaw, 1988.
[4] Osiński Z.: *General Mechanics* (in Polish), PWN, Warsaw, 1997.
[5] Wudarczyk S.: *Method of Synthesizing Mechatronic Trajectory Generator and Algorithm of its Control* (in Polish), PhD thesis, Wrocław, 2002.

Analiza dokładności redundantnego generatora trajektorii

Płaski układ mechatroniczny o trzech stopniach swobody – mechanizm dźwigniowy o strukturze zamkniętej wyposażony w sterowane napędy – może realizować dowolną trajektorię. Trzeci napęd zwiększa strefę roboczą, a jednocześnie pojawia się problem wyboru funkcji napędowych dla realizacji określonej trajektorii. W pracy przedstawiono wpływ dokładności ustawienia napędów na odchyłki realizowanych punktów strefy roboczej. Pokazano możliwy sposób optymalizacji odchyłek trajektorii, przedstawiono charakterystykę przykładowego układu pod kątem dokładności jego pracy.

ARCHIVES OF CIVIL AND MECHANICAL ENGINEERING

Vol. IV 2004 No. 1

The behaviour of CuSi5 silicon bronze during deformation along the complex strain path

ZBIGNIEW GRONOSTAJSKI, KAROL JAŚKIEWICZ
Wrocław University of Technology, Wybrzeże Wyspiańskiego 27, 50-370 Wrocław

The effect of different complex strain paths on the behaviour of silicon bronze CuSi5 has been examined. The strain paths contain various sequences of cyclic torsion and tension. The amplitude was changed in the range of 0.05–0.5, a temperature from 20 °C to 800 °C and the strain rate from 0.01 to 1 s^{-1}. The properties and structure obtained in complex strain paths are compared with those gained in monotonic torsion and tension. The silicon bronze containing about 5% of Si is a very curious alloy, because the stacking fault energy is very low, so its substantial deformation is obtained mainly by twinning. The strain paths similar to those applied in the experiments being carried out are observed in such industrial processes as: rolling, forging, rotary swaging and others. It has been found that by a proper choice of strain paths and deformation conditions, the decrease of flow stress and increase of limit strain can be obtained.

Keywords: *strain paths, silicon bronze, mechanical properties, structure*

1. Introduction

The relation of the true stress to the true strain is basic mechanical property of materials in each numerical simulation of material behaviour in forming processes. The effect of temperature, strain rate and strain on a flow stress and structure has been widely known and examined. So just now, when new generation of computers and commercial FEM programmers create the possibility of analyzing even very complicated metal forming processes with high accuracy, the meaning of a proper work hardening curves is fully appreciated. In the past, such processes could be analysed mainly for perfectly plastic model of materials. So due to the progress in computers, some new factors affecting the work hardening curves can be introduced into them. A basic new factor is strain path which should be used for numerical simulation of metal-forming processes, especially for non-monotonic and non-proportional flows of materials.

The effect of strain path on the formability in the case of sheet-metals forming processes has been examined for a long time. It has been found that such an effect is very strong, so there is even difficult to use forming-limit diagrams FLDs in sheet metal-forming processes design without taking into account the strain path.

In the case of massive processes, the effect of strain path on the structure and mechanical properties of materials is very little known because the examinations are more

difficult and complex. Only a small number of the experiments being aimed at the effect of strain path on the behaviour of metals and alloys were performed.

In the case of massive processes, it is easier to investigate the effect of strain path on the behaviour of metals and alloys in complex laboratory tests (CLT) than in industrial practice. In the last years, the cyclic torsion (CT) [1–8] versus monotonic torsion (MT) [9–11] is often used to show the effect of the former on the behaviour of metals and alloys during deformation. Such investigations were performed for copper [1, 2], interstitial free steel in the ferrite and austenite ranges [3, 4] and in strain reversal under torsion of HSLA steel [5].

In the papers [1–4] the stress–strain curves of commercially pure copper and interstitial free steel in hot cyclic torsion test with strain amplitude range of 0.025–0.4 and, for the sake of comparison, the curve from monotonic torsion test at the same temperature of 500 °C and strain rate of 0.1 s^{-1} were presented. It has been found that the stress–strain curves for cyclic torsion are significantly different from those obtained in monotonic loading tests. The cyclic torsion stress–strain curves did not show the peak stress characteristic of dynamic recrystallization, which suggested the absence of this phenomenon.

The authors show that the cyclic steady-state stress σ_{ps}^{c} with an increase of strain amplitude is quite close to that corresponding to monotonic dynamic recrystallization steady-state flow σ_{ps}, and for the highest strain amplitude applied in the experiments (0.4) no increase of cyclic straining σ_{ps}^{c} above σ_{ps} was observed.

However, all results reported in the above-mentioned papers were obtained for a narrow range of deformation, below 2.5 only; for a wider range, even at the same amplitude equal to 0.4, for CuAl8 aluminium bronze there was observed the cyclic steady-state stress σ_{ps}^{c} above the monotonic dynamic recrystallization steady-state flow σ_{ps} [7].

In order to analyse the mutual effects of monotonic and cyclic torsion, a composite test was carried out in which the sample was initially deformed under monotonic straining, then under cyclic loading with the amplitude ε_{at}=0.03, and finally under monotonic loading again [7, 8]. The results are shown in Figure 1. From Figure 1 it can be seen that cyclic torsion leads to extensive softening of steel. Cyclic torsion applied after monotonic torsion at the strain equal to 1 caused the flow stress at a strain of 2 to decrease to the same level it would have reached under pure cyclic straining at the same amplitude [4].

The results presented in the papers [1–4] have serious reservation. During cyclic deformation each histeresis loop contains elastic and plastic deformation, and the relative fraction of elastic strain in the total deformation rapidly increases with diminution of the deformation ampilitude and increases the number of the cycles in whole deformation process. With the increase of deformation during the monotonic straining the

relative fraction of elastic strain in total deformation is decreased. So the stress–total strain relation in cyclic deformation and monotonic deformation, where the relative fraction of elastic strain is quite different, cannot be compared. For a proper comparison of the above-mentioned curves, the elastic deformation must be removed from the total deformation in the case of cyclic and monotonic stress–strain relations.

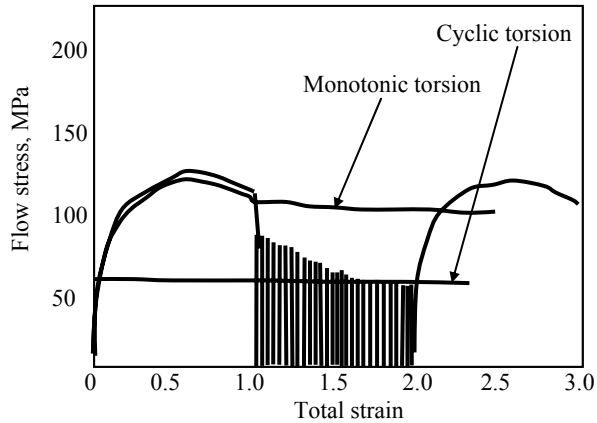

Fig. 1. The composite test: monotonic torsion at the strain of 1, next cyclic torsion at the strain of 2 and repeated monotonic torsion in comparison to monotonic and cyclic torsion in the whole range of deformation [4]

The other papers [12–14] present the experimental characteristic of flow stress of metallic materials under various deformation conditions and theoretical analysis of plastic flow identification during change of strain paths. Examining the effect of principal stresses' orientation on the course of M1E copper, titanium alloy Ti-3.5Al-1.5Mn and OH18N9 steel confirmed an essential influence of strain path on the forces needed for deformation, and thus on the work hardening curves. Such an information can be used for numerical simulation of metal-forming processes, especially for non-monotonic and out-of-proportion flow of materials.

The effect of complex deformation on the flow stress–strain relationship in the case of the following variants: torsion–tension–torsion in the same direction as before, torsion–tension–torsion in the opposite direction as before, and torsion–torsion–torsion with the change of direction in each next cycle was examined. In each variant of deformation, the same value of total strain was applied, it was equal to 0.3. This means that in each deformation cycle the strain is 0.1.

The curves obtained were shown in Figures 2–4. From these figures it can be seen that in tensile test, after work hardening by torsion, the flow stress–strain relationship is nearly linear. The renewed torsion in the same direction caused further increase of the flow stress in comparison with that in tensile test, but the maximum value obtained in the third cycle of deformation (torsion) is slightly lower than in the first one.

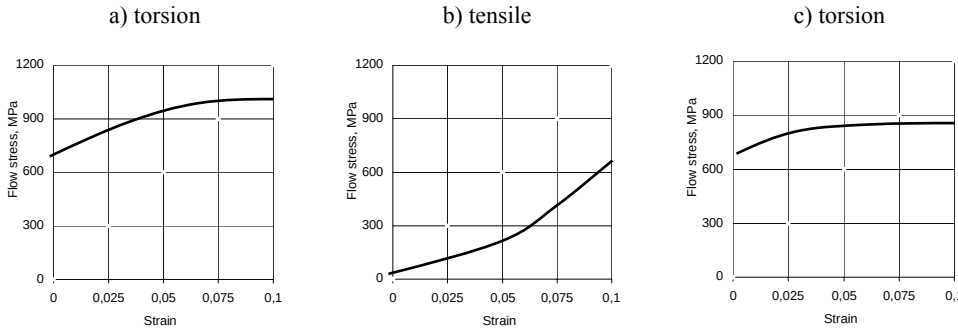

Fig. 2. Relationship between flow stress and strain for titanium alloy for the first variant of complex deformation [12]

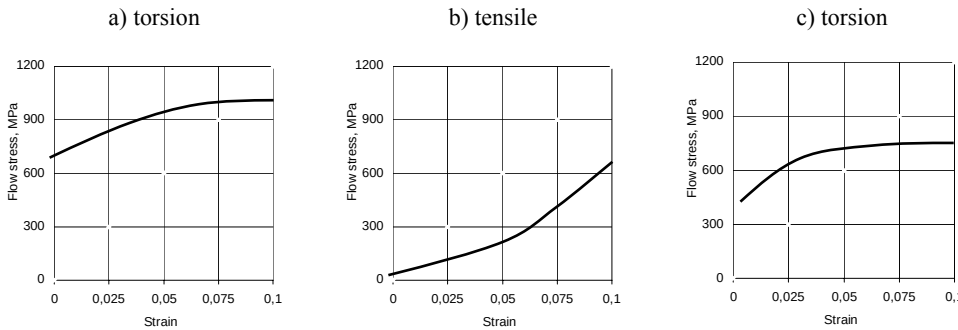

Fig. 3. Relationship between flow stress and strain for titanium alloy for the second variant of complex deformation [12]

In the second variant of deformation, the change in torsion direction in the third cycle causes significant decrease of flow stress in comparison with that in the first cycle (torsion) (Figure 3).

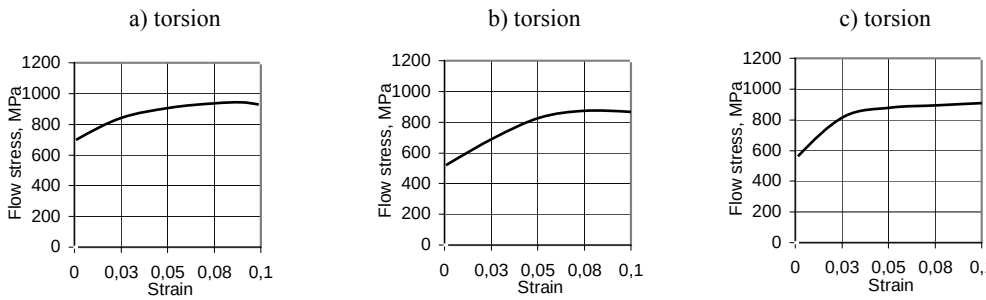

Fig. 4. Relationship between flow stress and strain for titanium alloy for the third variant of complex deformation [12]

In the case of successive change of torsion direction (the third variant of deformation), the maximum flow stress is stabilized on the same level in the first and the third cycles of deformation when torsion is realized in the same direction. But in the second cycle when torsion direction is opposite, a small decrease of flow stress can be seen. In the papers cited earlier, there is no information relating to the use of total strain or plastic strain only. It is difficult to imagine that the differences between the work hardening curves in torsion and tensile tests are so noticeable (Figures 2 and 3).

On the basis of the presented results [17] of the low energetic deformation of metallic materials in strain paths' control the laboratory and industrial processes were proposed.

Another investigation was carried out by using plastometer, where samples were simultaneously subjected to cyclic torsion with different amplitudes and the tension of various sequences [15, 16]. It has been found that cyclic amplitude and temperature have a substantial effect on the behaviour of CuAl8 aluminium bronze.

The strain paths similar to those occurring in cyclic torsion are observed in such industrial processes as: rolling [17], ingot turning [18], rotary forging [19], rotary swaging [20], extrusion [21] and others. From the above-given examples it is clearly visible that by the change of strain path in massive processes the great progress in metal-forming can be obtained and new technologies more effective in saving both energy and material consumption could be developed.

The main aim of the paper is to analyse the effect of complex strain path on the behaviour of CuSi5 silicon bronze containing 4.86% of Si, on the stress–strain relationship under different deformation conditions and on the structure and to avoid the above-mentioned errors.

2. Experimental procedure

In order to evaluate the mechanical properties, the plastometer for complex strain paths (Figure 5) was used [15].

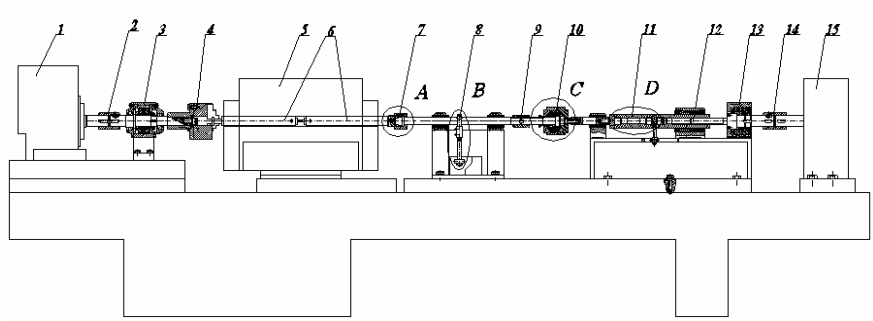

Fig. 5. Scheme of plastometer: 1 – asynchronous machine of 13 kW power, 2 – sleeve clutch, 3 – constant support, 4 – swivel head, 5 – furnace, 6 – sample holder, 7 – self-centric clutch, 8 – torque sensor, 9 – cluch, 10 – rotating head, 11 – compresion and tensile sensor, 12 – screw mechanism, 13 – constant support, 14 – sleeve clutch, 15 – asynchronous machine of 13 kW power

The specimens made from CuSi3.5 silicon bronze were deformed at the temperature range of 20–800 °C. The temperature was measured by a thermocouple being in contact with surface of the gauge length of the specimens. The specimens were subjected to monotonic tension with the strain rate of 0.01 s^{-1} and monotonic tension with the same strain rate applied simultaneously with symmetrical or pilger cyclic torsion with the strain rate of 0.1 s^{-1} and different total amplitudes ε_{at} = 0.05, 0.1, 0.2, 0.3, 0.4, 0.5 and 0.6. For microstructural observation the optical, scanning and transition microscopes were used.

The specimen shown in Figure 6 was used. The work-hardening surface layer of samples caused by mechanical turning was removed by heating them at a higher temperature.

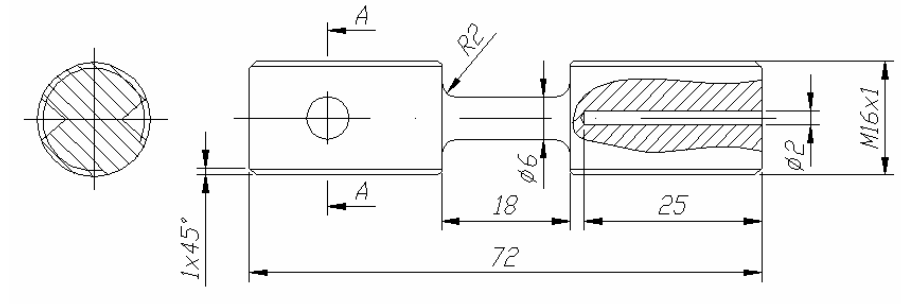

Fig. 6. The scheme of specimen used for complex strain paths

As it was explained in the former chapter, for a proper determination of the effect of strain paths on the flow stress–plastic strain relationship and on the limit strain the elastic deformation must be removed from total deformation. The method of partition of total strain during complex deformation of elastic and plastic parts is shown in Figure 7.

In the succeeding hysteresis loop, the elastoplastic strain was calculated using courses of the total strain as a function of time together with the courses of flow stress at the same time. From Figure 7 it can be seen that the zero values of torsional flow stress correspond to finite values of strain. When the torsional flow stress is equal to zero the power transmission system, recording system and specimen are loaded with tensile flow stress only, so on the assumption that stiffness of whole plastometer is much higher than that of deformed specimen alone, the elastic strain caused by tensile stress is accumulated in specimen only.

At that very moment the strains shown by arrows are plastic strains. This way the plastic strain can be calculated for arbitrary cycle of deformation, and as a final result of investigation a proper relation between flow stress and plastic strain can be obtained.

At that very moment the deformation contains plastic deformation caused by torsion ε_{pt1} and total deformation caused by tension ε_{cr1}. For the known Young's modulus

E the elastic deformation caused by tension can be easily calculated as follows: $\varepsilon_{sr1} = \sigma_{pr}/E$. Finally the plastic strain caused by torsion and tension ε_{ptr1} in successive half-cycles of deformation is given by the following formula: $\varepsilon_{pt1}+\varepsilon_{cr1}-\varepsilon_{sr1}$ (Figure 7a).

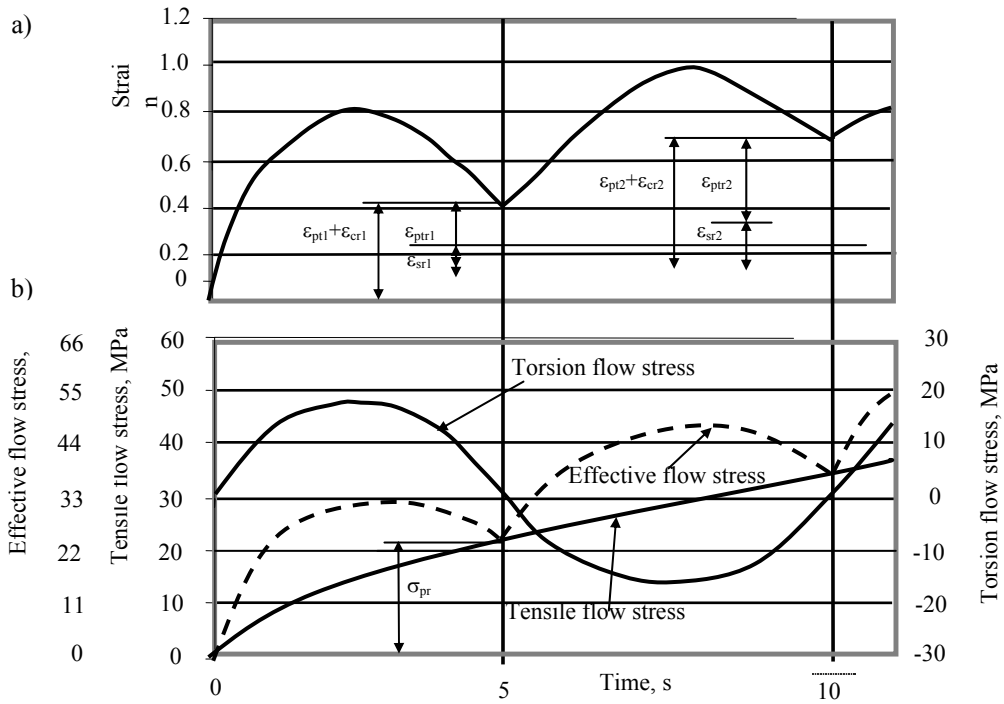

Fig. 7. Scheme of the method of calculation of plastic strain in complex deformation containing cyclic torsion with monotonic tension: a – strain and b – stress as a function of time. Arrows show values of plastic strain in successive half-cycles of deformation

The total plastic strain in the whole deformation process is the sum of particular plastic strains in successive half cycles of deformation $\varepsilon_{pti}+\varepsilon_{cri}-\varepsilon_{sri}$. This way the plastic strain can be calculated for arbitrary cycle of deformation, and as a final result of investigation a proper relationship between flow stress and plastic strain can be obtained.

In the case of principal stress orientation changes in successive monotonic torsion and tension, the plastic strain was calculated by using Young's modulus.

In Figure 7b, an effective plastic stress determined from Equation (1) is represented by dotted line. The BASIC program for plastic strain calculation in complex strain paths was designed.

Till now the universal method of stress and strain calculation in torsion test has not been developed. There are a few different methods given in the papers [9–11]. Taking into account that the main aim of the work is to compare the flow stress–strain curves

obtained at complex strain path with those of monotonic strain, the simple classical method of flow stress and strain determination was used.

The equivalent stress is due to simultaneous operation of torsion and tension and can be calculated according to the Huber–Misses criterion

$$\sigma_{pe} = \sqrt{\left(\frac{3\sqrt{3}M_s}{2\pi r_{or}^3}\right)^2 + \left(\frac{F}{2\pi r_{or}^2}\right)^2}. \tag{1}$$

The equivalent plastic strain

$$\varepsilon_{pe} = \frac{1}{\sqrt{3}}\sqrt{3\varepsilon_p^2 + \gamma_p^2}, \tag{2}$$

where ε_p is the strain caused by the tensile force F,

$$\varepsilon_p = \ln\frac{l_k}{l_p}, \tag{3}$$

and γ_p is the shear strain caused by torque M_s,

$$\gamma_p = \frac{r_{or}\omega_p}{l_k}, \tag{4}$$

where l_p and l_k are initial and final gauge lengths of complex deformed specimen, and ω_p stands for the angle of plastic rotation of sample.

The shear strain rate

$$\dot{\gamma} = \frac{r_{or}\dot{\omega}_p}{L_r}, \tag{5}$$

and tensile strain rate

$$\dot{\varepsilon} = \frac{d\varepsilon_p}{dt}, \tag{6}$$

where $\dot{\omega}_p$ is the plastic rotation speed.

The equivalent plastic strain rate of complex straining

$$\dot{\varepsilon}_e = \frac{1}{\sqrt{3}}\sqrt{3\dot{\varepsilon}_p^2 + \dot{\gamma}_p^2} \ . \tag{7}$$

3. Results and discussion

The equivalent flow stress–plastic strain relationship obtained in the minor cyclic torsion together with monotonic tension of specimens and the work hardening curves obtained in monotonic torsion and tensile tests at ambient temperature and at 600 °C are shown in Figure 8 and Figure 9, respectively.

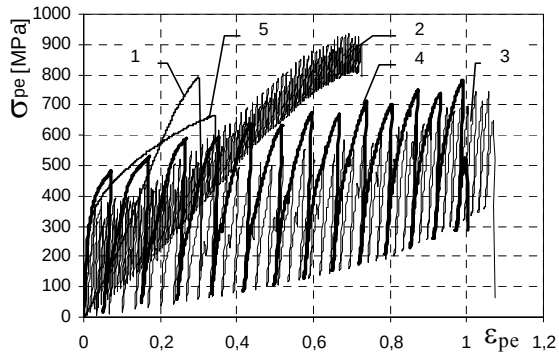

Fig. 8. The effect of tension and symmetrical minor cyclic torsion with amplitudes: 0.05 (2), 0.1 (3) and 0.2 (4) on the equivalent stress–plastic strain relationship in comparison with monotonic tension (1) and torsion (5) at ambient temperature

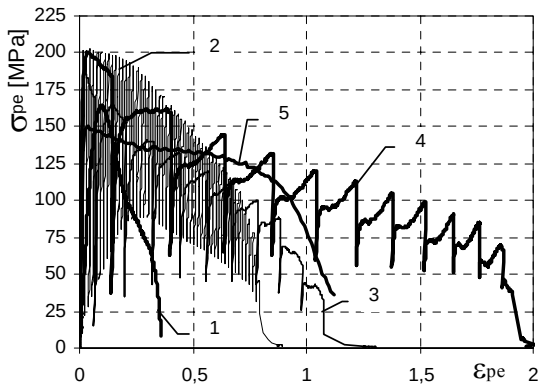

Fig. 9. The effect of tension and symmetrical minor cyclic torsion with amplitudes: 0.05 (2), 0.2 (3) and 0.4 (4) on the equivalent stress–plastic strain relationship in comparison with monotonic tension (1) and torsion (5) at a temperature of 600 °C

From Figure 8 it can be seen that at ambient temperature the limit plastic strains for both monotonic torsion and tensile tests are nearly the same (about 0.3). In this range of deformation, the highest value of flow stress for complex straining is slightly lower than that for monotonic torsion and much lower than that for tension. But the differences between the lowest value of flow stress in complex straining and flow stress in both monotonic tests are very large. An increase of deformation behind limit strain of both monotic tests causes the rise of the highest and the lowest values of flow stress in complex straining, more intensively for the smallest amplitude applied (0.05).

A radically different situation arises at a higher temperature of 600 °C (Figure 9). The limit strain determined in monotonic tension is very small in comparison with this in monotonic torsion and complex deformation. The same limit strain was obtained for monotonic torsion and complex deformation with the amplitude of 0.2, and the greatest limit for deformation with the amplitude of 0.4. In these ranges of equivalent plastic strain, an unfavourable phenomenon takes place, i.e. the increase of flow stress for complex straining is larger than that for monotonic torsion and tension. With an increase of an equivalent plastic strain the continous decrease of flow stress is observed.

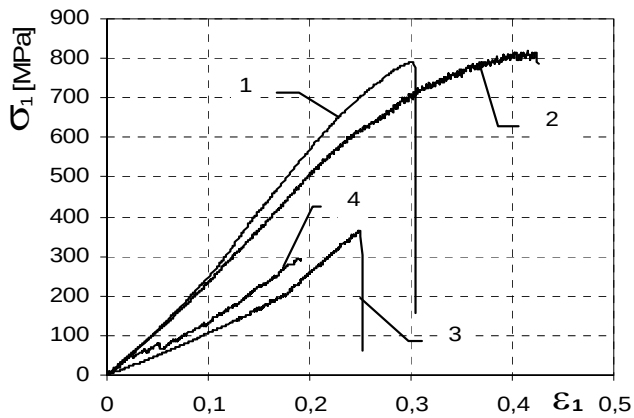

Fig. 10. The effect of symmetrical minor cyclic torsion with amplitudes: 0.05(2), 0.2(3) and 0.4(4) and tension (1) on the relation between σ_1 and ε_1 determined in tensile direction at an ambient temperature

The flow stress and limit strain in the tensile direction of complex specimens deformed at an ambient temperature and at 600 °C are shown in Figure 10 and Figure 11, respectively. During deformation at 600 °C a decrease of limit strain by application of cyclic torsion is observed. It can be explained by strain localization in shearing bands and dynamic recrystallization in these bands, which leads to quick fracturing of samples. During deformation at lower temperature the localization of strain is not intensified by dynamic recrystallization and limit strains in the tensile direction for the used strain paths are rather comparable (Figure 10).

The initial structure contains equiaxial grains of an average diameter equal to about 500 μm. The microstructure after monotonic tensile test at an ambient temperature shows highly deformed structure with two active slip systems only. Similar structure was obtained after monotonic torsion, but in the outer layers of a sample, slip lines are more numerous compared to the inner layers.

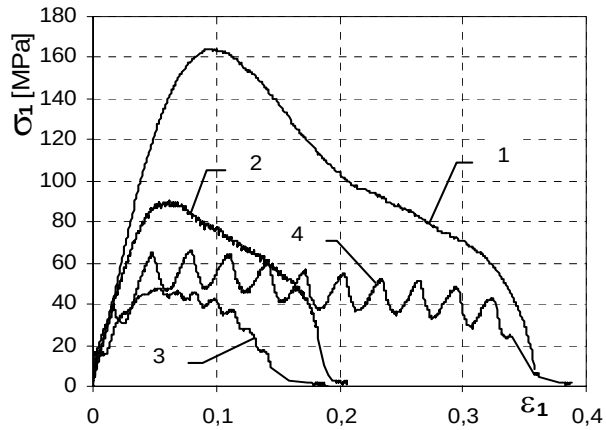

Fig. 11. The effect of symmetrical minor cyclic torsion with amplitudes: 0.05 (2), 0.2 (3) and 0.4 (4) and tension (1) on the relation between σ_1 and ε_1 determined in tensile direction at a temperature of 600 °C

After tension and torsion at 600 °C a significant decrease in grain size takes place, which is caused by dynamic recrystallization DRX. Microstructure of CuSi5 silicon bronze after monotonic tensile together with cyclic torsion at an ambient temperature is similar to microstructure after monotonic tensile or monotonic torsion at the same temperature. The only visible difference is that the complex deformation activates more slip systems than each simple monotonic deformation separately activates.

The cyclic torsion superimposed on the monotonic tension lowers the energy stored in material in comparison with pure monotonic deformation. This can completely eliminate the DRX if amplitude is very low (0.05), and on the other hand by the increase of amplitude the DRX is produced. This means that at a high temperature cyclic straining affects profoundly the microstructures, while at lower temperature these effects are small.

The silicon bronze containing about 5% of Si is a very curious alloy, because the stacking fault energy is very low, nearly equal to zero. The mechanism of deformation is special; a large deformation can be obtained mainly by twinning in the case of cyclic process, therefore it is a new aspect of large deformation.

4. Conclusions

It has been found that complex strain paths have significant effect on the behaviour of CuSi5 silicon bronze during deformation. The effect of cyclic torsion together with uniaxial tension on the flow stress and limit strain is dependent on the temperature. Cyclic straining eliminates the DRX if amplitude is very low (0.05), and the increase of amplitude activates the DRX.

From the examples given above it is clearly visible that by the change of strain path in massive processes the great progress in metal-forming processes can be obtained and new technologies more effective in energy and material saving can be developed.

Acknowledgements

The authors are grateful to the State Committee for Scientific Researches for the financial support.

References

[1] Pinheiro J.P., Barbosa R., Cetlin P.R.: *Dynamic restoration during the hot cyclic straining of copper*, Scripta Mater., 1998, Vol. 38, pp. 53–57.
[2] Pinheiro J.P., Barbosa R., Cetlin P.R.: *Effect of the cyclic straining amplitude on the hot dynamic restoration of copper*, Scripta Mater., 2001, Vol. 44, pp. 187–193.
[3] Pinheiro J.P., Barbosa R., Cetlin P.R.: *Warm cyclic straining of ferritic interstitial free steel*, Proc. of Symposium of Thermomechanical Processing of Steel, Ottawa, the Metallurgical Society of the Canadian Institute of Metallurgy, 2000, pp. 221–233.
[4] Pinheiro J.P., Barbosa R., Cetlin P. R.: *The effect of cyclic torsion on the hot dynamic restoration of interstitial free steel in the austenitic range*, J. Mater. Proc. Technol., 2002, Vol. 125–126, pp. 125–129.
[5] Bartolomé R., Gutiérrez I., Fuents M.: *Effect of strain reversal on the recrystallization of a microalloyed steel*, Proc. of the 4th Int. Conf. on Recrystallization and Related Phenomena, Taskuba, The Japan Institute of Metals, 1999, pp. 709–714.
[6] Zhang X.J.: *The effect of strain history on properties and structure of deformed metals*, Department of Materials Engineering, Monash University, Clayton, Victoria, Australia, 1998.
[7] Gronostajski Z., Misiołek N., Jaśkiewicz K.: *Wpływ małocyklowego skręcania oscylacyjnego na naprężenie uplastyczniające oraz odkształcenie graniczne brązu CuAl8*, Materiały Konf. Forming'2002, Luhacovice, 2002, pp. 93–98.
[8] Gronostajski Z., Misiołek N.: *The effect of amplitude in minor cyclic torsion on the behaviour of CuAl8 aluminium bronze*, Proc. of Int. Sc. Conf. Achievements in Materials and Mechanical Engineering, AMME'2002, Zakopane, 2002, pp. 219–222.
[9] Gronostajski Z.: *Analiza wyznaczania naprężenia uplastyczniającego w próbie skręcania*, Rudy i Metale Nieżelazne, 1999, Vol. 44, pp. 236–242.
[10] Hadasik E., Płachta A., Gronostajski Z., Schindler I.: *Analiza sposobów wyznaczania naprężenia uplastyczniającego w próbie skręcania na gorąco*, Materiały Konf. Forming'2001, Stara Leśna, 2001, pp. 77–84.

[11] Gronostajski Z.: *Modele konstytutywne opisujące zachowanie się wybranych stopów miedzi w zakresie dużych odkształceń plastycznych*, Prace Naukowe Instytutu Technologii Maszyn i Automatyzacji, Ser. Monografie, 2000, Vol. 23, pp. 1–225.
[12] Pawlicki J., Grosman F.: *Naprężenie uplastyczniające w warunkach wymuszonej zmiany orientacji osi głównych stanu naprężenia wybranych materiałów metalicznych*, Materiały Konf. Forming'99, Ustroń, pp. 208–213.
[13] Pawlicki J., Grosman F.: *Wpływ zmiany orientacji osi głównych stanu naprężenia na wartość naprężenia uplastyczniającego*, Rudy i Metale Nieżelazne, 1997, Vol. 42, pp. 501–503.
[14] Pawlicki J., Grosman F.: *Wpływ przebiegu odkształcania na wartość naprężenia uplastyczniającego polikryształów*, Rudy i Metale Nieżelazne, 1999, Vol. 10, pp. 565–568.
[15] Gronostajski J., Gronostajski Z., Jaśkiewicz K., Misiołek N., Weiler W.: *Plastometr realizujący złożone drogi odkształcania*, Obróbka Plastyczna Metali, 2001, Vol. 12 pp. 5–10.
[16] Gronostajski Z., Jaśkiewicz K.: *The effect of complex strain path on the hot dynamic restoration of silicon bronze CuSi3.5*, Proc. of Int. Sc. Conf. Achievements in Materials and Mechanical Engineering, AMME'2002, Zakopane, pp. 215–218.
[17] Hurley P.J., Hodgson P.D., Muddle B.C.: *Analysis and characterization of ultrafine ferrite produced during a new steel strip rolling process*, Scripta Materialia, 1999, Vol. 40, pp. 433–438.
[18] Armstrong P.E., Hockett J.E.: *Large strain multidirectional deformation of 1100 aluminium at 300 K*, J. Mech. Phys. Solids, 1982, Vol. 30, pp. 37–58.
[19] Garczyński Z.: *Kształtowanie odkuwek metodą prasowania obwiedniowego*, Materiały Konferencji Obróbka Plastczna Metali,'98, Poznań-Kierz, 1998, pp. 29–34.
[20] Piela A., Grosman F.: *Designing the Swaging Process*, Proc. of the 8th International Conference on Metal Forming 2000, Kraków, 2000, pp. 617–624.
[21] Korbel A., Bochniak W.: *Method of plastic forming of materials*, U.S. Patent No. 5, 737.959 (1998).

Zachowanie się brązu krzemowego CuSi5 podczas odkształcania wzdłuż złożonej drogi

Przedstawiono wpływ złożonej drogi odkształcania na zachowanie się brązu krzemowego CuSi5. Złożona droga odkształcania obejmowała różne sekwencje małocyklowego odkształcania połączonego z monotonicznym rozciąganiem. Amplitudę odkształcenia zmieniano w zakresie od 0.05 do 0.5, temperaturę – od 20 °C do 800 °C, a prędkość odkształcania – od 0.01 do 1 s^{-1}. Właściwości i strukturę uzyskiwane wskutek złożonych sposobów odkształcania porównywano z tymi samymi wielkościami uzyskiwanymi w procesach monotonicznego skręcania i rozciągania. Brąz krzemowy zawierający około 5% Si jest szczególnym materiałem, ponieważ energia jego błędów ułożenia jest bardzo niska, niemal bliska zera. Zaobserwowano, że duże odkształcenia w złożonym procesie odkształcania takiego materiału są w dużym stopniu osiągane przez bliźniakowanie.

Stwierdzono, że złożony sposób odkształcania ma duży wpływ na zachowanie się brązu krzemowego CuSi5, przy czym inaczej wpływa na jego właściwości i strukturę określane w ni-

skiej temperaturze aniżeli w wyższej temperaturze. Małocyklowe odkształcanie eliminuje rekrystalizację dynamiczną, jeśli amplituda odkształcenia jest bardzo mała (0.05) i dopiero zwiększenie amplitudy powoduje aktywację rekrystalizacji dynamicznej.

W procesach obróbki objętościowej przez zmianę drogi odkształcenia można osiągnąć znaczny postęp w procesach kształtowania plastycznego, opracowując bardziej energo- i materiałochłonne technologie.

Sposoby odkształcania podobne do tych, które stosowano w badaniach, są wykorzystywane w przemysłowych procesach kształtowania plastycznego takich jak: walcowanie, walcowanie z poprzecznym ruchem walców, prasowanie wahającą matrycą, kucie przy użyciu kowarek, wyciskanie z cyklicznie skręcaną matrycą itp.

ARCHIVES OF CIVIL AND MECHANICAL ENGINEERING

Vol. IV 2004 No. 1

Approximate fundamental solutions of equilibrium equations for thin plates on elastic foundation

KAZIMIERZ MYŚLECKI
Wrocław University of Technology, Wybrzeże Wyspiańskiego 27, 50-370 Wrocław

In this paper, a new approximate method of determining fundamental solutions for thin plates on elastic foundation is considered. Various models of foundations (Winkler, Pasternak, elastic half-space) are analysed. The approximate fundamental solutions are obtained through the analysis of power series of their Fourier's transform images. In the inversion procedure from images to originals, the well-known fundamental solutions of the *n*-th power of the Laplace operator are used. The effectiveness of the approximate fundamental solutions is verified by some test examples.

Keywords: *fundamental solution, boundary element method, thin plate, elastic foundation*

1. General relations of thin-plate theory

Let us consider a thin plate of a uniform thickness h with midplane S and boundary curve C lying on a plane (x_1, x_2) (Figure 1).

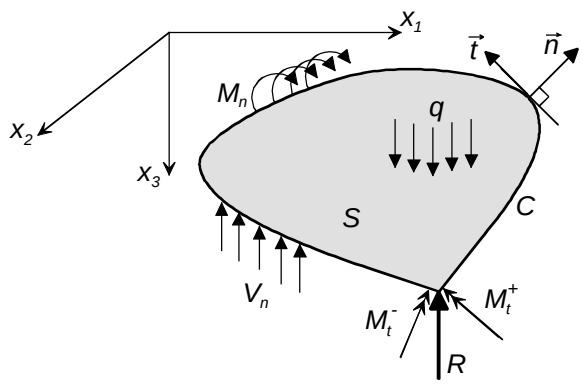

Fig. 1. Definition of thin plate

Generalized stress–displacement relation for moments and shear forces are [1]:

$$M_{\alpha\beta} = -D[(1-\nu)w_{,\alpha\beta} + \nu\delta_{\alpha\beta}w_{,\gamma\gamma}],$$
$$Q_\alpha = -D\Delta w_{,\alpha}, \quad \alpha,\beta,\gamma \in \{1,2\}, \tag{1}$$

where v is Poisson's ratio, $D = Eh^3/12(1-v^2)$ – the plate stiffness, $\delta_{\alpha\beta}$ – Kronecker's symbol, Δ – Laplace's operator. The comma before index denotes partial differentiation and repeated indices' summation convention.

The relations for such boundary quantities as: rotation, moments, Kirchhoff's shear force and concentrated reaction in the corner are as follows:

$$\begin{aligned} &\varphi_n = -w_{,\alpha}\, n_\alpha, \\ &M_n = M_{\alpha\beta} n_\alpha n_\beta, \quad M_t = M_{\alpha\beta} t_\alpha t_\beta, \\ &V_1 = Q_1 + M_{12,2}, \quad V_2 = Q_2 + M_{12,1}, \quad V_n = V_\alpha n_\alpha, \\ &R = M_t^+ - M_t^-, \end{aligned} \tag{2}$$

where n_α and t_α are the unit normal and the vector tangent to the boundary curve C, respectively.

2. Governing equations for plates on elastic foundation

The equilibrium equation for the plate on elastic foundation has a general form

$$D\Delta^2 w + p(w) = q. \tag{3}$$

The foundation reaction $p(w)$ is expressed by a linear operator of the deflection of a plate and depends on a foundation's model.

The simplest model is Winkler's foundation with the reaction of the form

$$p(w) = k_1 w. \tag{4}$$

The foundation's stiffness k_1 depends on mechanical properties of soil. This model of foundation can be interpreted as a set of independent springs (Figure 2).

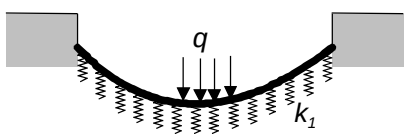

Fig. 2. Winkler's foundation

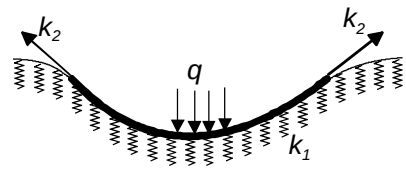

Fig. 3. Pasternak's foundation

Two parameter Pasternak's foundation is another model of an elastic foundation

$$p(w) = -k_2 \Delta w + k_1 w. \tag{5}$$

The second stiffness parameter k_2 can be interpreted as a tension in the membrane that covers the foundation (Figure 3).

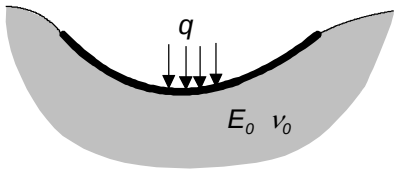

Fig. 4. Half-space foundation

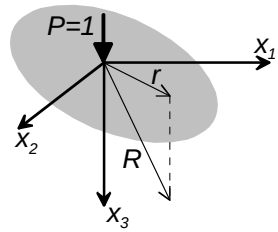

Fig. 5. Boussinesq's problem

The most advanced model is an elastic half-space (Figure 4). In that case, a simple differential expression for foundation reaction does not exist. In order to determine a form of the reaction, a classical Boussinesq's problem [2] will be recalled (Figure 5)

$$\begin{aligned} &u_3 = \frac{1+\nu_0}{2\pi E_0}\left[\frac{x_3^2}{R^3} + \frac{2(1-\nu_0)}{R}\right], \\ &r = \sqrt{x_1^2 + x_2^2}, \\ &R = \sqrt{r^2 + x_3^2}, \\ &x_3 = 0 \quad \Rightarrow \quad u_3 = \frac{1-\nu_0^2}{\pi E_0}\frac{1}{r}. \end{aligned} \tag{6}$$

Then a deflection of the plate caused by the foundation reaction takes the form of convolution

$$w(x_1, x_2) = \int_{-\infty}^{\infty}\int_{-\infty}^{\infty} u_3(x_1 - \xi_1, x_2 - \xi_2)p(\xi_1, \xi_2)d\xi_1 d\xi_2 = u_3 * p. \tag{7}$$

Thus the problem is described by a system of two differential-integral equations [3]

$$\begin{cases} w = u_3 * p, \\ D\Delta^2 w + p = q \end{cases} \tag{8}$$

with two unknown functions, i.e. reaction of the foundation p and deflection of the plate w.

3. Fundamental solutions

A fundamental solution of the differential equation is defined as a particular solution of it with the right-hand side in the form of Dirac's δ [4, 5], i.e. the unit concentrated force:

$$L(x_1, x_2)\overline{w}(x_1 - \xi_1, x_2 - \xi_2) = \delta(x_1 - \xi_1, x_2 - \xi_2), \tag{9}$$

where L is a differential operator, (ξ_1, ξ_2) – the source point and (x_1, x_2) – the reference point.

The fundamental solutions of powers of the Laplace operator [6] are worth mentioning, since they are of a great importance in subsequent derivations of the approximate fundamental solutions of plate on elastic foundations:

$$\begin{aligned} &\Delta^n \overline{w}_n = \delta, \\ &\overline{w}_n = \frac{1}{2\pi} r^{2(n-1)} \left(A_n \ln \frac{r}{r_0} - B_n\right), \quad r = \sqrt{(x_1 - \xi_1)^2 + (x_2 - \xi_2)^2}, \\ &A_n = \frac{1}{4^{n-1}[(n-1)!]^2}, \quad B_n = A_n \sum_{j=1}^{n-1} \frac{1}{j}, \quad n \geq 1, \end{aligned} \tag{10}$$

where r_0 is an arbitrary constant of length's dimension.

Let us rewrite the general equation for plate on elastic foundation (3) so as to obtain the form with a small parameter ε

$$D\Delta^2 \overline{w} + \varepsilon p(\overline{w}) = \delta. \tag{11}$$

To this end we apply a generalised Fourier transform and then expand the image of fundamental solution $\widetilde{\overline{w}}$ into a power series of ε. The useful properties of a Fourier transform are as follows [7, 8]:

$$\begin{aligned} &\Im[f(x_1, x_2)] = \int_{-\infty}^{\infty} \int_{-\infty}^{\infty} f(x_1, x_2) e^{i(\alpha_1 x_1 + \alpha_1 x_1)} \, dx_1 dx_2 = \widetilde{f}(\alpha_1, \alpha_2), \\ &\Im^{-1}[\widetilde{f}(\alpha_1, \alpha_2)] = \frac{1}{4\pi^2} \int_{-\infty}^{\infty} \int_{-\infty}^{\infty} f(\alpha_1, \alpha_2) e^{-i(\alpha_1 x_1 + \alpha_1 x_1)} \, d\alpha_1 d\alpha_2 = f(x_1, x_2), \\ &\Im[f * g] = \widetilde{f}\,\widetilde{g}, \quad \Im[\delta] = 1, \quad \Im[\Delta^n f] = (-1)^n \rho^{2n} \widetilde{f}, \quad \rho = \sqrt{\alpha_1^2 + \alpha_2^2}, \end{aligned} \tag{12}$$

and

$$\begin{aligned}
&\Im[\overline{w}_n] = \frac{(-1)^n}{\rho^{2n}}, \\
&\Im[r^{6n-1}] = \frac{1}{C_n}\frac{1}{\rho^{6n+1}}, \qquad C_n = \frac{(-1)^n}{2\pi}\prod_{j=1}^{n}\frac{1}{(6j-1)^2(6j-3)^2(6j-5)^2}, \qquad n \geq 0.
\end{aligned} \tag{13}$$

Applying a Fourier transform to Equation (11) for all considered models of elastic foundations (Winkler, Pasternak and half-space (4), (5), (8)) we can find the following forms of fundamental solutions:

$$\begin{aligned}
\widetilde{\overline{w}}_W &= \frac{1}{D\rho^4 + \varepsilon k_1} = \frac{1}{D\rho^4} - \frac{\varepsilon k_1}{D^2\rho^8} + \frac{\varepsilon^2 k_1^2}{D^3\rho^{12}} - \frac{\varepsilon^3 k_1^3}{D^4\rho^{12}} + \ldots, \\
\widetilde{\overline{w}}_P &= \frac{1}{D\rho^4 + \varepsilon(k_2\rho^2 + k_1)} \\
&= \frac{1}{D\rho^4} - \frac{\varepsilon(k_2\rho^2 + k_1)}{D^2\rho^8} + \frac{\varepsilon^2(k_2\rho^2 + k_1)^2}{D^3\rho^{12}} - \frac{\varepsilon^3(k_2\rho^2 + k_1)^3}{D^4\rho^{12}} + \ldots, \\
\widetilde{\overline{w}}_H &= \frac{1}{D\rho^4 + \varepsilon k_3\rho} \\
&= \frac{1}{D\rho^4} - \frac{\varepsilon k_3}{D^2\rho^7} + \frac{\varepsilon^2 k_2^2}{D^3\rho^{10}} - \frac{\varepsilon^3 k_3^3}{D^4\rho^{13}} + \frac{\varepsilon^4 k_3^4}{D^5\rho^{16}} - \ldots, \quad k_3 = \frac{E_0}{2(1-\nu_0^2)}.
\end{aligned} \tag{14}$$

After inversion of the images (14) using formulae (12), (13) and fixing the parameter $\varepsilon = 1$ we can find originals of fundamental solutions:

$$\begin{aligned}
\overline{w}_W &= \frac{1}{D}\overline{w}_2 + \sum_{i=1}^{\infty}(-1)^i\frac{k_1^{i-1}}{D^i}\overline{w}_{2(i+1)}, \\
\overline{w}_P &= \frac{1}{D}\overline{w}_2 + \sum_{i=1}^{\infty}\frac{(-1)^i}{D^{i+1}}\sum_{j=0}^{i}\binom{i}{j}k_1^j k_2^{i-j}(-1)^{i+j}\overline{w}_{2+i+j}, \\
\overline{w}_H &= \frac{1}{D}\overline{w}_2 + \sum_{i=1}^{\infty}\left[(-1)^i\frac{k_3^{2i}}{D^{2i+1}}\overline{w}_{3i+2} - \frac{k_3^{2i-1}}{D^{2i}}C_i r^{6i-1}\right].
\end{aligned} \tag{15}$$

In practical applications, the infinite series (15) are truncated to several terms, thus we obtain approximate fundamental solutions. Additionally, the author has inverted the images (14) for the Winkler half-space foundation and found exact originals:

$$\overline{w}_W = \frac{l^2}{2\pi D}\frac{i}{2}\left[K_0\left(\frac{\eta r}{l}\right) - K_0\left(\frac{\overline{\eta}\, r}{l}\right)\right], \quad l = \sqrt[4]{\frac{D}{k_1}}, \eta = \frac{\sqrt{2}}{2} + i\frac{\sqrt{2}}{2}, \quad i = \sqrt{-1},$$

$$\overline{w}_H = \frac{l^2}{12D}\left\{\mathbf{H}_0\left(\frac{r}{l}\right) - Y_0\left(\frac{r}{l}\right) - Re\left[\mathbf{H}_0\left(\frac{\omega r}{l}\right) - Y_0\left(\frac{\omega r}{l}\right)\right]\right\} \tag{16}$$

$$+\frac{l^2}{12D}\left\{-\sqrt{3}Im\left[\mathbf{H}_0\left(\frac{\omega r}{l}\right) - Y_0\left(\frac{\omega r}{l}\right)\right]\right\}, \quad l = \sqrt[3]{\frac{D}{k_3}}, \quad \omega = -\frac{1}{2} + \frac{\sqrt{3}}{2}i,$$

where K_0, Y_0 are the Bessel functions, $\mathbf{H}_0$ is Struve's function, *Re*, *Im* are real and imaginary parts of complex functions, and $\overline{\eta}$ is complex conjugate of η.

4. Algorithm of boundary element method (BEM)

The boundary integral equations of the problem are derived from Betti's reciprocity theorem [1]. Let us consider two systems of displacement and force fields: the first given in Figure 1 and the second corresponding to an infinite plate subjected to a unit concentrated force (9), i.e. obtained from relation (2) using the fundamental solution (15). The Betti's reciprocity theorem can be expressed by the following equation:

$$\int_S q\overline{w}\,dS + \int_C \left(M_n\overline{\varphi}_n + V_n\overline{w}\right)dC + \sum_i R_i\overline{w}_i$$
$$= \int_S \overline{q}\,w\,dS + \int_C \left(\overline{M}_n\varphi_n + \overline{V}_n w\right)dC + \sum_i \overline{R}_i w_i, \qquad \overline{q} \equiv \delta. \tag{17}$$

In accordance with Diraca's δ properties we can write

$$\int_S w(x_1,x_2)\delta(x_1-\xi_1, x_2-\xi_2)\,dS(x_1,x_2) = \begin{cases} w(\xi_1,\xi_2), & (\xi_1,\xi_2)\in S, \\ \dfrac{1}{2}w(\xi_1,\xi_2), & (\xi_1,\xi_2)\in C, \\ 0, & (\xi_1,\xi_2)\notin S\cup C. \end{cases} \tag{18}$$

We take advantage of the third relation in (18) which is the basis of Kupradze's collocation method [9]. Plates on elastic foundation have usually free edges so we can assume $M_n = V_n = R_i = 0$ and Equation (17) takes the form

$$\int_S q\overline{w}\,dS - \int_C \left(\overline{M}_n\varphi_n + \overline{V}_n w\right)dC - \sum_i \overline{R}_i w_i = 0. \tag{19}$$

Equation (19) should be satisfied in any point (ξ_1, ξ_2) outside the domain S. The boundary curve C is divided into linear elements. The unknown functions w and φ_n are also approximated by linear functions (Figure 6). Kupradze's method gives us such advantage as avoiding singular integrals in Equation (19).

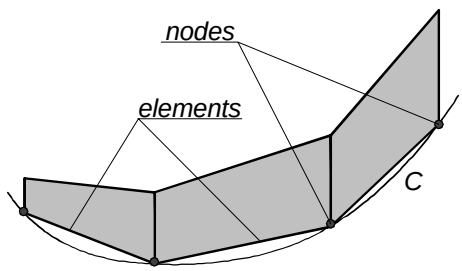

Fig. 6. Linear boundary element

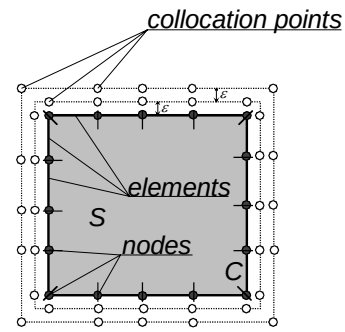

Fig. 7. Collocation points

The collocation points are located on two outer contours. The number of collocation points depends on the number of unknown values in nodal points. Figure 7 shows location of collocation points for a rectangular plate with free edges. The distance ε of outer contours is of a great importance in Kupradze's method: too short one requires more precise procedures of numerical integration, while too long leads to badly conditioned matrix of linear equations system. Author's experience learns that the distance ε is estimated as 1/10 of the mean length of boundary elements.

5. Numerical examples

The square plate of free edges is under consideration (Figure 8). The side of plate is a = 5 m, its bending stiffness D = 1923 kNm and Poisson's ratio v = 0.2. The plate is loaded with a concentrated force P = 69.44 kN [10]. The boundary side of the plate is divided into four equal linear boundary elements.

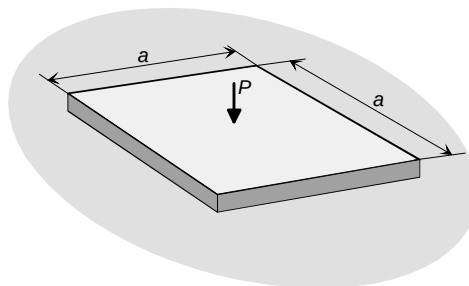

Fig. 8. Free-edge square plate

Deflections of the axes of symmetry of the Winkler's and Pasternak's plates are presented in Figure 9 and Figure 10. The stiffnesses of foundations are: $k_1 = 10^4$ kN/m^3, $k_2 = 3.472 \cdot 10^3$ kN/m.

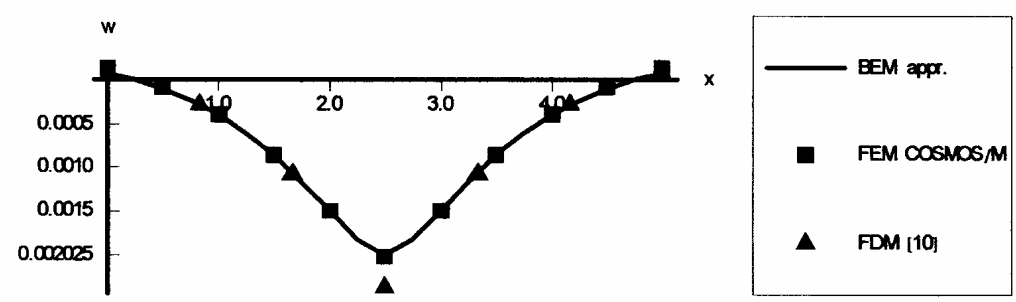

Fig. 9. Deflection of Winkler's plate

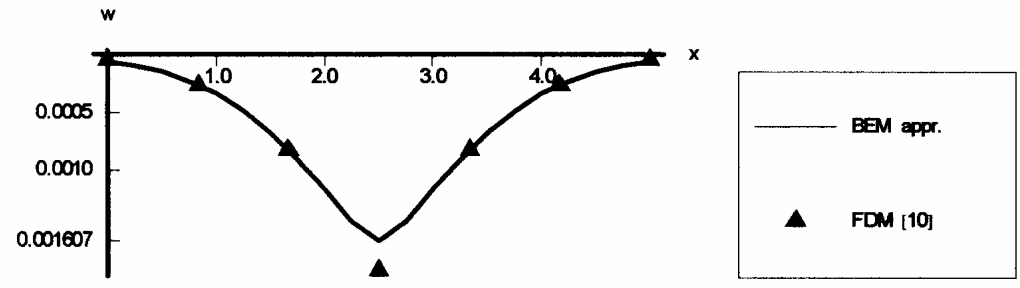

Fig. 10. Deflection of Pasternak's plate

Deflection of the axis of symmetry of the plate in elastic half-space is presented in Figure 11. The elastic constants of the half-space were estimated from relation $k_1 = 2.5E_0/a$ [11] ($\nu_0 = 0$) to compare the results with the results obtained using other models of foundations.

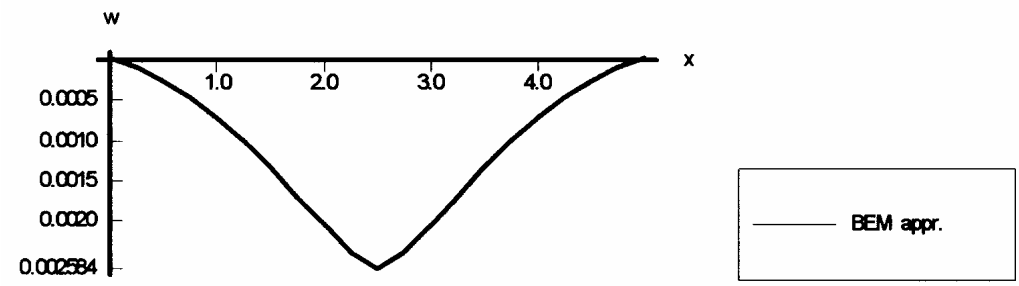

Fig. 11. Deflection of plate on a half-space

All these results are in a good agreement with those available from other numerical methods using the finite difference method (FDM) and the finite element method (FEM) in the COSMOS/M code. It is worth mentioning that the calculation convergence using the approximate fundamental solutions (15) was obtained even for a few terms of series (5–7).

6. Concluding remarks

A new method of finding approximate fundamental solutions for plates on various elastic foundations has been presented. The approximate fundamental solutions have simple forms of power series. Numerical results of the practical computation of some exemplary plates show that the approximate fundamental solutions have a satisfactory accuracy.

References

[1] Banerjee P.K., Butterfield R.: *Boundary Element Methods in Engineering Science*, McGraw-Hill, London, 1981.
[2] Nowacki W.: *Teoria sprężystości*, PWN, Warszawa, 1970.
[3] Łukasiewicz S.: *Obciążenia skupione w płytach, tarczach i powłokach*, PWN, Warszawa, 1976.
[4] Kythe P.K.: *Fundamental Solutions for Differential Operators and Applications*, Birkhäuser, Boston, 1996.
[5] Burczyński T.: *Metoda elementów brzegowych w mechanice*, WNT, Warszawa, 1995.
[6] Cheng A.H.-D.: *Particular solutions of Laplacian, Helmholtz-type, and polyharmonic operators involving higher order radial basis functions*, Eng. Anal. Bound. Elem., 2000, 24.
[7] Кеч В., Теодореску П.: *Введение в теории обобщенных функций с приложениями в технике*, Мир, Москва, 1978.
[8] Saichev A.I., Woyczyński W.A.: *Distributions in the Physical and Engineering Sciences*, Birkhäuser, Boston, 1997.
[9] Верюжский Ю.В.: *Численные методы потенциала в некоторых задачах прикладной механики*, Вища школа, Киев, 1978.
[10] Lisowski A.: *Obliczanie konstrukcji na ciągłym podłożu sprężystym*, PWN, Warszawa, 1974.
[11] *Budownictwo betonowe*, t. IX. *Fundamenty*, Arkady, Warszawa, 1963.

Przybliżone rozwiązania podstawowe równań równowagi płyt cienkich na podłożu sprężystym

Podano przybliżoną metodę wyznaczania rozwiązań podstawowych równań równowagi dla płyt cienkich na podłożu sprężystym. Rozpatrzono jednoparametrowe podłoże Winklera, dwuparametrowe podłoże Pasternaka i półprzestrzeń sprężystą. Przybliżone rozwiązania podstawowe otrzymano, rozwijając transformaty Fouriera ścisłych rozwiązań podstawowych wzglę-

dem małego parametru. Do odwracania obrazów transformat Fouriera wykorzystano znane rozwiązania podstawowe *n*-tej potęgi operatora Laplace'a. Otrzymana postać przybliżonych rozwiązań podstawowych (szeregi podstawowe) jest dużo prostsza od postaci ścisłych rozwiązań podstawowych (funkcje specjalne Bessela i Struvego).

Znalezione przybliżone rozwiązania podstawowe zastosowano w metodzie elementów brzegowych w wersji Kupradzego. Zaletą tej wersji jest to, że nie musi się obliczać osobliwych całek na brzegu obszaru płyty, a brzegowe równania całkowe mają prostą postać.

Dla każdego rodzaju podłoża wykonano przykład numeryczny rozwiązania płyty metodą elementów brzegowych z zastosowaniem przybliżonych rozwiązań podstawowych. Prezentowane wyniki obliczeń porównano z opublikowanymi literaturze wynikami otrzymanymi dzięki zastosowaniu metody różnic skończonych. Część wyników porównano z wynikami otrzymanymi metodą elementów skończonych w systemie COSMOS/M. Analiza przykładów wykazuje użyteczność przybliżonych rozwiązań podstawowych w praktycznych zastosowaniach oraz szybką zbieżność szeregów potęgowych reprezentujących te rozwiązania – wystarcza 5–7 wyrazów, aby osiągnąć zadowalającą zbieżność.

ARCHIVES OF CIVIL AND MECHANICAL ENGINEERING

Vol. IV 2004 No. 1

Hybrid knowledge representation in BMS

JAN BIEŃ, PAWEŁ RAWA
Wrocław University of Technology, Wybrzeże Wyspiańskiego 27, 50-370 Wrocław

Development of computer technology enables implementation of expert tools supporting decision processes in the Bridge Management Systems. The proposed expert tools utilise both data base and knowledge base of the system. Decisions in bridge management are very often based on a mixture of accurate data and fuzzy or uncertain information. This requires a proper technology for information acquisition, representation and processing. The paper presents the technology of hybrid knowledge representation integrating symbolic and non-symbolic knowledge representation. The proposed technology of the multilevel hybrid network enables the integration of various techniques in one computer tool. According to the problem that should be solved and to the type of available information the hybrid network can be built of the neural, fuzzy and functional components.

Keywords: *knowledge representation, Bridge Management Systems, hybrid networks, neural networks, fuzzy logic*

1. Information in the Bridge Management Systems

In the traditional computer-based Bridge Management Systems (BMS), information is stored as the data in the form of the database (e.g. [1–4]). The development of the computer technology currently enables representation of information also in the form of the advanced knowledge base (e.g. [5–9]). General diagram of the information flow in the data & knowledge-based BMS is presented in Figure 1.

The information coded in the form of data is stored and processed in the computer system and after the interpretation in the specific context is used in the decision processes [10–12]. The knowledge representation in the computer-based BMS needs much more complex procedures. The following main steps of these procedures can be itemized [1]:

- selection of the knowledge representation method corresponding to the form of the available information;
- acquisition of the knowledge as a special type of the information;
- construction of the computer knowledge base coupled with the system database;
- selection of the proper inference mechanisms for each particular application;
- analysis and interpretation of the results of the computer reasoning and the application of the conclusions in the decision processes.

The analysis of the information taken into account in the bridge management shows that decisions are very often based on the fuzzy information and on the information of various degree of uncertainty, e.g. [13–15]. The classification of the information utilized in the BMS, proposed in [13], is presented in Table 1.

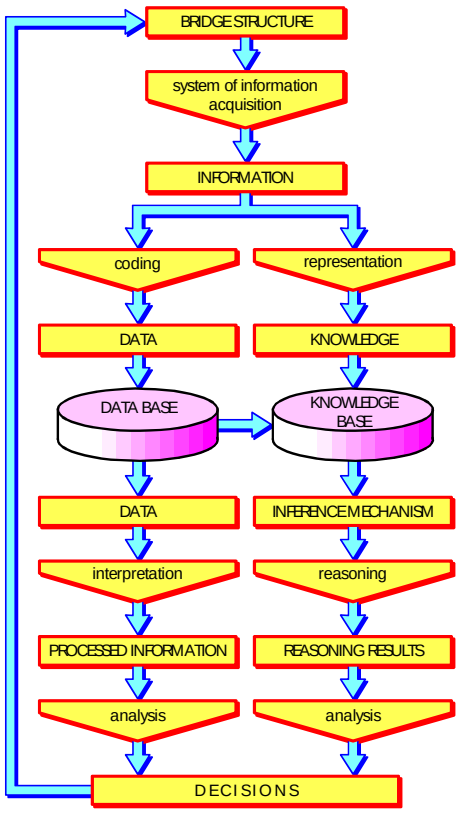

Fig. 1. Information flow in the data and knowledge-based Bridge Management Systems

The classification is based on the information fuzziness and takes into account two basic aspects: fuzziness of the information definition and fuzziness of the information measure.

In the proposed classification, three types of the information definitions are itemized:

- *precise definitions* (P), e.g. geometrical parameters, material characteristics, which are based on the standards, manuals, etc.;
- *imprecise, fuzzy definitions* (F), e.g. technical condition, serviceability, etc., which are partly based on the subjective interpretation;
- *undecided definitions* (U), e.g. aesthetics of bridge structures, which are completely based on the individual, subjective impressions.

The information can be described using two types of the measures:

- *precise measures* (P) expressed usually by means of the numbers, e.g. span length: 24 m, condition state: 2, load capacity: 30 t;
- *fuzzy measures* (F) expressed by means of the fuzzy numbers (e.g. about 20 m, between 20 t and 30 t) or by means of the fuzzy linguistic values (e.g. large, intensive, insignificant).

Table 1. Types of the information utilized in the BMS – classification based on the information fuzziness

Definition	Measure	
	Precise (P)	Fuzzy (F)
Precise (P)	PP	PF
Fuzzy (F)	FP	FF
Undecided (U)	UP	UF

The combination of the three types of the information definitions and the two types of the information measure creates six classes of information presented in Table 1. All the classes of information are usually used in the bridge management.

2. Technology of hybrid networks

A variety of information types taken into account in the bridge management process requires effective tools for data and knowledge acquisition, processing and utilization. One of the promising methods of the knowledge representation seems to be the technology of the multilevel hybrid networks [13, 16, 17]. This technology enables the integration of the various knowledge representation techniques in one expert tool.

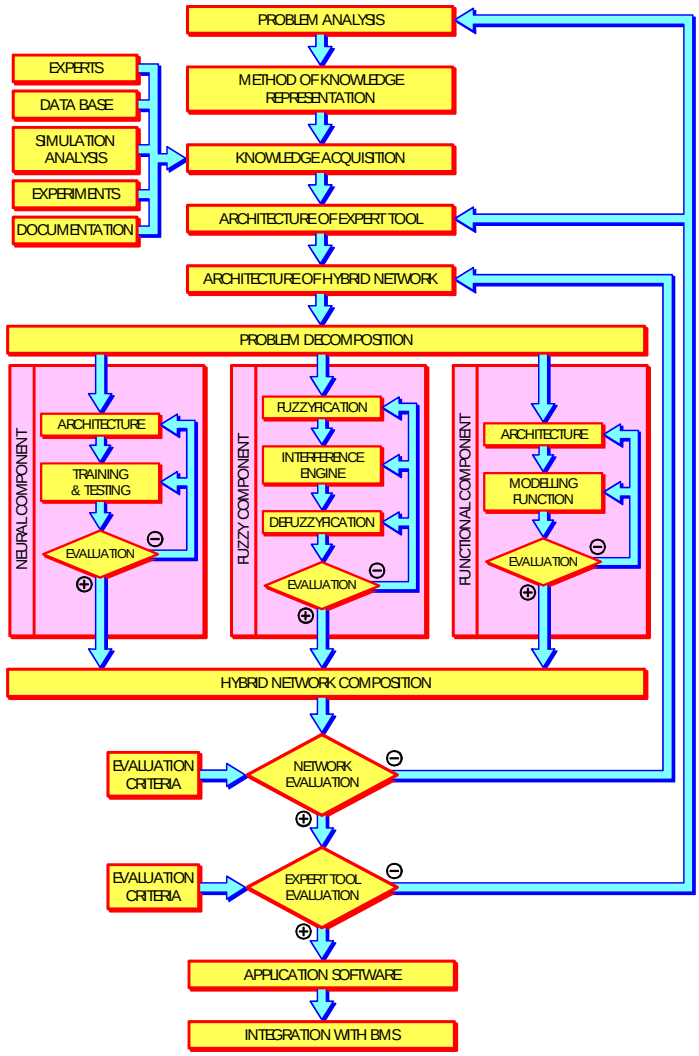

Fig. 2. Creation of the expert tool with hybrid knowledge representation

The process of the creation of the expert application by means of the hybrid network technology is presented in Figure 2. After the general analysis of the problem and the acquisition of the available knowledge – the architecture of the final network should be designed. Depending on the form and class of the accumulated information (see Table 1), the analyzed problem should be divided into subproblems. In the next step, a dedicated component of the network is created for each subproblem. All the components are prepared in the form of the prefabricated "blocks" which are stored in the library of the computer system and can be used in various networks. In the last step of the creation process, the components are connected to one another to form a multilevel network. For the creation of the components and the final network the specialized computer system NEURITIS [13, 18] can be used. The system is now available only in Polish version, therefore Figures 3, 5 and 9 are in Polish.

The illustration of the process of the components connecting to obtain a multilevel hybrid network is presented in Figure 3. In the system NEURITIS, the number of the network levels as well as the number of the network components are not limited and depend only on the application needs.

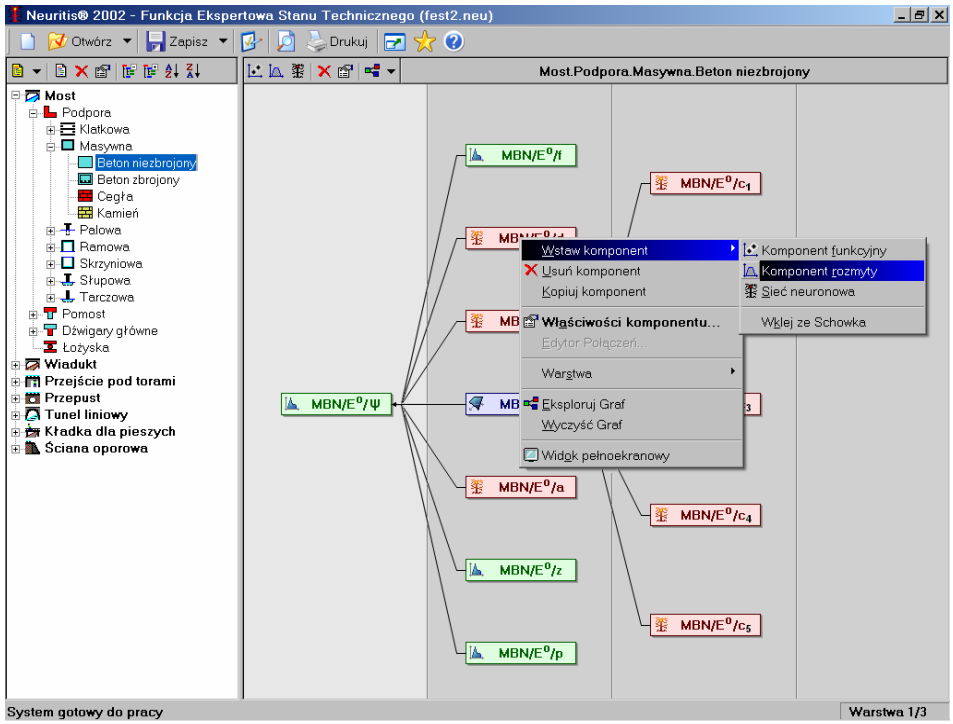

Fig. 3. Process of the components connecting to obtain the multilevel hybrid network

3. Components of the hybrid networks

In the presented system NEURITIS, three main types of network components can be used:

- *functional components*, which enable the implementation of the analytical functions in the knowledge representation;
- *neural components* based on the application of the multilayer neural networks;
- *fuzzy components* based on the fuzzy logic and fuzzy inference methods applied in the knowledge representation.

Table 2. Characteristics of the hybrid network components available in the NEURITIS

Definable elements of component		Functional component	Neural component	Fuzzy component
Input data	Form of input data	real number x_i	real number x_i	real number x_i
		matrix of real numbers $[\mathbf{X}_i]$		fuzzy number $\hat{x}_i$
				linguistic variable x_i*
	Number of inputs	unlimited	unlimited	2
Internal mechanisms	Internal resources	functions of n variables in the analytic form	neural network topology	membership functions for inputs
		functions of n variables in the discrete form	neuron activation functions	membership functions for outputs
				fuzzy rule base
	Internal operations	mathematical operations on the input data	training of the neural network	aggregation of rule premises
				conclusion activation
		mathematical operations on the internal resources of the component	testing of the neural network	output composition
				defuzzification
Output data	Form of output data	real number y_i	real number y_i	real number y_i
		matrix of real numbers $[\mathbf{Y}_i]$		
	Number of outputs	unlimited	unlimited	1

The selection of the type of components depends on the quality, quantity and form of the available information. Each component has to be prepared individually and has to pass all the needed tests before being applied as a "brick" of the final network.

In the preparation of each type of components, the following main steps can be itemized:

- defining the number of the component inputs and form of the input data;

• defining the internal mechanisms of the component: the internal resources specific to the component and the internal operations which can be prescribed on the input data and internal resources;

• defining the number of the component outputs and form of the output data.

Definable elements of each type of the hybrid network components are compared in Table 2. The following figures present the procedures of the preparation of the main types of the network components.

The diagram of the creation process of the functional component is presented in Figure 4. Some selected steps of the procedure are illustrated by the screen shots in Figure 5.

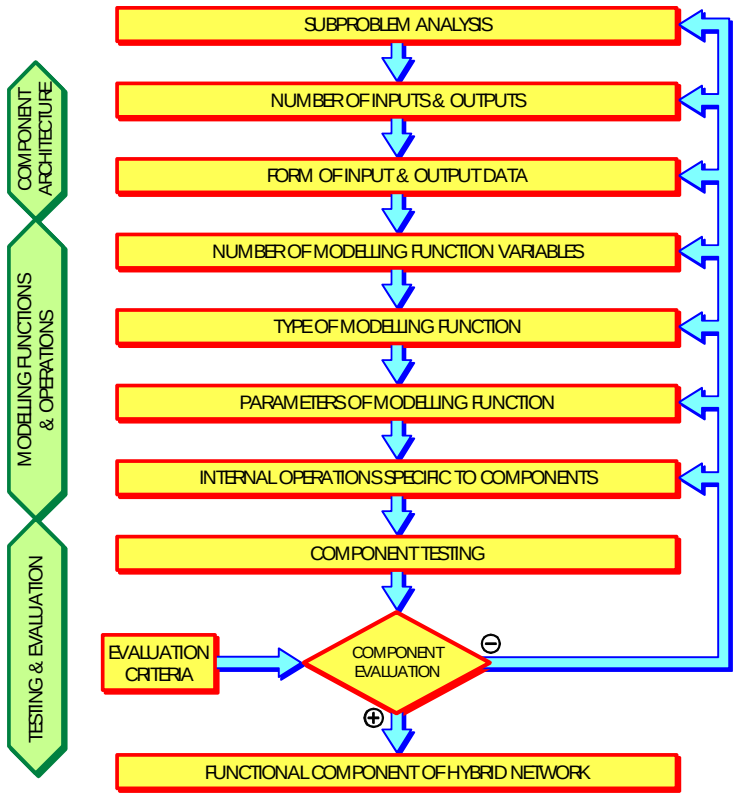

Fig. 4. Functional component of the hybrid network-defining procedure

The procedure of the neural component defining is shown in Figure 6. Figure 7 presents visualization of the neural component topology in the system NEURITIS.

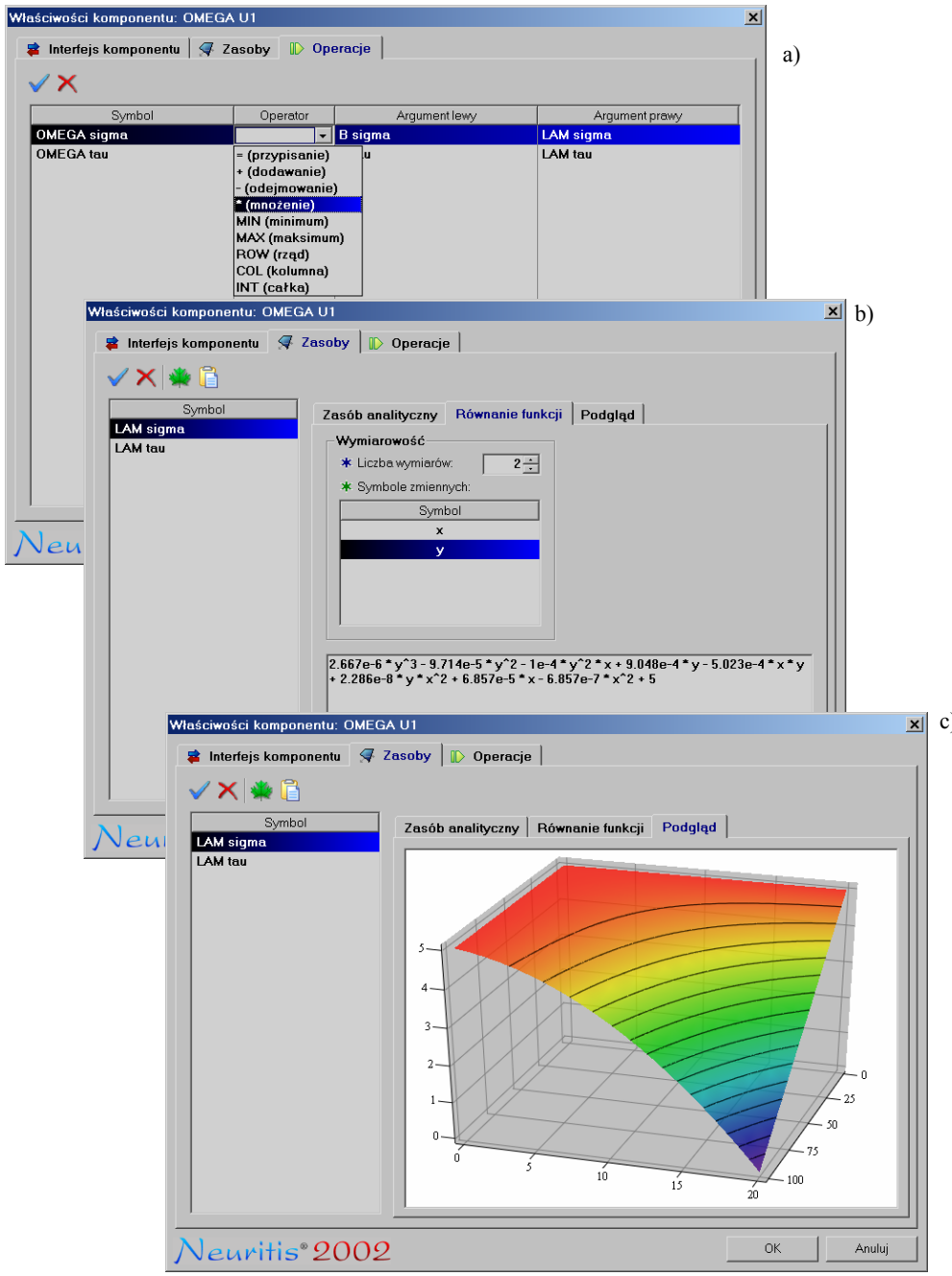

Fig. 5. Selected steps of the functional component defining: a) internal operations, b) internal resources, c) visualization of internal function

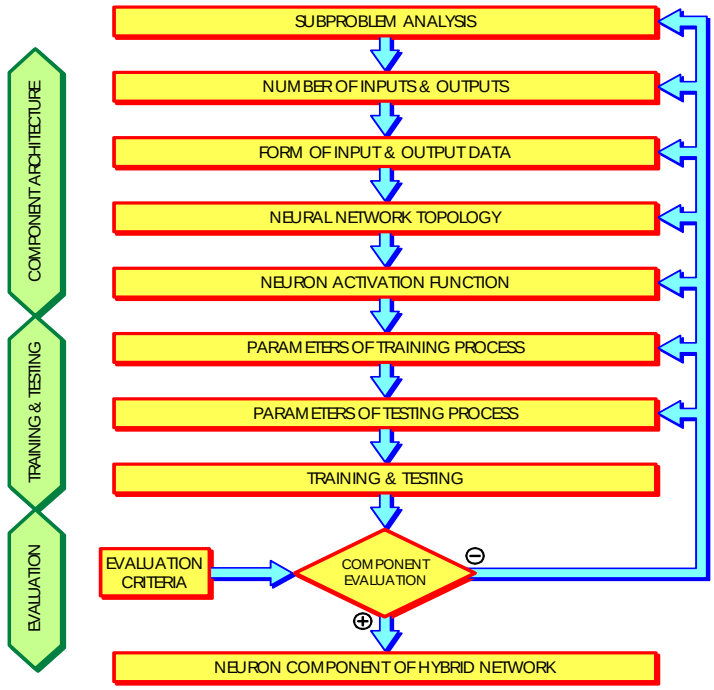

Fig. 6. Neural component of the hybrid network-defining procedure

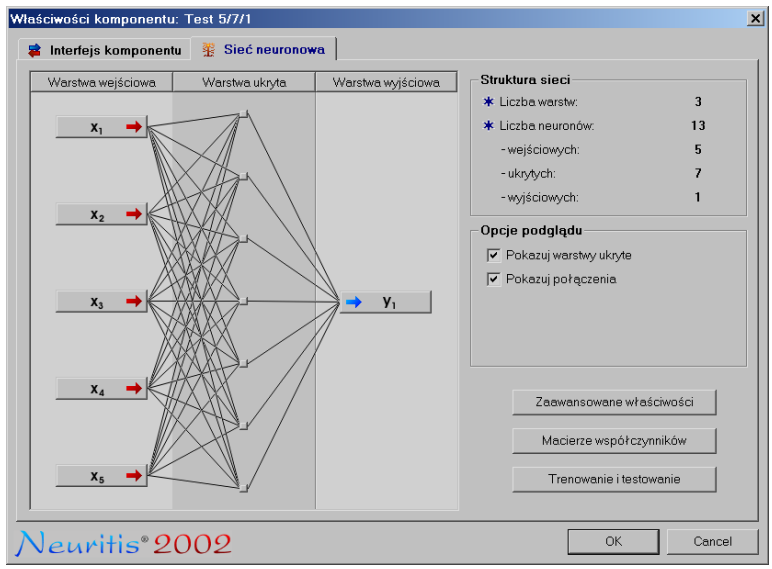

Fig. 7. Neural component topology definition

Defining the fuzzy component requires specification of the fuzzy inference mechanism. The sequence of the basic steps of the component-defining procedure is presented in Figure 8. The process of the fuzzy component creation in the NEURITIS system is illustrated in Figure 9.

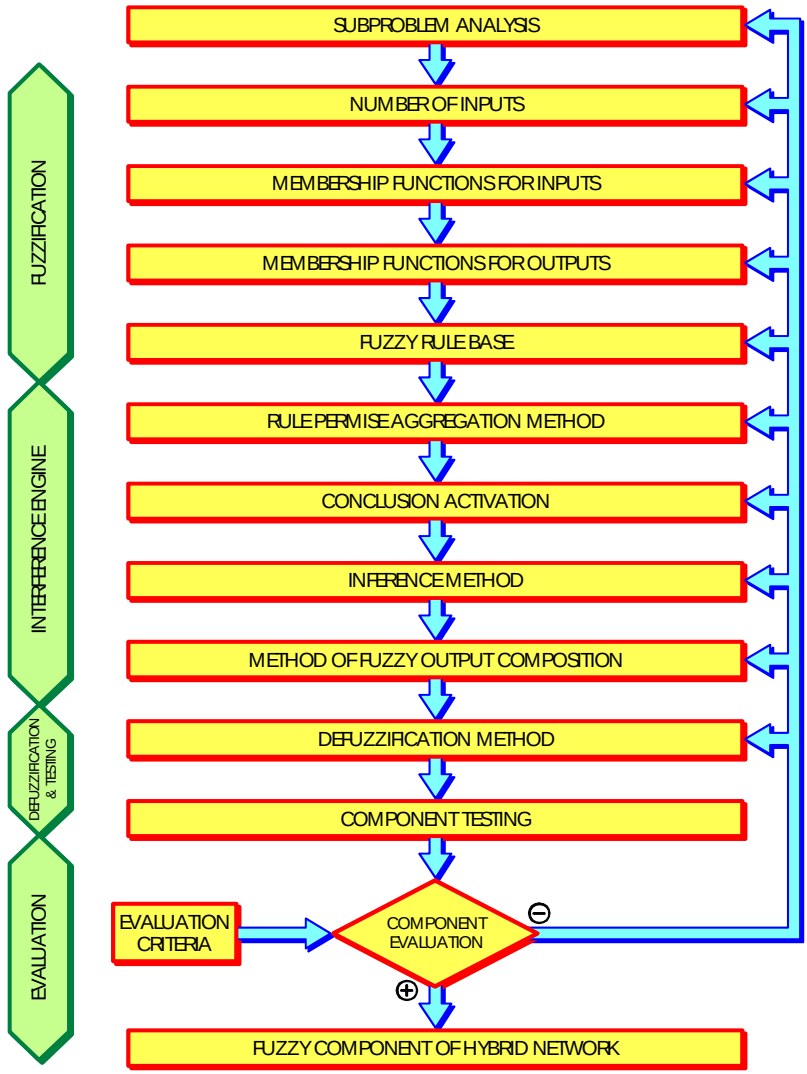

Fig. 8. Fuzzy component of the hybrid network-defining procedure

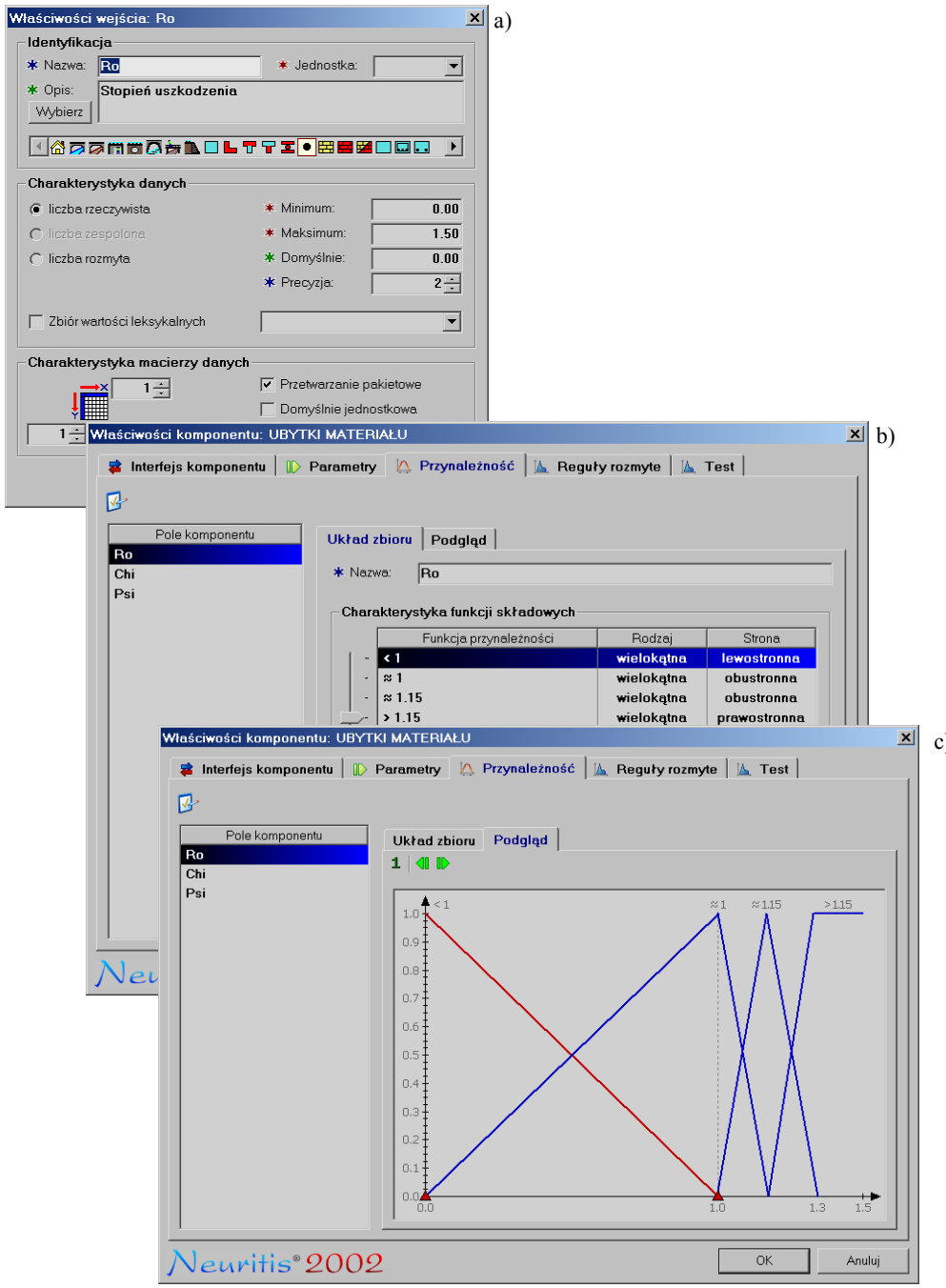

Fig. 9. Selected steps of the fuzzy component creation: a) component inputs, b) description of the membership functions, c) visualization of the membership functions

4. Applications in BMS

The presented technology of the knowledge representation by means of the hybrid networks has been successfully applied in the Railway Bridge Management System SMOK developed at Wrocław University of Technology for the Polish State Railways [19]. A functional scheme of this system is presented in Figure 10, where two expert tools are shown:

- Bridge Evaluation Expert Function (BEEF) supporting evaluation of the technical condition of the main elements of the bridge structures [14, 16].
- Prognosis Expert Function (PEF) aiding prediction of the bridge condition changes [17, 18].

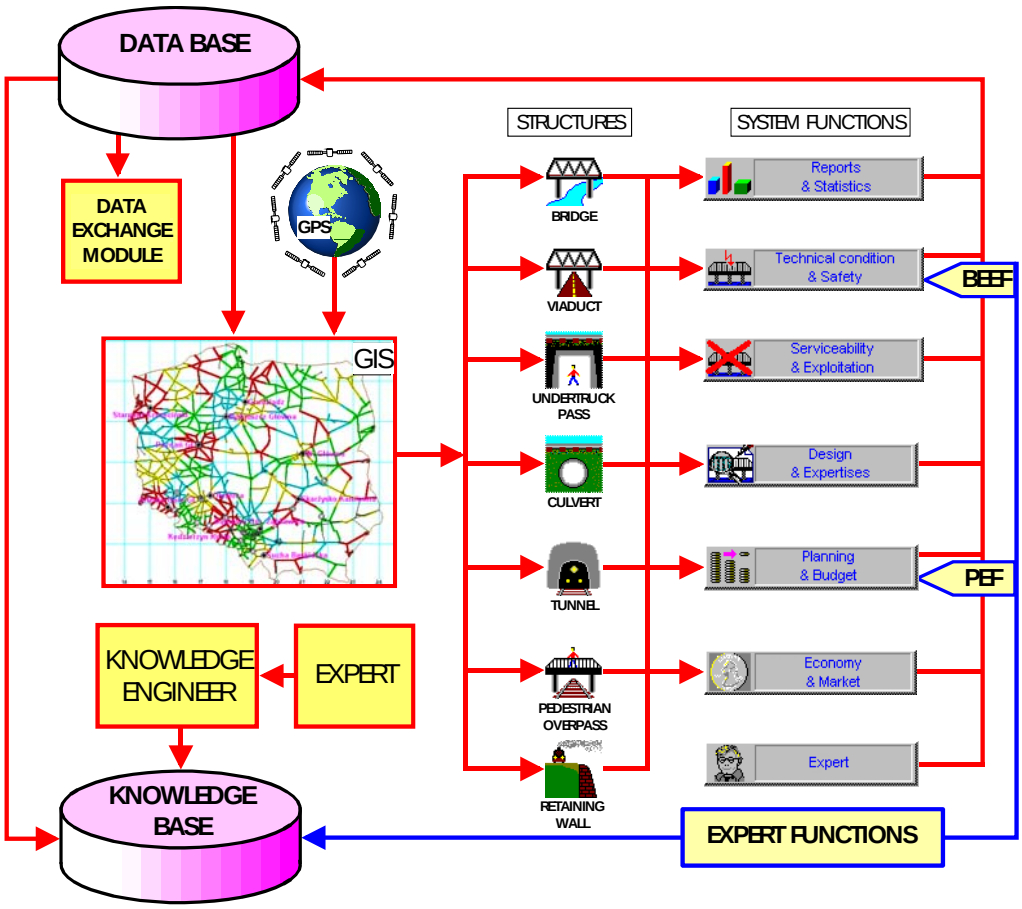

Fig. 10. Functional scheme of the Railway Bridge Management System SMOK

Figure 11 shows an example of the hybrid network used in the BEEF for the evaluation of the Technical Condition Index (TCI) of the column bridge pier made of the reinforced concrete. A three-level hybrid network of neural, fuzzy and functional components has been constructed.

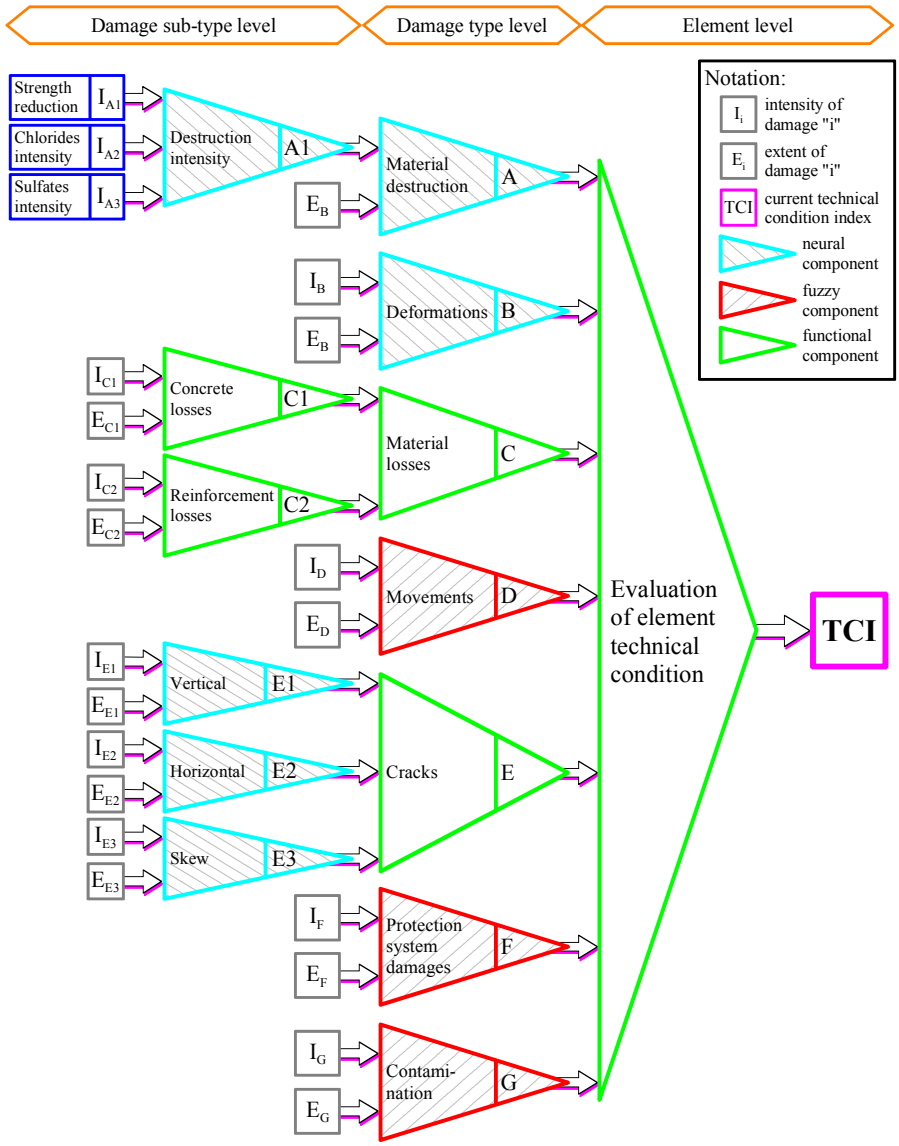

Fig. 11. Architecture of the hybrid network used in the BEEF for evaluation of the TCI of the column bridge pier made of the reinforced concrete

The evaluation of the TCI is based on the intensity and extent of the structure damages, according to the rules described in the Bridge Damage Catalogue [20]. About 200 hybrid networks have been created and implemented in the whole BEEF for the combinations of the following parameters:

- type of the structure (bridge, footbridge, underpass, etc.);
- type of the structure element (main girders, deck, bearings, etc.);
- type of the construction (plate, box, beam, etc.);
- type of the construction material (steel, reinforced concrete, stone, etc.).

The presented version of the BEEF, as a part of the system SMOK, has been used in the bridge management offices of the Polish State Railways since the year 2000.

5. Conclusions

The technology of multilevel hybrid networks is a powerful and effective tool of the knowledge representation in the Bridge Management Systems. The main advantages of the presented methodology of the information processing and utilization can be listed as follows:

- effective composition of the data and knowledge in the computer-based BMS;
- integration of the diverse types of information on various levels of uncertainty in one expert tool;
- unification of the decisions in the BMS due to application of the specialized expert tools;
- applications based on the hybrid network technology can be easily modified by the improvement or replacement of the network components, without decomposition of the whole network;
- technology of the hybrid networks can be developed by adding new types of components and implementation of the self-modification mechanisms in the components.

On the other hand, it should be underlined that the preparation of network components and the creation of practically effective networks is a very time-consuming process, engaging quite large group of specialists. The preparation of the knowledge-based expert tools for the BMS requires the cooperation of civil engineering experts, knowledge engineers, computer scientists, etc. The presented technology needs the continuation of the research and the extensive application study to create a more and more effective knowledge representation.

References

[1] Grob J., *Data Base System for the Maintenance of Highway Structures*, Proceedings of the 4th International Conference on Safety of Bridge Structures, Wrocław, 1992, pp. 293–300.

[2] Thompson P.D., Small E.P., Johnson M., Marshall A.R., *The Pontis Bridge Management System*, Structural Engineering International, 1998, Vol. 8, No. 4, pp. 303–308.

[3] Soderqvist M.K., Veijola M., *The Finnish Bridge Management System*, Structural Engineering International, 1998,Vol. 8, No. 4, pp. 315–319.
[4] *Management of Highway Structures*, edited by Parag C. Das, Thomas Telford Publishing, London, 1999.
[5] Bień J., Rewiński S., *Artificial Intelligence in Bridge Management System*, Second Workshop on Bridge Engineering Research in Progress, Reno, Nevada, USA, 1990, pp. 159–162.
[6] Brito de J., Branco F., *Concrete Bridges Management Using Knowledge-Based Systems*, Proceedings of the Conference on Maintenance of Bridges and Civil Structures, Paris, Presses de l'Ecole Nationale des Ponts et Chaussees, Paris, 1994, pp. 383–392.
[7] Miyamoto A., Kushida M., Kinoshita K., *Concrete Bridge Rating Expert System with Machine Learning*, Colloquium of the International Association for Bridge and Structural Engineering "Knowledge Support Systems in Civil Engineering", Bergamo, IABSE, Zurich, Switzerland, 1995, Vol. 72, pp. 301–306.
[8] Yang H.-L., *Information/Knowledge Acquisition Methods for Decision Support Systems and Expert Systems*, Information Processing and Management, 1995, Vol. 31, No. 1, pp. 47–58.
[9] Furuta H., Frangopol D.M., Saito M., *Life-Cycle Cost Design of Deteriorating Bridges Using Genetic Algorithm*, ASCE Structures Congress, New Orleans, LA, USA, 1999, pp. 243–246.
[10] Turban E., *Decision Support and Expert Systems: Management Support Systems*, MacMillian, New York, 1993.
[11] Sugidate M., Ichikawa A., Koshiba A., Horiguchi T., *Development of a Bridge Maintenance Consulting System*, Symposium of the International Association for Bridge and Structural Engineering "Extending the Lifespan of Structures", San Francisco, California, USA, IABSE, Zurich, Switzerland, 1995, Vol. 73/1, pp. 413–418.
[12] Garrett J.H. et. al., *Design of Computer Support for Field Operations*, Symposium of the International Association for Bridge and Structural Engineering "Structures for the Future – The Search for Quality", Rio de Janeiro, Brazil, IABSE, Zurich, Switzerland, 1999, pp. 1000–1007.
[13] Bień J., *Modelling of Bridge Structures During Operation* (in Polish), Wrocław University of Technology, Wrocław, 2002.
[14] Bień J., *Expert Functions in Bridge Management Systems*, 8th International Bridge Management Conference, Denver, Colorado, USA, 1999, Transportation Research Circular, No. 498, June 2000, pp. H-3/1–15.
[15] Bień J., *Neural Networks in Bridge Management Systems*, Structures Congress of the American Society of Civil Engineers "Advanced Technology in Structural Engineering", Philadelphia, USA, 2000, pp. 1–8.
[16] Bień J., *Multi-Level Hybrid Networks in Bridge Management Systems*, World Multiconference on Systemics, Cybernetics and Informatics, Orlando, Florida, USA, 2001, Vol. II, Information Systems, pp. 316–321.
[17] Bień J., *Hybrid Networks in Bridge Condition Evaluation and Prediction*, First International Conference on Bridge Maintenance, Safety and Management, IABMAS, Barcelona, 2002, pp. 451–452 + CD.

[18] Bień J., *Computer Models of Bridge Degradation Process. Expert Function Creator* (in Polish), Wrocław University of Technology, Institute of Civil Engineering, Report SPR-85/98, Wrocław, 1998.
[19] Bień J., *SMOK – Integrated Railway Bridge Management System* (in Polish), Inżynieria i Budownictwo, 1996, No. 3, p. 180–184.
[20] Bień J., Kmita J., Rawa P., *Scientific and Technical Basis of the RBMS SMOK. Part V/9: Bridge Damage Catalogue* (in Polish), Wrocław University of Technology, Institute of Civil Engineering, Report SPR-93/98, Wrocław, 1998.

Hybrydowa reprezentacja wiedzy w systemach zarządzania mostami

Rozwój technologii komputerowych umożliwia stosowanie narzędzi ekspertowych wspomagających procesy decyzyjne w Systemach Zarządzania Mostami. Zaproponowane w niniejszym artykule narzędzia ekspertowe wykorzystują zarówno bazę danych, jak i bazę wiedzy systemu wspomagającego zarządzanie. Decyzje w procesie zarządzania infrastrukturą komunikacyjną są bardzo często podejmowane na podstawie kompozycji różnego rodzaju informacji: precyzyjnych, rozmytych, a także niepewnych. Wymaga to stosowania specyficznych technologii pozyskiwania informacji, ich reprezentacji oraz przetwarzania w systemie komputerowym wspomagającym zarządzanie. W artykule zaprezentowano technologię hybrydowej reprezentacji wiedzy łączącą symboliczną i niesymboliczną reprezentację wiedzy. Zaproponowana technologia wielopoziomowych sieci hybrydowych umożliwia integrację różnych technik reprezentacji wiedzy w jednym narzędziu komputerowym. W zależności od rodzaju rozwiązywanego problemu, a także od typu dostępnych informacji sieci hybrydowe mogą być tworzone z komponentów neuronowych, rozmytych, a także funkcyjnych.

ARCHIVES OF CIVIL AND MECHANICAL ENGINEERING

Vol. IV 2004 No. 1

Determination of the design model for simulating vibrations of steel beam bridges under moving trains

MONIKA PODWÓRNA
Wrocław University of Technology, Wybrzeże Wyspiańskiego 27, 50-370 Wrocław

The paper deals with single-track, single-span, simply supported steel railway bridges with two plate steel girders and a ballasted closed platform; they are called *steel beam bridges* for short. A simplified model, i.e. a design model, of the bridge–track–moving train system is constructed that simulates dynamic processes with the accuracy acceptable in practice. A physical non-linear high-performance planar model of the system reflecting its all main structural features and mechanical properties and simulating dynamic processes with high accuracy is applied as a comparative model. In a high-performance model, there are taken into account, among other things, the Timoshenko effects in the superstructure, physically nonlinear properties of the ballast layer and fasteners, vertical inertia forces of moving wheel sets, the first- and the second-stage suspensions of rail-vehicles. Six main simplifications of the high-performance model, creating the simplified models, are considered. Dynamic analysis of the bridge–track–moving train system, aimed at determining the design model, has been carried out for a series-of-types of steel beam bridges.

Keywords: *steel beam railway bridge, moving train, design model*

1. Introduction

One of the standard types of railway bridges is built out of single-track, single-span, simply supported structures, with the plate girders and a ballasted closed deck. Jointless railway track is placed on a breakstone bed. This type of bridges is simply called *steel beam bridges*.

The bridge–track–moving train system (BTT) has a fast-varying configuration and is subject to forced and parametric excitations [1]. A problem of physical and mathematical modelling of such systems is still valid as modern passenger trains are moving at speed up to 360 km/h [2]. In Poland, the travels at a service velocity as high as 160–250 km/h on some selected railway lines are planned.

The majority of papers on dynamics of BTT systems do not deal with relative flexibility of a rail-track, among others those by Matsuura [3] and Klasztorny and Langer [4]. Klasztorny [1] and Fryba [5] assumed a model of a track in the form of an Euler beam on a linear viscoelastic base. In recent papers, more complex superstructures of railway bridges are modelled as spatial bar structures using FEM [6–8].

A physical non-linear high-performance model (HPM) of the BTT system has been developed in [9]. All basic structural features as well as mechanical properties of the BTT system were taken into consideration. However, it is difficult to carry out dy-

namic analyses using the HPM model because of difficulties in evaluating the values of a few dozen parameters of the model and too long time of computations. Therefore, determination of a simplified model of the BTT system, which simulates dynamic processes with the accuracy acceptable in practice, seems to be valid. In this paper, such a model has been termed *the design model* (DM).

2. Quasi-exact modelling the bridge–track–moving train system

The experimental and theoretical investigations of single-track, single-span steel railway bridges prove that vibrations in the vertical plane that coincides with the track's axis are separated from lateral-torsional vibrations [1, 3, 5–8, 10]. Lateral-torsional vibrations (swings) are of a secondary importance and are excited, first of all, by snaking of wheel sets and random deviations of the system from ideal symmetry with respect to the longitudinal vertical plane. In these circumstances, planar modelling of the BTT system is acceptable. Moreover, vibrations of the system can be treated as geometrically linear (small displacements), and microroughness of rolling surfaces of the rails can be neglected.

A scheme of a planar model of the BTT system, reflecting all main structural features and mechanical properties, is presented in Figure 1. This model is termed *a high-performance planar model* (HPM) which enables simulation of dynamic processes with high accuracy. A simplified assumption has been made that the model takes into account the flexibility of the track over the bridge and in finite zones of access. This leads to distortion of the dynamic response of the system at the ends of the zones of access. If the zones are long enough, these distortions will not affect considerably dynamic response of the superstructure as damping of the ballast layer is very heavy.

There are 6 mass subsystems in the HPM model: a bridge superstructure, subsoil in the zones of access, sleepers on the bridge and in the access zones, rails on the bridge and in the access zones, moving wheel sets, sprung masses of rail-vehicles (bodies and truck frames).

A bridge superstructure is modelled as a sectionally-prismatic Timoshenko beam of linear viscoelastic properties. Subsoil in the zones of access is modelled as discrete set of linear viscoelastic oscillators which approximate a deformable pile under the ballast layer [1]. A real continuous layer of the ballast is substituted for a set of vertical, nonlinear, elastic-damping constraints. These constraints are located under sleepers. A one-sided type and initial compression of the constraints under the weight of sleepers, fasteners and rails are taken into account in the model of the ballast. The damping properties of the ballast are described as dry friction proportional to elastic interactions carried by the ballast. The ballast mass is included either in the superstructure mass or in the subsoil mass.

Prestressed concrete sleepers are reflected by a set of point masses vibrating vertically. Fasteners are modelled as physically nonlinear viscoelastic elements. Different stiffness with respect to compression and tension as well as initial compression of the

fasteners are taken into account. There is assumed that damping properties are viscous in character due to vibro-insulating pads, first of all. Rails are described by a prismatic Euler beam of linear viscoelastic properties.

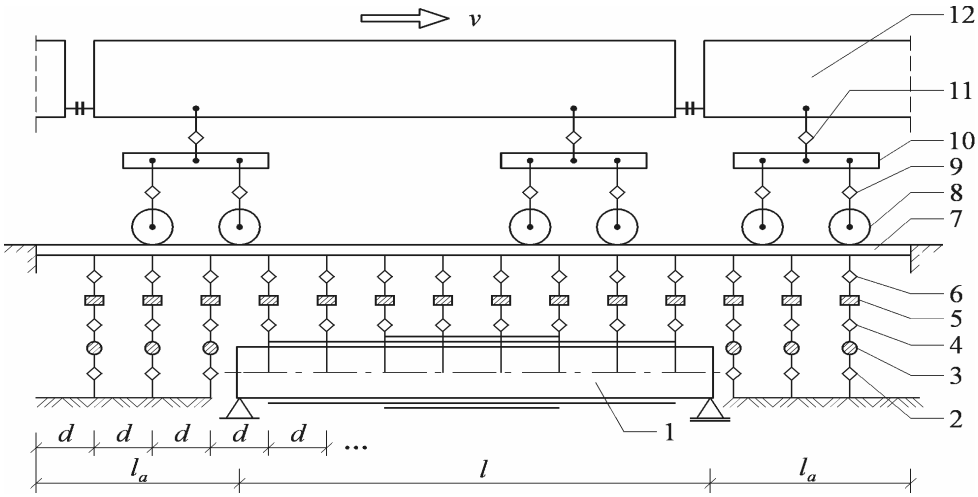

Fig. 1. A conceptual scheme of the planar physical model of the bridge–track–moving train system [9]: 1 – a bridge superstructure; 2, 3 – track subsoil in the zones of access (2 – concentrated linear viscoelastic elements; 3 – concentrated masses); 4 – ballast; 5 – sleepers; 6 – fasteners; 7 – rails; 8 – wheel sets of rail-vehicles; 9 – first-stage suspensions; 10 – bogie frames with track engines; 11 – second-stage suspensions; 12 – bodies of rail-vehicles

Only conventional passenger trains are taken into consideration. Each rail-vehicle has two independent double-axle trucks. A vehicle model is assumed as in [1, 3]; it consists of four unsprung point masses reflecting wheel sets, two rigid mass disks reflecting bogie frames with track engines and a rigid mass reflecting the body of the vehicle model. Four first-stage suspensions and two second-stage suspensions exist in the vehicle. Each suspension is shown as a discrete vertical linear viscoelastic constraint. Sprung masses of the vehicle are stiffly guided in the horizontal direction coinciding with the track axis.

A Timoshenko beam modelling the bridge superstructure is discretised mathematically using a finite beam element with 8 degrees-of-freedom (DOF). This element is not affected by a shear-locking effect [11]. Generalised coordinates of the beam have been assumed to satisfy all kinematical and kinetic boundary conditions.

A rail beam has been discretised with 6 DOF finite beam elements [11]. These elements protect continuity of the acceleration following positions of moving wheel sets as well as zero curvatures at the ends of the beam. Dynamic pressure of moving wheel sets on the track is then continuous as in reality.

Nodal points of the superstructure and the rails coincide with sleepers' positions. This makes calculating the interactions carried by the ballast and fasteners easier.

Moreover, this allows us to calculate deflections and normal stresses in the superstructure with good accuracy.

A method for deriving equations of motion of the BTT system partly in an implicit form has been applied [1]. In this method, each subsystem is loaded with interactions carried by ballast, fasteners and vehicles' suspensions. The only exception are wheel sets treated as moving unsprung masses without their own DOFs. These masses generate vertical inertia forces inserted in an explicit form into the rail equations of motion. Matrix equations of dynamic equilibrium of the subsystems of the BTT system are obtained using Lagrange's equations of the second kind, applied separately in each subsystem. Finally one obtains five matrix equations of motion partly in an implicit form, i.e.

$$\begin{aligned}
&\mathbf{B}_b\ddot{\mathbf{q}}_b + \kappa\mathbf{K}_b\dot{\mathbf{q}}_b + \mathbf{K}_b\mathbf{q}_b = \mathbf{F}_b,\\
&\mathbf{B}_a\ddot{\mathbf{q}}_a + \kappa_a\mathbf{K}_a\dot{\mathbf{q}}_a + \mathbf{K}_a\mathbf{q}_a = \mathbf{F}_a,\\
&\mathbf{B}_s\ddot{\mathbf{q}}_s = \mathbf{F}_s,\\
&(\mathbf{B}_r + \widetilde{\mathbf{B}}_r)\ddot{\mathbf{q}}_r + (\kappa\mathbf{K}_r + \widetilde{\mathbf{C}}_r)\dot{\mathbf{q}}_r + (\mathbf{K}_r + \widetilde{\mathbf{K}}_r)\mathbf{q}_r = \mathbf{F}_r,\\
&\mathbf{B}_o\ddot{\mathbf{q}}_o = \mathbf{F}_o,
\end{aligned} \tag{1}$$

where:

a dot describes a regular derivative with respect to time variable,

$\mathbf{B}_b$, $\mathbf{K}_b$ – mass and stiffness matrices for a bridge superstructure,

$\mathbf{B}_a$, $\mathbf{K}_a$ – mass and stiffness matrices for subsoil in the zones of access,

$\mathbf{B}_s$ – mass matrix for sleepers of the bridge and in the zones of access,

$\mathbf{B}_r$, $\mathbf{K}_r$ – mass and stiffness matrices for rails on the bridge and in the zones of acess,

$\mathbf{B}_o$ – mass matrix for sprung masses of rail vehicle series,

$\widetilde{\mathbf{B}}_r$, $\widetilde{\mathbf{C}}_r$, $\widetilde{\mathbf{K}}_r$ – matrices varying in time, resulting from vertical inertia forces of wheel sets being in complex motion,

$\mathbf{q}_b$, $\mathbf{q}_a$, $\mathbf{q}_s$, $\mathbf{q}_r$, $\mathbf{q}_o$ – subvectors of generalised coordinates describing vibrations of the subsystems of the BTT system, respectively,

$\mathbf{F}_b$, $\mathbf{F}_a$, $\mathbf{F}_s$, $\mathbf{F}_r$, $\mathbf{F}_o$ – subvectors of generalised loads dependent on interactions related to the subsystems of the BTT system,

κ – time of retardation for steel,

κ_a – time of retardation for subsoil in the deformable zones of access.

Couplings and nonlinear influences are hidden in the generalised load vectors.

A full description of complex non-linear mathematical modelling of the BTT system is presented in ref. [9]. There is shown a full mathematical description of finite beam elements, calculations of non-linear interactions carried by constraints modelling ballast and fasteners, calculations of linear interactions carried by rail-vehicles' suspensions, calculations of vertical inertia forces of wheel sets being in complex motion, calculations of subvectors of generalised loads for mass subsystems having their own DOFs.

Equations (1) describe physically non-linear and geometrically linear vibrations, transient and quasi-steady state of the BTT system. Quasi-steady state vibrations occur for a train consisting of several repeatable driving or wagon units. A recurrent – iterative algorithm for numerical integration of these equations, using Newmark's average acceleration method, has been developed [9].

3. A definition of the design model and a conception of its determination

In this study, dynamic and quasi-static responses in the design model (DM) coincide, by definition, qualitatively and quantitatively with respective responses in the high-performance model (HPM), with accuracy acceptable in practice. The qualitative and quantitative compatibility relates to time histories of displacements and normal stresses in the bottom fibres of the bridge superstructure. The solutions coincide if relative errors are less than 1.5%.

A conception of determining the design model is as follows. The HPM model is treated as a comparative model. A set of simplified models is created. The solutions for simplified models are compared with respective solutions for the HPM model. The DM model is in the set of simplified models. In this study, the following simplifications are made:

U1 – neglecting the sub-grade deformability,

U2 – assuming linear viscoelastic constraints that model both fasteners and ballast,

U3 – neglecting deformability of fasteners and assuming linear viscoelastic constraints modelling ballast,

U4 – neglecting deformability of fasteners, neglecting deformability of ballast in the zones of access, assuming linear viscoelastic constraints modelling ballast on the bridge,

U5 – neglecting Timoshenko's effects (shear deformability and rotational inertia) in the bridge superstructure,

U6 – neglecting vertical inertia forces of moving wheel sets.

The simplified models were built as combinations of the above-mentioned simplifications. The models are coded by means of the combination of 6 digits (0 – a simplification is not taken into account; 1 – a simplification is taken into account). For example, a code of 000000 describes the HPM model, a code of 111000 – the model with U1, U2, U3 simplifications.

Dynamic analysis, whose aim being determination of the model design, was performed for a series of types of steel beam bridges. In this way, one can derive a design model for a selected type of bridges.

Dynamic analysis for a series of types of steel beam bridges is also presented in ref. [12]. The analysis was aimed at classic dynamic coefficient of displacements and normal stresses versus service velocity of a train. The 100011 model was used, partly applying the vibration theory developed in ref. [9].

4. A series of types of steel beam bridges

Dynamic analysis of the BTT systems, aimed at determining the DM model, has been carried out for a series of types of steel beam bridges designed by Machelski [13], according to all requirements of Polish Standards [14, 15]. In this study, the static calculations given in [13] are improved.

The main dimensions of a cross-section at the midspan of the SB15 (l = 15 m) bridge are shown in Figure 2. The following parameters of the cross-section depend on a span length: a height of the main beam, dimensions of the cover plates and a distance between the main beams. The parameters data describing a series of types of steel beam bridges is listed in Table 1 (l – the span length, m – the bridge mass per unit length at the midspan (without sleepers and rails, J – the moment of inertia of a cross-section with respect to the central horizontal axis).

Table 1. Values of the basic parameters of the bridges

Bridge code	SB15	SB18	SB21	SB24	SB27	SB30
l [m]	15.00	18.00	21.00	24.00	27.00	30.00
M [kg/m]	4820	5380	5970	6580	6620	6720
J [m^4]	0.04452	0.06812	0.09840	0.14439	0.19770	0.27356

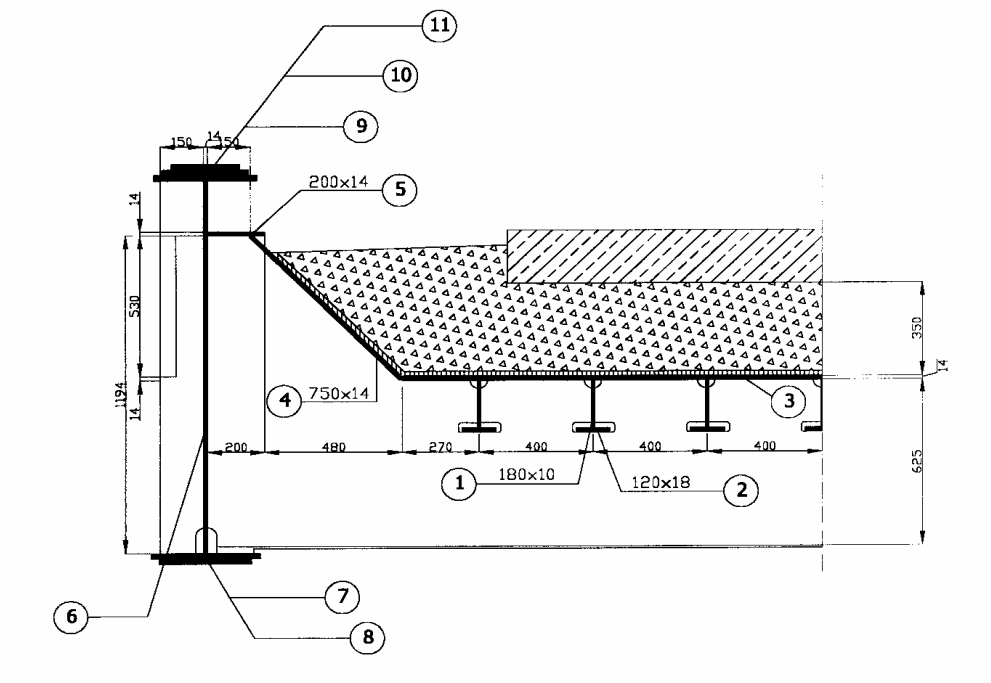

Fig. 2. A cross-section at the midspan of SB 15 bridge [13]

5. Determination of the design model

Discretisation of the BTT system according to FEM in some cases gives 652 DOFs, in total. The algorithm has been programmed in PASCAL. A method for deriving equations of motion partly in an implicit form yields strip matrices of the width of 7, 11 or 15, and also diagonal matrices. This results in shortening 2–3 times the time of computations.

Simulations of dynamic processes of the BTT system have been carried out for a stabilised track in a summer period. The track contains S60 rails, SB3 fasteners and PS94 concrete sleepers. Average values of the physical parameters of the track, describing a nonlinear model assumed in this study, were estimated based on a number of references [1, 5, 6, 16, 17, 18]. They are given as follows:

$$m_r = 130\,\text{kg/m},\quad I_r = 6110\,\text{cm}^4,\quad m_s = 294\,\text{kg},$$
$$k_c = 120\ \text{MN/m},\quad k_t = 32.5\ \text{MN/m},\quad c_f = 16\ \text{kNs/m},$$
$$k_b = 165\ \text{MN/m},\quad \mu = 0.36,\ m_{ba} = 3150\ \text{kg/m},\ c_b = 50\ \text{kNs/m},$$
$$E_a = 150\ \text{MN/m}^2,\ b_a = 4\ \text{m},\ h_a = 1\ \text{m},\ \rho_a = 1750\ \text{kg/m}^3,\ \kappa_a = 0.002\ \text{s},$$

where:

m_r – the mass per unit length of a pair of rails, including weight of fasteners,

I_r – the moment of inertia of a cross-section of a pair of rails, with respect to the horizontal central axis,

m_s – the weight of a sleeper,

k_c – the stiffness with respect to compression of fasteners per one sleeper,

k_t – the stiffness with respect to tension of fasteners per one sleeper,

c_f – the viscous damping coefficient of fasteners per one sleeper,

k_b – the stiffness with respect to compression of ballast per one sleeper,

μ – the dry friction coefficient of ballast,

m_{ba} – the ballast mass per unit length in the zones of access,

c_b – the viscous damping coefficient of subsoil of the length d,

E_a – the Young's modulus of subsoil,

b_a – the width of deformable pile of subsoil,

h_a – the height of deformable pile of subsoil,

ρ_a – the mass density of subsoil,

κ_a – the retardation time for subsoil.

The rules for selecting the values of numerical parameters ε , h, λ are presented in ref. [9], where: h [s] – the integration step, λ [m/s] – the smoothing parameter of a dry friction characteristic of ballast, ε [N] – the parameter of accuracy in an iteration loop.

A Shinkansen superexpress passenger train, whose mass, stiffness and damping parameters of a repeatable vehicle being collected in [1, 3], runs across the bridges. The train consists of 8 repeatable power units.

Numerical analysis has been performed based on dynamic time-histories of the bridge superstructure's deflections at the midspan and at ¼ of the span and based on dynamic time-histories of the bridge superstructure's bottom normal stresses at the same cross-sections. The numerical results showing the influence of the simplifications on the extreme values of the displacements and stresses are listed in Table 2. These values correspond to forced resonance velocities of a train for individual bridges [12], provided that the train consists of four repeatable vehicles.

Neglecting the subgrade deformability (100000) lead to an insignificant increase in the maximum displacements (up to 0.10%) and in stresses (up to 0.29%) in comparison to the HPM model. This is associated, first of all, with neglecting the energy dissipation in the subsoil.

Neglecting the subgrade deformability and assuming linear viscoelastic constraints modelling fasteners and ballast (110000) lead also to insignificant increase in the maximum displacements (up to 0.16%) and in stresses (up to 0.22%) in comparison to the HPM model.

Making the U1 and U2 simplifications and neglecting deformability of fasteners (111000) we increase the maximum displacements up to 1.23% and the stresses – up to 1.30% in comparison to the HPM model.

Neglecting the above features as well as deformability of the ballast in the zones of access (111100) leads to significant differences in the maximum displacements (up to 2.82%) and in stresses (up to 3.90%) in comparison to the HPM model.

There was analysed the dynamic response of the main girders related to the access zones of the length ranging from 0.30 to 12.30 m. Shortening the access zones from 12.3 m to 6.3 m yields the differences in the maximum displacements and stresses up to 0.87%. Shortening the access zones from 12.3 m to 3.3 m results in the differences in the maximum displacements and stresses up to 0.19%. These results prove that the access zones of 12.3 m length are acceptable in the problem undertaken.

The Timoshenko effects (000010) should be taken into account in the design model because of valuable differences, both qualitative and quantitative, in comparison to the HPM model. Deviations in the maximum values of displacements and stresses reach 2.70% and 5.63%, respectively.

Neglecting vertical inertia forces of moving wheel sets (000001) may lead to significant qualitative and quantitative differences in comparison to the HPM model. Deviations in the maximum values of displacements and stresses reach 15.68% and 17.90%, respectively.

Table 2 shows that the U1, U2, U3 simplifications are acceptable in the BTT system (provided that subgrade deformability, non-linearity of constraints modelling ballast, and deformability of fasteners are neglected). The DM model has then the code 111000.

Table 2. The influence of simplifications on the maximum values of deflections and bottom normal stresses in a series of types of steel beam bridges

Bridge code	SB15	SB18	SB21	SB24	SB30	max
v [km/h]	270	250	270	240	280	
model 100000						
$\Delta w\,(0.5l,t)$ [%]	0.10	0.02	0.01	0.01	0.01	0.10
$\Delta\sigma\,(0.5l,t)$ [%]	0.29	0.03	0.00	0.01	0.04	0.29
model 110000						
$\Delta w\,(0.5l,t)$ [%]	0.16	0.07	0.04	0.01	0.03	0.16
$\Delta\sigma\,(0.5l,t)$ [%]	0.22	0.10	0.08	0.08	0.10	0.22
model 111000						
$\Delta w\,(0.5l,t)$ [%]	1.23	0.11	0.11	0.24	0.05	1.23
$\Delta\sigma\,(0.5l,t)$ [%]	1.30	1.05	0.26	0.26	0.10	1.30
model 111100						
$\Delta w\,(0.5l,t)$ [%]	2.82	0.38	0.20	0.80	0.21	**2.82**
$\Delta\sigma\,(0.5l,t)$ [%]	3.90	2.74	0.42	1.17	0.22	**3.90**
model 000010						
$\Delta w\,(0.5l,t)$ [%]	2.70	1.07	0.16	0.39	1.46	**2.70**
$\Delta\sigma\,(0.5l,t)$ [%]	5.63	1.41	0.98	1.02	2.58	**5.63**
model 000001						
$\Delta w\,(0.5l,t)$ [%]	15.68	5.02	0.73	0.43	1.07	**15.68**
$\Delta\sigma\,0.5l,t)$ [%]	17.90	4.30	1.56	1.41	2.41	**17.90**

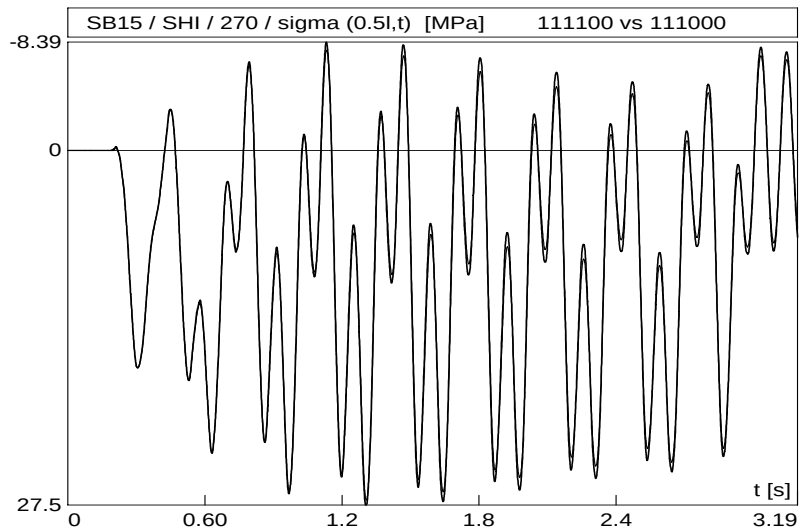

Fig. 3. The dynamic time-history of bottom normal stresses at the midspan of the main girders of the SB 15 bridge. Load: Shinkansen train, 8 repeatable vehicles, v = 270 km/h. The effect of deformability and damping of the ballast in the zones of access

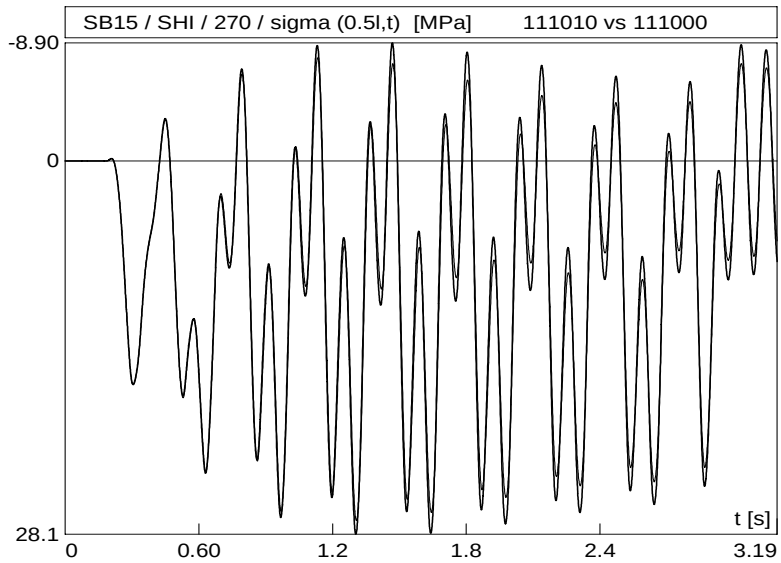

Fig. 4. The dynamic time-history of bottom normal stresses at the midspan of the main girders of the SB 15 bridge. Load: Shinkansen train, 8 repeatable vehicles, v = 270 km/h. The effect of shear deformability and rotational inertia of the bridge superstructure

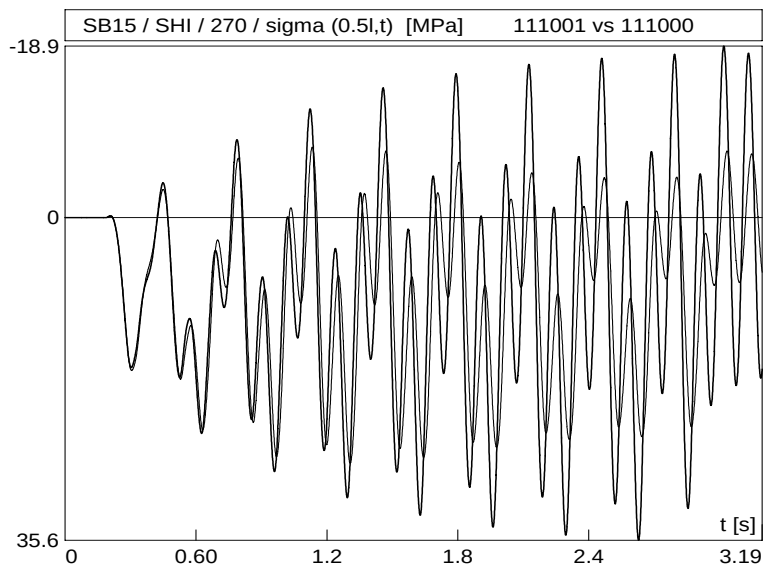

Fig. 5. The dynamic time-history of bottom normal stresses at the midspan of the main girders of the SB 15 bridge. Load: Shinkansen train, 8 repeatable vehicles, v = 270 km/h. The effect of vertical inertial forces of moving wheel sets

The influence of the U4, U5, U6 simplifications on normal stresses in the bottom fibres of main girders of the SB15 bridge is illustrated in Figures 3–5. Figure 3 illustrates the influence of subsoil deformability in the access zones. A heavy curve represents the approximate solution for the 111100 model, while a light curve – the solutions for the design model (111000). Figure 4 shows the Timoshenko effects in bridge superstructure. A heavy curve represents the approximate solution for the 111010 model, whereas a light curve – the solutions for the design model (111000). Figure 5 presents the effects of the inertia forces of wheel sets. A heavy curve represents the approximate solution for the 111001 model, and a light curve – the solutions for the design model (111000). Solutions for the DM model coincide practically with the solutions for the HPM model (000000).

6. Conclusions

In dynamic analysis of steel-beam bridges under high-speed trains, one should take into account:

- vertical inertia forces of wheel sets of moving vehicles,
- shear deformations of a bridge superstructure,
- track deformability in the zones of access and on the bridge.

On the other hand, one can neglect:

- deformability of subsoil,
- non-linear features of ballast,
- deformability of fasteners.

The design model, i.e. a model with simplifications acceptable in practice, seems to be linear. Due to dynamic analyses carried out with the DM model it was possible to shorten the calculation time 2–3 times. Using a PC with Pentium IV processor and 700 MHz clock we are able to arrive at an average computation time of 1.3 hour.

The results presented in this study have to be validated by respective experiments, before applying them in engineering practice.

The design model is useful for evaluating the displacement and stress states of the bridge superstructure. However, some dynamic problems such as track stability require simulations run on a non-linear HPM model.

Acknowledgements

This paper has been supported by the State Committee for Scientific Research, Poland, under Grant No. 8 T07E 024 20, coordinated by Professor M. Klasztorny, Warsaw University of Technology.

References

[1] Klasztorny M., *Vibrations of single-track railway bridges caused by trains moving at high speeds* (in Polish), Wydawnictwo Politechniki Wrocławskiej, Wrocław, 1987.

[2] Niemierko A.: *Some design and performance problems related to behaviour of bridge structures on high speed railway lines*, Arch. Civil Eng., 1996, Vol. 42, No. 4, 401–423.
[3] Matsuura A., *Dynamic behaviour of bridge girder for high speed railway bridge,* RTRI Quarterly Reports, 1979, Vol. 20, No. 2.
[4] Klasztorny M., Langer J.: *Dynamic response of single-span beam bridges to series of moving loads*, Earthquake Eng. & Struct. Dynamics, 1990, Vol. 19, No. 8, 1107–1124.
[5] Fryba L.: *Dynamics of railway bridges*, Academia, Praha, 1996.
[6] Clark G. et al., *Bridge No 9 at Brotherton*, Report TM CES 142, British Rail Research, 1990.
[7] ERRI D 181/DT 329, *Lateral forces on railway bridges. Parametric study*, Utrecht, 1995.
[8] Niemierko A.: *Theoretical and experimental analysis of the railway bridge with an orthotropic deck* (in Polish), Research Institute of Roads and Bridges Works, 1987, No. 1–2, 120–186.
[9] Klasztorny M., Podwórna M.: *New computational algorithms in dynamics of bridge–track–moving train system*, CD Proceed. 2nd Europ. Conf. on Computational Mechanics ECCM-2001, Minisymp. 28, Cracow, 2001, paper 110, pp. 1–20.
[10] Klasztorny M.: *Spatial vibrations of a multi-span railway steel bridge under a train moving at high speed*, Arch. Civil Eng., 2000, Vol. 46, No. 2, 287–311.
[11] Klasztorny M.: *Finite beam elements of Euler and Timoshenko type* (in Polish), Computer Methods in Civil Eng., 1992, Vol. 2 7–32.
[12] Klasztorny M., Myślecki K., Machelski Cz., Podwórna M.: *Dynamic analysis of a series-of-types of steel beam bridges loaded with fast train* (in Polish), Proc. 48th Conference of Polish Academy of Sciences, 2002, Vol. 1, pp. 85–92, Krynica.
[13] Machelski Cz.: *A series-of-types of steel railway bridges*, Report SPR No. 135/01, Inst. of Civil Eng., Wrocław Univ. Technol., Wrocław, 2001.
[14] Polish Standards, 1982. PN-82/S-10050. *Bridges. Steel structures. Design.*
[15] Polish Standards, 1985. PN-85/S-10030. *Bridges. Loads.*
[16] Ahlbeck D.R. et al.: *The development of analytical models for railroad track mechanics*, Proc. Symp. on Railroad Track Mechanics, 1975, 239–263.
[17] Dukkipati R.V., Amyot J.R.: *Computer aided simulation in railway dynamics*, Series: Mechanical Engineering, Marcel Dekker, Inc., New York–Basel, 1988.
[18] Esveld C.: *Modern railway track*, Esveld Press, Germany, 1989.

Wyznaczenie modelu projektowego do symulacji drgań belkowych mostów stalowych obciążonych przejeżdżającymi pociągami

W artykule rozpatruje się jednotorowe, jednoprzęsłowe, swobodnie podparte stalowe belkowe mosty kolejowe z dwoma pełnościennymi dźwigarami głównymi i balastowanym pomostem zamkniętym. Celem pracy jest wyznaczenie tzw. modelu projektowego układu most–tor–pociąg ruchomy, tj. modelu z uproszczeniami dopuszczalnymi z inżynierskiego punktu widzenia. Jako model porównawczy przyjęto tzw. model quasi-ścisły, odwzorowujący wszystkie główne cechy i właściwości mechaniczne układu oraz symulujący z dużą dokładnością drgania układu w płaszczyźnie pionowej. Model quasi-ścisły uwzględnia m.in. efekty Timoshenki w konstrukcji nośnej, fizycznie nieliniowe właściwości podsypki i przytwierdzeń szyn do podkładów, pionowe siły bezwładności ruchomych zestawów kołowych, zawieszenia pierwszego

i drugiego stopnia pojazdów szynowych. Rozpatrzono 6 głównych uproszczeń modelu quasi-ścisłego, które tworzą modele uproszczone. Analizę dynamiczną układu most–tor–pociąg ruchomy, ukierunkowaną na wyznaczenie modelu projektowego, wykonano na typoszeregu belkowych mostów stalowych.

ARCHIVES OF CIVIL AND MECHANICAL ENGINEERING

Vol. IV 2004 No. 1

Internal forces due to live loads in a bridge structure comprising a steel space frame and a concrete slab

CZESŁAW MACHELSKI, WOJCIECH ZIELICHOWSKI-HABER
Wrocław University of Technology, Wybrzeże Wyspiańskiego 27, 50-370 Wrocław

The possibility of using two models of geometry in the analysis of bridges consisting of a tubular frame combined with a concrete slab is presented. The first model is derived from the orthotropic plate theory and the second one is a discrete model including beam elements (the structure) and shell elements (the slab). This makes it possible to adopt some easy to model flat two-dimensional elements. Also, the use of the Guyon–Massonnet distribution method is possible, if preliminary dimensions of structural elements are chosen. The concept of evaluation of torsional stiffness for equivalent orthotropic plate is developed. The algorithms for determining the influence of the surface of internal forces and normal stresses in structural members in the case of discrete model are given, which is necessary for a detailed static analysis. The algorithm based on kinematic method is essential for the use of standard FEM software. The practical use of the algorithms proposed is shown by numerical examples.

Keywords: *internal forces, bridge structures, composite structures, steel space frame*

1. Bridge profile and configuration

A steel tubular grid space frame has been usually used for masts, towers, long-span roofs and offshore structures. In recent years, the steel tubes have been more commonly used also in bridge engineering. The composite structures combining steel tubular space frame with a concrete slab experience their renaissance nowadays. As a result of the composite action, the structure maximizes the advantages of strength characteristics of both materials. Concrete used to form the deck slab, i.e. the top plane of bridge, is subjected to compression and to the largest fatigue loading. Steel used in the middle and bottom planes of bridge is exposed to the greatest tension. The combination of both components aims at optimizing the structural performance of concrete deck acting along with a steel frame so as to obtain the effect that surpasses that offered by the traditional bridge system and best meets the contemporary requirements (Figure 1).

The steel space frame is very effective construction solution that is suitable for highway and railway bridges, arch bridges and for the deck system of cable-stayed and suspension bridges [1]. One can regulate the stiffness of the cross-section of bridge by applying various diameters of tubes and by affecting geometric configuration of grid and concentration of elements on the length and width of bridge section, adjusting it to needs and requirements. The construction can be also adjusted to a variety of static schemes which allows us to achieve a particular architectural shape. The high tor-

sional and transverse stiffness and great resistance to distortion during the various stages of erection renders it suitable for aerodynamic and stability-sensitive cable-supported bridges and for broad range of curved in plan and skew bridges.

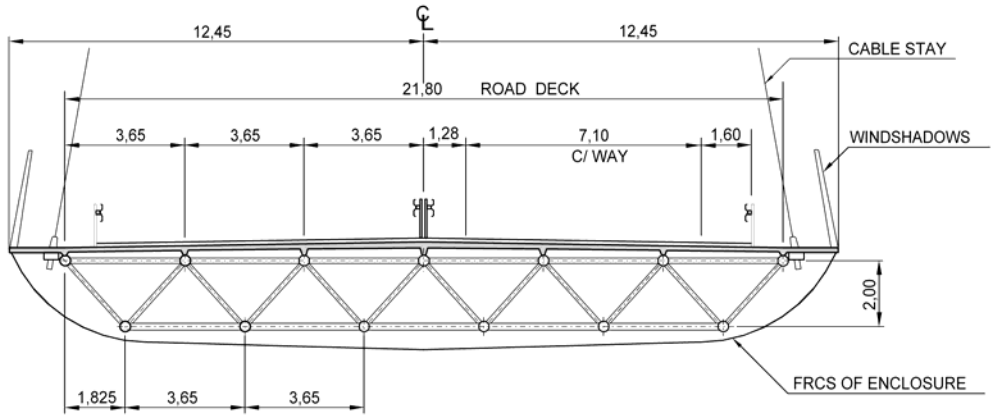

Fig. 1. Examplary cable-stayed bridge application (taken from [1])

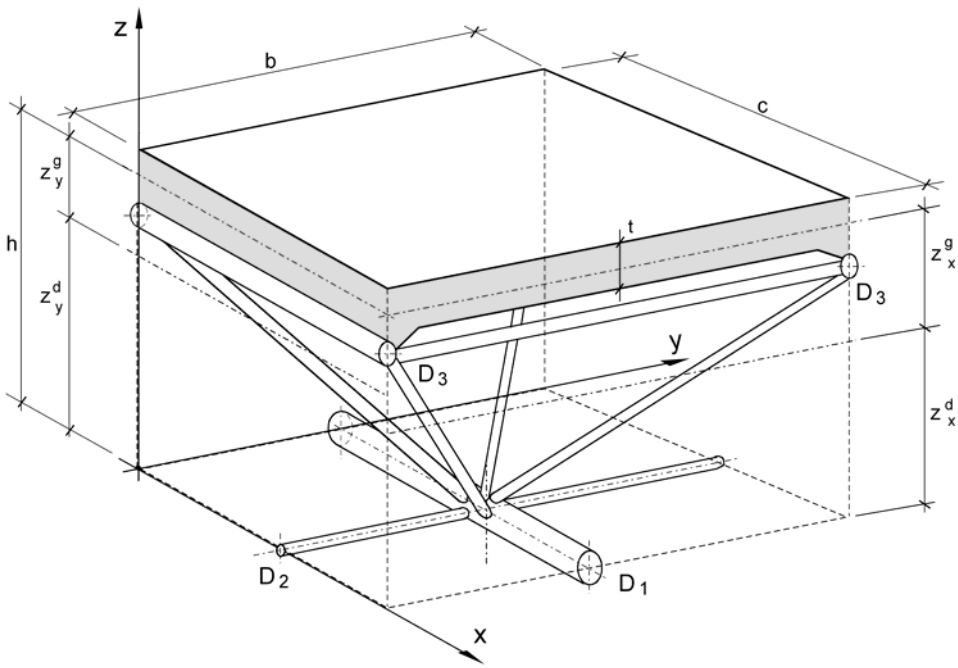

Fig. 2. Section of the part of the span

The space frame is constructed from steel tubular members with the use of cast or welded steel nodes. The members are cut, profiled and bevelled by automatic machines [2]. All joints are made as circumferential butt welds in semi-automatic high-quality welding processes. The cast steel nodes characterized by considerable fatigue strength are usually used in bearing area and in high-stress concentration nodes where the danger of negative effect of fatigue exists. The other braces of chord joints are very complicated due to geometry configuration (three-dimensional KK pattern, Figure 2) and require computer precision to perform cutting and welding. The concrete slab is connected with the top-plane longitudinal primary members by shear connectors. Furthermore it can be connected with the top-plane transverse secondary members in the case of wide deck. Whenever it is required, the system of post-tensioning cables may be used to prestress the concrete slab over intermediate supports in continuous construction to eliminate tensile stresses. The external cables, easy to reach and accessible for inspection, can be also successfully applied.

2. Influence surface for axial forces

The steel space frame combined with the concrete slab can be modelled by means of one-dimensional beam elements (the steel space frame members) and two-dimensional shell elements (the concrete slab) which in the case of the construction described is considered to be utterly correct model to carry out static analysis. To ensure the compatibility of rotational and linear displacements all elements are connected to each other rigidly. The joints can be modelled as well taking into consideration local distortion which means that the incompatibility of rotational displacement is assumed [3].

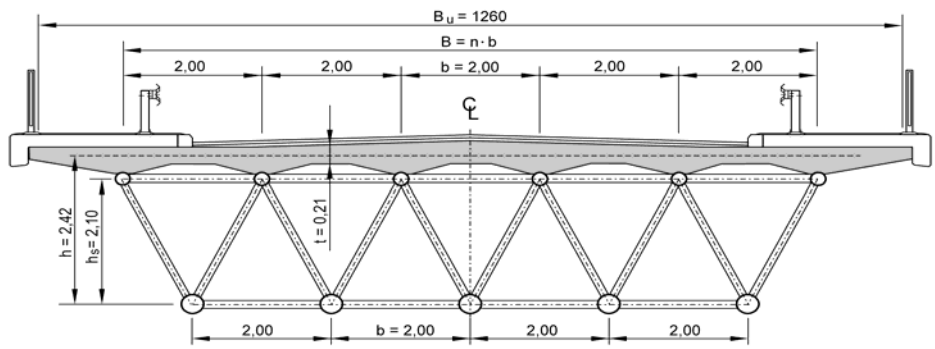

Fig. 3. Cross-section of bridge to be analyzed

A general rule governing this kind of structures proves that the crucial static effort is that of steel members. The concrete slab in such a combination takes concentrated loads from vehicles and braces the structure, especially when subjected to horizontal

loads. Usually, the concrete deck is not used fully if its ultimate load capacity is taken into account. For that reason, in the paper only the issue of internal forces in the space frame is addressed. The cross-section of bridge to be analyzed is shown in Figure 3. The specificity of behaviour of structure due to moving load (live load) is studied with the help of the concept of influence surface for internal forces. Owing to the position of moving load on the deck and bars intersecting at nodes, the characteristic internal forces for that type of construction are the axial ones. Thus, the influence surface $\xi(x,y)$ determines the axial force N in a selected element in space frame, depending on the position of the external force $P(x_p,y_p)$ acting vertically to the surface of slab

$$N = P \cdot \xi(x_p, y_p). \tag{1}$$

An effective numerical algorithm for the influence surfaces is the kinematic method explained in [4, 5]. The substitute load for the member of structure under consideration is then an imposed kinematic displacement, which results in the deflection surface of the bridge deck. The displacement perpendicular to the plane of slab can be considered as the influence surface of axial load $\xi(x,y)$, as in (1).

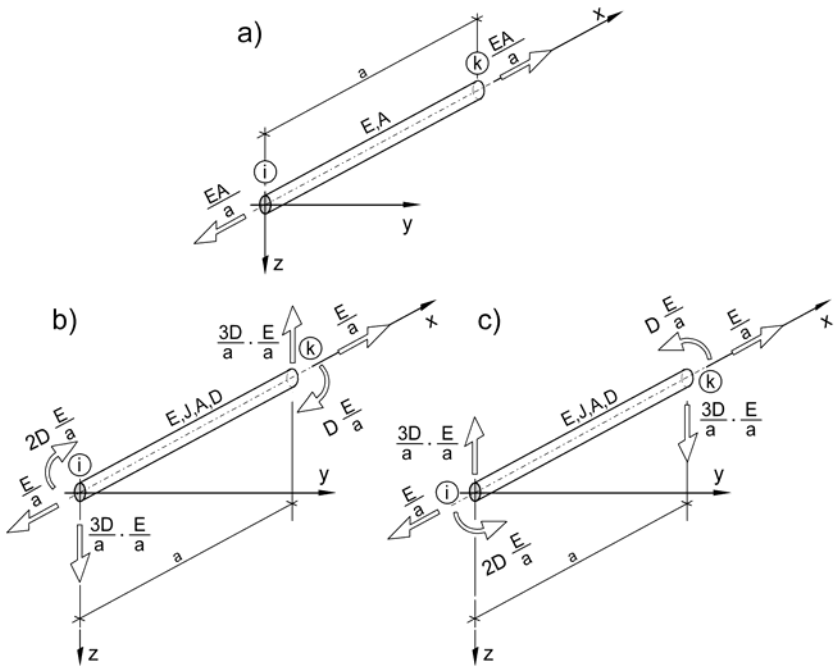

Fig. 4. Node loading of the imposed kinematic displacement for influence surface at internal forces and normal stresses

The imposed kinematic displacement for axial force in the bar fixed at the nodes *i, k* is in equilibrium with two coaxial forces, as shown in Figure 4a, which yields

$$N_i = N_k = \left(\frac{EA}{a}\right)_{ik}, \tag{2}$$

where EA is the axial stiffness of a bar of the length a.

It is assumed that those forces cause the bar to elongate by unit value. The second kind of the imposed kinematic displacement as effective as the first one is in the form of the linear change of temperature Δt of this bar, which can be calculated using the formula

$$1 = \left(\frac{N \cdot a}{EA}\right)_{ik} = (\alpha \cdot \Delta t) a_{ik} \tag{3}$$

and which takes the following form

$$\alpha \cdot \Delta t = \frac{1}{a_{ik}}, \tag{4}$$

where a is the coefficient of thermal expansion. It enables us to apply the imposed kinematic displacement in each single member of structure.

For bridges of a regular shape (in plan), the influence surface can take three characteristic forms. They are shown as contour plans in Figure 5. The plans were obtained from the analysis of the simply-supported, single-span bridge of the length L=35.20 m and of such construction dimensions as t = 0.21 m, b = 2.00 m, h = 2.10 m shown in Figure 3, and concern the bottom-plane longitudinal bar members, the bottom-plane transverse bar members and diagonal braces (n = 10 and $B_u = B$ = 20 m). The centers of the bars under consideration have the following coordinates:

- longitudinal bar, x = 5.40 m and y = 10.00 m;
- transversal bar, x = 16.50 m and y = 12.00 m;
- cross brace, x = 5.50 m and y = 16.50 m.

In Figure 5, the axis system has its origin in the bottom left-hand corner. Directions in Figure 5 are as follows: the horizontal x-axis parallel to the length L of span, the y-axis is perpendicular to the first one (vertical in Figure 5).

The influence surfaces for axial forces given in Figure 5a, b are very similar to the influence surfaces for the bending moment of longitudinal and transverse girders in the multibeam bridges. The influence surfaces for axial force in diagonal braces, see in Figure 5c, express the nature of local behaviour of that member.

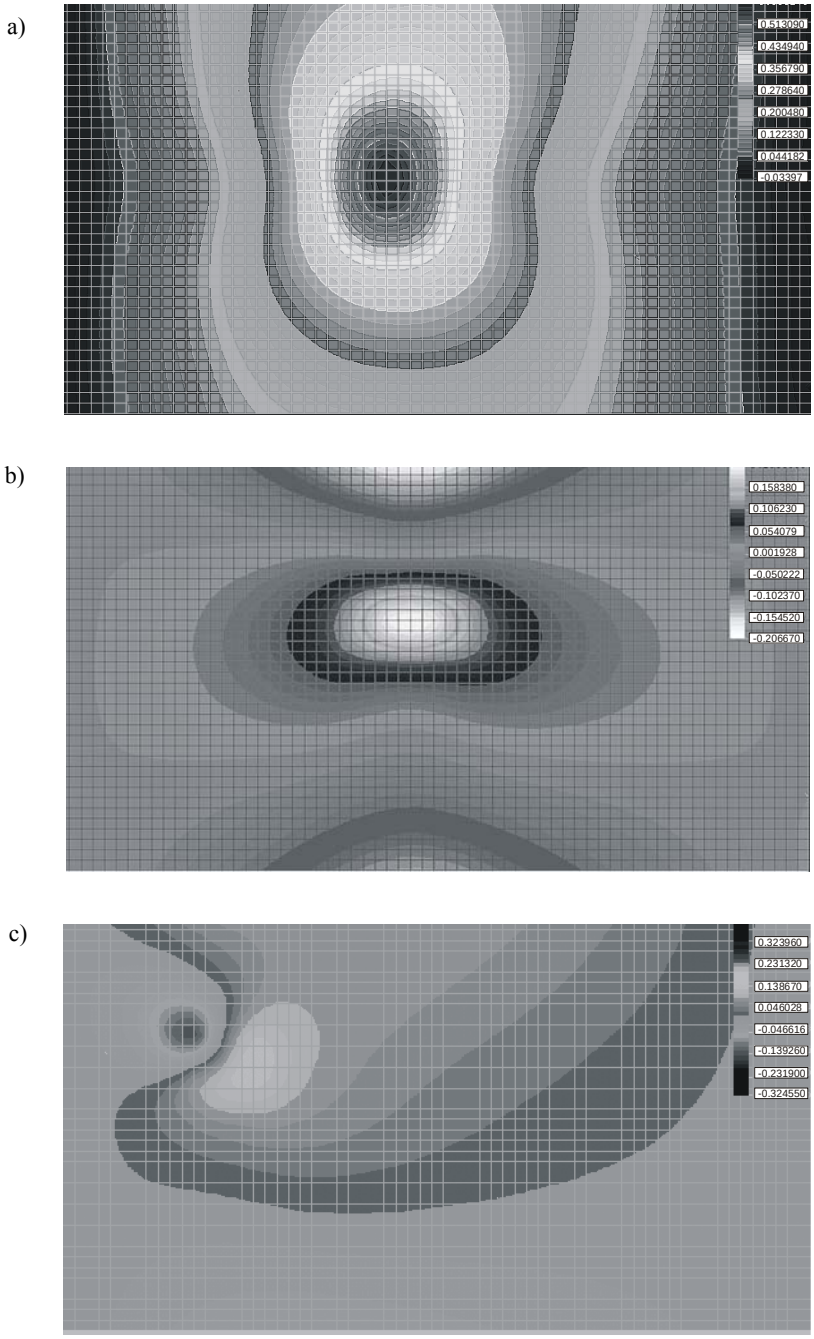

Fig. 5. Influence surface for axial forces in the members of the space frame for single-span bridge: a) bottom-plane longitudinal bar, b) bottom-plane transverse bar, c) diagonal bar

3. Influence surface for normal stresses

At the structure nodes, besides the axial forces there occur the bending moments, which are highly significant to normal stresses. In order to estimate the effort of the bar cross-section, it is essential to take into consideration simultaneously the axial forces N and the bending moments M, which are included in the following equations

$$\sigma_{\min} = \left(\frac{N}{A} - \frac{M}{I} \cdot \frac{D}{2} \right)_{ik} \tag{5}$$

and

$$\sigma_{\max} = \left(\frac{N}{A} + \frac{M}{I} \cdot \frac{D}{2} \right)_{ik}, \tag{6}$$

where: A – the area and I – the moment of inertia are the geometric characteristics of the cross-section of a tube, and D is its diameter.

The imposed kinematic displacement method for the normal stresses $s_{\min}$ and $s_{\max}$ can be formulated in terms of equivalent loads given in Figure 4b, c. The boundary forces take the following values:

- For the node i one can obtain

$$M_i = 4\frac{EI}{a} \cdot \frac{D}{2I} = 2D\frac{E}{a},$$

$$V_i = 6\frac{EI}{a^2} \cdot \frac{D}{2I} = 3D\frac{E}{a^2}, \tag{7}$$

$$H_i = \frac{EA}{a} \cdot \frac{1}{A} = \frac{E}{a}.$$

- For the node k one arrives at

$$M_k = 2\frac{EI}{a} \cdot \frac{D}{2I} = D\frac{E}{a},$$

$$V_i = 6\frac{EI}{a^2} \cdot \frac{D}{2I} = 3D\frac{E}{a^2}, \tag{8}$$

$$H_k = H_i = \frac{EA}{a} \cdot \frac{1}{A} = \frac{E}{a}.$$

The influence surface for normal stresses can be compared to the results shown in Figure 5. The imperceptible differences in the shape of graphs are due to a small influence of bending moments. In the special case, where $M = 0$, the shape (but not the ordinate) of the influence surface N and of the influence surface s are identical.

4. The model of orthotropic plate

In the past, the bridges of a regular configuration, for example beam-plate bridges, have been modelled based on the theory of technical orthotropy. By means of the equivalent orthotropic model proposed, one can reduce the complex structure with a great number of nodes and elements to a considerably simpler model which at the same time ensures an the appropriate accuracy of results – especially for the preliminary stage of design [5].

In the case of structure being analyzed that is shown in Figure 3, due to vertical loads perpendicular to its surface $p(x,y)$, one can express the solution in terms of orthotropic plate equation

$$D_x \frac{\partial^4 w}{\partial x^4} + 2H \frac{\partial^4 w}{\partial x^2 \partial y^2} + D_y \frac{\partial^4 w}{\partial y^4} = p(x,y)\,. \tag{9}$$

In Equation (9), there are the flexural rigidities D_x and D_y that can be obtained considering the strip of deck (i.e. equivalent beam) separated from the structure. This strip is a repetitive element of the cross-section of bridge. The stiffness properties of one strip shown in Figure 6 should be determined like for the steel-concrete composite cross-section where the concept of equivalent cross-section being made of one homogeneous material (for example, steel) of the values EI_x and EI_y is accepted. Hence, one can calculate

$$D_x = \frac{EI_x}{b} \tag{10}$$

and

$$D_y = \frac{EI_y}{c}\,. \tag{11}$$

In such a case, the torsional stiffness of the orthotropic plate H is the implicit function of several variables of geometric parameters. Hence, in order to estimate it, the comparative analysis was carried out. It allowed the conclusion that the results calculated from orthotropic plate equation were in conformity with the results obtained based on the discrete model (being discussed in chapter 2). As a result of analysis, the flexural stiffness of orthotropic plate H was evaluated assuming a criterion of consis-

tency of the transverse profile of the influence line for axial forces in the bottom, longitudinal elements of structure.

Fig. 6. Value of the parameter *a*, depending on the number of segments (strips) in transverse cross-section of bridge

The dimensions of the cross-section of bridge, i.e. *b*, *t*, *h*, and the number of longitudinal strips *n* were assumed as variable parameters. The range of change of geometric parameters is represented by the coefficient $0.75 < \mu < 1.25$ related to basic dimensions given in Figure 3 according to the relationships

$$b = 2.00 \cdot \mu,$$

$$t = 0.21 \cdot \mu \qquad \text{[m]}, \tag{12}$$

$$h = 2.15 \cdot \mu.$$

The value of the torsional stiffness *H* is determined as in Figure 6 and 7 in terms of the parameter α. Its value is a characteristic parameter of the solution of orthotropic plate equation (9) presented in the form

$$\alpha = \frac{H}{\sqrt{D_x D_y}}, \tag{13}$$

which gives

$$H = \alpha \sqrt{D_x D_y}\ . \tag{14}$$

The number of segments (in other words beams or strips) set in the cross-section of bridge is of crucial importance for the value of *H* (assuming that the segments have

the same dimensions being independent of n) and causes the significant reduction of parameter α in (13). This reduction can be omitted in the analysis of beam-plate bridges because it is considered that the number of n influences the value of the second characteristic parameter of orthotropic plate rectangularly shaped (in orthogonal projection) in linear manner

$$\vartheta = \frac{n \cdot b}{L} \sqrt[4]{\frac{D_x}{D_y}} \,. \tag{15}$$

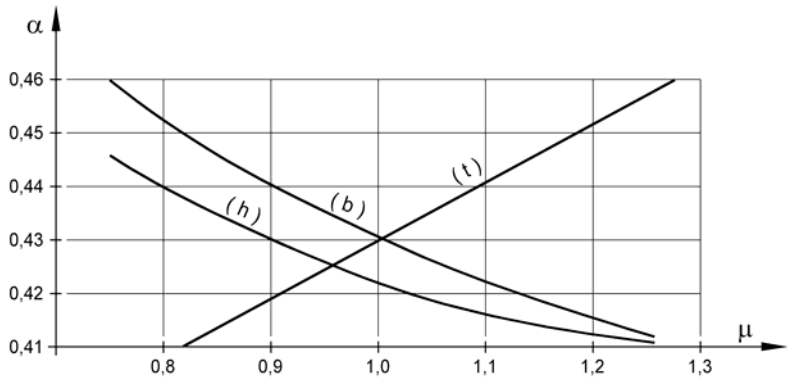

Fig. 7. Value of parameter a depending on the dimensions of bridge elements

The change in the dimensions of cross-section does not lead to increasing significantly difference in the values of H. In Figure 7, there is shown the graph of the function $a(n)$ provided that in the changes one selected dimension (b, h, t) is taken into account.

5. Summary

Internal forces due to dead load depend on the technology of erection of bridge and the construction of connection of concrete slab with the top plane of steel frame. As a result of rheological processes, which occur inside the concrete slab, the redistribution of internal forces in composite steel-concrete structure occurs. For that reason, determining of internal forces due to dead constant load is treated as a distinct problem.

In the paper, two algorithms of static analysis based on various models of geometry were given. For the model defined on the basis of orthotropic plate, the method of determining the torsional stiffness with the help of the parameter α (13) was presented. In such a type of construction, the dependence of α on the geometry of span (of horizontal projection) determined by the values of q (15) was analysed. The model established in such a way makes it possible to carry out all calculations by hand.

In the case of the discrete model comprising one-dimensional elements (the bars) and two-dimensional element (the slab), the solution is developed in the form of the influence surface for internal forces. That solution can be applied to constructions of various shapes (as well as of space frame transversally variable in depth) and of any boundary conditions (supports, for example cable-stayed bridges) and of any configuration in its own plane (irregular outline of deck). Numerical algorithm makes it possible to couple with FEM programs [5].

Comparing the values of a shown in graphs, one can claim that they are localized in proper place with reference to the box girder bridges ($\alpha \approx 1$) and multibeam bridges ($\alpha \to 0$).

References

[1] Churchman A.E., Cadei J.M.: *SPACES: A new concept in bridge construction*, International Conference *New Technologies in Structural Engineering*, Lisbon, 1997.
[2] Cadei J.M., Churchman A.E.: *The design approach for a new composite space frame bridge system*, IABSE Conference on Composite Construction – Conventional and Innovative, Innsbruck, 1997.
[3] Weiss S., Giżejowski M.: *Stateczność konstrukcji metalowych. Układy prętowe*, Arkady, Warszawa, 1991.
[4] Machelski Cz.: *Zastosowanie metody kinematycznej do wyznaczania funkcji wpływu sił wewnętrznych w układach prętowych*, Inżynieria i Budownictwo, 1998, R. 54, nr 7, s. 372–375.
[5] Kmita J., Bień J., Machelski Cz.: *Komputerowe wspomaganie projektowania mostów,* WKiŁ, Warszawa, 1989.

Siły wewnętrzne od obciążeń zmiennych w mostowych strukturach prętowych zespolonych z płytą pomostową

Niniejsza praca dotyczy mostów utworzonych ze stalowej struktury prętowej zespolonej z betonową płytą pomostową. Przedstawiono w niej możliwości wykorzystania do analizy sił wewnętrznych dwóch modeli geometrycznych w postaci: 1) płyty ortotropowej oraz 2) układu dyskretnego, utworzonego z elementów prętowych (struktura) i płaskich elementów powłokowych (płyta pomostowa). Dla modelu przęsła w postaci płyty ortotropowej podano sposób określania sztywności na skręcanie H, uciążliwej do określania w obliczeniach. W przeprowadzonej analizie wskazano na istotną zależność parametru H od liczby segmentów n oraz niewielki wpływ parametrów geometrycznych przekroju poprzecznego przęsła.

W przypadku modelu dyskretnego podano rozwiązanie w postaci powierzchni wpływu sił wewnętrznych w elementach struktury prętowej. Dotyczy ono zarówno wielkości przekrojowych M, N, T (momentów zginających, sił osiowych czy też poprzecznych), jak również naprężeń normalnych σ. Podane rozwiązanie odnosi się do obciążeń ruchomych, zmieniających swoje położenie na płycie pomostowej obiektu.

Siły wewnętrzne od obciążeń stałych w tych konstrukcjach zależą w znacznym stopniu od technologii montażu przęsła i sposobu zespalania płyty ze strukturą stalową. W wyniku zachodzących w betonie procesów reologicznych wpływ obciążeń stałych na siły wewnętrzne należy rozpatrywać jako odrębne zagadnienie.

ARCHIVES OF CIVIL AND MECHANICAL ENGINEERING

Vol. IV 2004 No. 1

Nonlinear modelling of composite beams prestressed with external tendons

WOJCIECH LORENC, ERNEST KUBICA
Wrocław University of Technology, Wybrzeże Wyspiańskiego 27, 50-370 Wrocław

An algorithm for analysis of capacity and behaviour of steel-concrete beams prestressed with external cables has been presented. Nonlinear constitutive laws for concrete and constructional and reinforcing steel can be taken into account, in a way similar to that adopted in the case of nonlinear slip dependence and nonlinear studs' distribution along the beam. According to the method presented, completed computer program has been created and used for solving the problem of the influence of cable profile and the stiffness of shear connection on the forces in shear connection during prestressing.

1. Introduction

External prestressing of composite steel-concrete beams as a method of their strengthening is to be applied most of all in bridge engineering [3, 7, 8]. Symmetrical cable arrangement, while placed along the bottom flange of the beam, is most often applied. Cable profile can be straight [7] or rectilinear [8]. Shear connection stiffness and studs' distribution are to be found as important factors influencing the behaviour of whole beam, both in prestressing and serviceable states. The method enabling analysis of such structures based on nonlinear constitutive laws for concrete, steel and shear connection taken into account, nonlinear studs' distribution along the beam and any cable profile is presented in this paper. Taking advantage of this method, the results of the analysis of prestressing influence on the forces in shear connection are described.

2. Subject of the analysis and the method proposed

The idea of a beam is shown in Figure 1. For the sake of simplicity a simply supported beam has been taken into consideration.

The method proposed is the Ritz method which roughly consists of a solution with a finite set of shape functions selected from orthonormal base. It allows us to analyse monosymmetrical beams in elastoplastic range, both simply supported and continuous ones. Load pattern is any. Slab reinforcement can be included. Constitutive laws for structural steel, reinforcements, prestressing steel, concrete and shear connection can be different. The method enabling solving the problems without weak shear connection included was published [1].

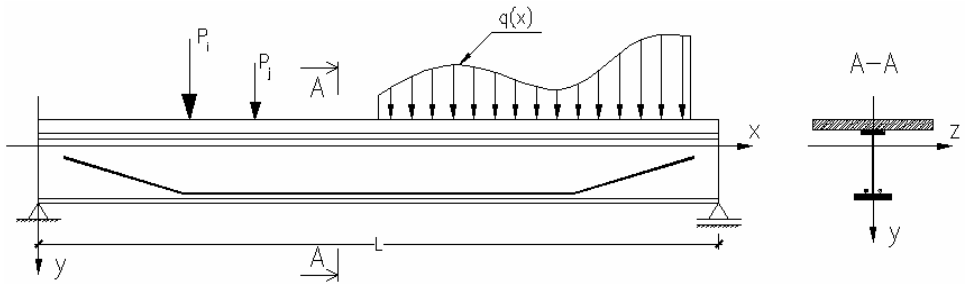

Fig. 1. Scheme of composite beam prestressed with external cables

3. Method without weak shear connection

Dall'Asta and Dezi [1] supposed cable slipping in contact points except anchorages, homogeneous cable material, small displacements and uni-axial bending and described the displacements of beam points by two functions $u(x)$ and $v(x)$. Strain field in the beam can presented as follows:

$$\varepsilon_b = \frac{\partial u_x}{\partial x} = u'(x) - y \cdot v''(x). \tag{1}$$

The beam displacements determine unambiguously the displacements of cable points and thereby axial strain of cable. After essential mathematical transformations one can arrive at axial strain in a cable:

$$\varepsilon_c = \frac{1}{\Lambda} \sum_{1}^{D} \alpha_d [\Delta_d u - \Delta_d (y \cdot v')] + \beta_d \Delta_d v, \tag{2}$$

where Λ is the cable length in an initial state, coefficients α_d and β_d stand for location of anchorages and saddle points, respectively (they depend on the y and z co-ordinates only) and the quantities Δ_d, according to the specific functions ($u(x)$, $v(x)$ and $v'(x)$), represent the difference in the values of these functions between two saddle points. Taking constitutive laws described by means of the function G_i, one can obtain respectively the stresses in steel, concrete and cable (for the sake of simplicity reinforcements are avoided):

$$\sigma_s = G_s(\varepsilon_s - \varepsilon_{s0}), \tag{3a}$$

$$\sigma_b = G_b(\varepsilon_b - \varepsilon_{b0}), \tag{3b}$$

$$\sigma_c = G_c(\varepsilon_c - \varepsilon_{c0}), \tag{3c}$$

where 0 in the subsciprt represents the initial strain field, e.g. prestressing.

A global balance condition of the system can be expressed in the form:

$$\int_0^L \int_{As} \sigma_s \cdot \delta\varepsilon_s \, dA_s \, dx + \int_0^L \int_{Ab} \sigma_b \cdot \delta\varepsilon_b \, dA_b \, dx + \Lambda \cdot A_c \cdot \sigma_c \delta\varepsilon_c = \int_0^L \int_{As+Ab} \mathbf{f} \cdot \boldsymbol{\delta}\mathbf{u} \, dx, \tag{4}$$

where A_s, A_b and A_c are the cross-sectional areas of steel beam, concrete slab and cable, respectively, and the right-hand side of the equation represents the work of external loads. After transformations to the parts responsible for energy from axial force and bending moment it can be rewritten in the form:

$$\int_0^L \left[N(u', v'')\delta u'\right] dx + \int_0^L \left[M(u', v'')\delta v''\right] dx$$

$$+ \Lambda \cdot T_c(u_d, v_d, v'_d)\delta\varepsilon_c(u_d, v_d, v'_d) = \int_0^L \left[n\delta u + q\delta v + m\delta v'\right]. \tag{5}$$

The functions u and v can be approximated by means of a finite set of shape functions to approximate solution of the functional problem. This was done by reducing the functional problem to an algebraic one:

$$u(x) = \sum_1^I u_i \cdot \phi_i(x) = \mathbf{u} \cdot \boldsymbol{\varphi}(\mathbf{x}), \tag{6}$$

$$v(x) = \sum_1^J v_i \cdot \psi_i(x) = \mathbf{v} \cdot \boldsymbol{\psi}(\mathbf{x}). \tag{7}$$

In order to hold the global balance condition for every-shape function, it is possible to derive the nonlinear set of $I + J$ equations:

$$\frac{\partial \Pi}{\partial u_i} = 0 \qquad \text{at} \qquad i = 1 \ldots I,$$

$$\frac{\partial \Pi}{\partial v_j} = 0 \qquad \text{at} \qquad j = I + 1 \ldots J. \tag{8}$$

There are two groups of equations in this set, and the number of equations in the group is equal to the number of shape functions of the group. The Newton–Raphson method can be used for solving nonlinear set of equations. To that end a square gra-

dient matrix should be assembled in every iterative step. A detailed description of the parameters and derivation of the formulas can be found in paper [1].

4. Taking weak shear connection into account

The approach that allows taking a weak shear connection into account was presented by Dall'Asta et al. [2], who described the strain field by functions representing the displacements of centroids of steel beam and concrete slab separately. In the present paper, there is presented an alternative approach where all functions treat the displacement of centroid of composite section in the initial state (no slip and all stresses amount to zero). According to this, strain field is described by three functions of displacements:

$u(x)$ – the displacement of points of steel beam in horizontal direction, i.e. in the x-direction (the composite beam axis consists of the points initially lying on the x-axis),

$h(x)$ – the function describing the displacement of the points of concrete slab in horizontal direction due to slip,

$v(x)$ – the displacement of the points of composite beam in vertical direction, i.e. in the y-direction.

Such a displacement field provides only the axial strains in a steel beam and concrete slab and slip, respectively:

$$\varepsilon_s = u'(x) - y \cdot v''(x), \tag{9a}$$

$$\varepsilon_b = h'(x) - y \cdot v''(x), \tag{9b}$$

$$s = u(x) - h(x). \tag{9c}$$

Description of the cable strain remains unchanged compared to that presented in the paper [1], assuming that the cable is connected with steel beam only, as the most often takes place in such structures. The three functions enable modelling of the structure based on nonlinear constitutive laws for steel, concrete and shear connection as nonlinear studs' distribution along the beam. Constitutive law for the shear connection needs to be applied:

$$F_z = G_z(s - s_0). \tag{10}$$

For the sake of simplicity the reinforcement of slab is avoided in equations, and a global balance condition (4) can be expressed as follows:

$$\int_0^L \int_{As} \sigma_s \cdot \delta\varepsilon_s \, dA_s \, dx + \int_0^L \int_{Ab} \sigma_b \cdot \delta\varepsilon_b \, dA_b \, dx + \int_L \upsilon(x) \cdot G_z(s) \cdot \delta s \cdot dx + \Lambda \cdot A_c \cdot \sigma_c \delta\varepsilon_c = \int_L \mathbf{f} \cdot \boldsymbol{\delta}\mathbf{u}^T dx. \tag{11}$$

The vector **f** remains unchanged if only vertical external load is considered. The function $\upsilon(x)$ describes a density of studs' distribution along the beam. The approximated solution can be expressed in the form:

$$u(x)=\sum_{1}^{I} u_i \cdot \phi_i(x), \qquad h(x)=\sum_{1}^{J} h_i \cdot \eta_i(x), \qquad v(x)=\sum_{1}^{J} v_i \cdot \psi_i(x). \tag{12}$$

According to Equations (12) nonlinear set of equations now consists of three equations:

$$\begin{aligned}
&\frac{\partial \Pi}{\partial u_i}=0 \quad \text{at} \quad i=1...I,\\
&\frac{\partial \Pi}{\partial h_i}=0 \quad \text{at} \quad i=I+1...K,\\
&\frac{\partial \Pi}{\partial v_i}=0 \quad \text{at} \quad i=K+1...J.
\end{aligned} \tag{13}$$

After substitutions and mathematical transformations it can be rewritten as follows:

$$\begin{aligned}
&\int_0^L \int_{As} G_s(\varepsilon_s-\varepsilon_{s0})\cdot \phi'_h \, dA_s\, dx+\int_L \upsilon(x)\cdot G_z(s-s_0)\cdot \phi_h dx\\
&+A_c G_c(\varepsilon_c-\varepsilon_{c0})\cdot \sum_1^D \alpha_d \Delta_d \phi_h=\int_0^L \int_{As} \sigma_s \phi_h \, dA_s\, dx, \qquad h=1...I,\\
&\int_0^L \int_{Ab} G_b(\varepsilon_b-\varepsilon_{b0})\cdot \eta'_h \, dA_b dx-\int_L \upsilon(x)\cdot G_z(s-s_0)\cdot \eta_h \, dx\\
&=\int_0^L \int_{Ab} \sigma_{bs}\, \eta_h \, dA_b\, dx, \qquad h=I+1...K,\\
&-\int_0^L \int_{As} G_s(\varepsilon_s-\varepsilon_{s0})\cdot y\cdot \psi''_h \, dA_s\, dx-\int_0^L \int_{Ab} G_b(\varepsilon_b-\varepsilon_{b0})\cdot \psi''_h \, dA_b\, dx\\
&+A_c G_c(\varepsilon_c-\varepsilon_{c0})\cdot \sum_1^D \left[\beta_d \Delta_d \psi_h-\alpha_d \Delta_d (y\cdot \psi'_h)\right]\\
&=\int_0^L \int_{As+Ab} \left[\tau_y \psi_h-y\cdot \sigma_x \psi'_h\right] dA\, dx, \qquad h=K+1...J.
\end{aligned} \tag{14}$$

The above set comprises three types of equations, which results in nine different types of components of gradient. Because of the symmetry of the gradient, it is possible to reduce the terms in order to compute six types of components:

- Derivatives of the *u*-type equations with respect to the *u*-type coefficients:

$$[\nabla a]_{hm} = \int_0^L \varphi'_h \cdot \varphi'_m \left\{ \int_{Ac} \frac{\partial G_s(\varepsilon_s - \varepsilon_{s0})}{\partial \varepsilon_s} d A_s \right\} d x + \int_0^L \upsilon(x) \cdot \frac{\partial G_z(s - s_0)}{\partial s} \cdot \varphi_h \cdot \varphi_m d x$$
$$+ A_c \frac{\partial G_c(\varepsilon)}{\partial \varepsilon_c} \cdot \sum_1^D [\alpha_d \Delta_d \varphi_h] \cdot \sum_1^D [\alpha_d \Delta_d \varphi_m].$$

- Derivatives of the *u*-type equations with respect to the *h*-type coefficients:

$$[\nabla a]_{hm} = -\int_0^L \upsilon(x) \cdot \frac{\partial G_z(s - s_0)}{\partial s} \cdot \varphi_h \cdot \eta_m.$$

- Derivatives of the *u*-type equations with respect to the *v*-type coefficients:

$$[\nabla a]_{hm} = -\int_0^L \varphi'_h \psi''_m \left\{ \int_{As} y \cdot \frac{\partial G_s(\varepsilon_s - \varepsilon_{s0})}{\partial \varepsilon_s} d A_s \right\} d x$$
$$+ A_c \frac{dG_c(\varepsilon)}{d\varepsilon_c} \cdot \sum_1^D [\alpha_d \Delta_d \varphi_h] \cdot \sum_1^D [\beta_d \Delta_d \psi_m - \alpha_d \Delta_d (y \psi'_m)].$$

- Derivatives of the *h*-type equations with respect to the *h*-type coefficients:

$$[\nabla a]_{hm} = \int_0^L \eta'_h \cdot \eta'_m \left\{ \int_{Ab} \frac{\partial G_b(\varepsilon_b - \varepsilon_{b0})}{\partial \varepsilon_b} d A_b \right\} d x + \upsilon(x) \cdot \frac{\partial G_z(s - s_0)}{\partial s} \cdot \eta_h \cdot \eta_m .$$

- Derivatives of the *h*-type equations with respect to the *v*-type coefficients:

$$[\nabla a]_{hm} = -\int_0^L \eta'_h \cdot \psi''_m \left\{ \int_{Ab} y \frac{\partial G_b(\varepsilon_b - \varepsilon_{b0})}{\partial \varepsilon_b} d A_b \right\} d x.$$

- Derivatives of the *v*-type equations with respect to the *v*-type coefficients:

$$[\nabla a]_{hm} = -\int_0^L \psi''_h \psi''_m \left\{ \int_{As} y^2 \cdot \frac{\partial G_s(\varepsilon_s - \varepsilon_{s0})}{\partial \varepsilon_s} d A_s \right\} d x$$
$$- \int_0^L \psi''_h \cdot \psi''_m \left\{ \int_{Ab} y^2 \cdot \frac{\partial G_b(\varepsilon_b - \varepsilon_{b0})}{\partial \varepsilon_b} d A_b \right\} d x$$
$$+ A_c \frac{\partial G_c(\varepsilon)}{\partial \varepsilon} \cdot \sum_1^D [\beta_d \Delta_d \psi_h - \alpha_d \Delta_d (y \psi'_h)] \cdot \sum_1^D [\beta_d \Delta_d \psi_m - \alpha_d \Delta_d (y \psi'_m)].$$

5. Analysis of the influence of cable shape and studs' distribution on forces in shear connection during prestressing of composite beam

In practice, there is usually no slip considered in the analysis of prestressing of composite beams, but as a rule the Kirchoff model is assumed for the beam deformation. Based on the experiments described in [3] and the results of theoretical analysis reported in [2] it is possible to show that the cable profile, shear connection stiffness and its changeability along the beam affect the shear forces in the connection during prestressing stage. In this paper, the results of theoretical analysis of composite beam are presented. Different cable profiles and studs' distribution have been considered. Few problems associated with designing of this kind of structures have been brought up.

The subject of this analysis is a composite beam (Figure 1) post-tensioned with external cables. Such a situation takes place when bridge is strengthened without a concrete deck replacement. In this paper, post-tensioning stage is considered before external load is to be applied. There are two kinds of cable profiles used in practice: "king-post" arrangement (Figure 1) and straight cables with no deviators on the beam. The cable is connected with a steel beam only and the forces in a concrete slab are induced due to a suitably stiff shear connection between steel and concrete. There are significant axial forces being induced in the beam near anchorages during prestressing stage. In this case, the assumption of the Kirchoff model for beam may be inappropriate because it does not reflect the real behaviour of the structure. As long as the conception of partial shear connection presented in [4] has no application in the bridge structures (according to [5]), omitting totally the possible slip can lead to a model which does not represent a real structure properly. The results of theoretical analysis confirm that such a problem appears [2] and it should not be avoided; however, detailed experiments have not been made yet.

In order to gain information about shear forces in the connection between steel and concrete during prestressing stage, theoretical simulation was carried out. Here we analysed the beam described in detail in paper [6]. Total length of the beam approaches 4.5 m, height of steel beam is 352 mm, width of slab is 915 mm and slab thickness is 76 mm. Cross-sectional area of cables is 402 mm^2. For the purposes of this analysis there have been considered three different cable profiles: 1) "king-post"

arrangement with a cable anchored near to top flange of steel beam and deviators placed 1.20 m from the beam ends, 2) "king-post" arrangement with a cable anchored near to centroid of composite beam and deviators placed 1.20 m from the beam ends, 3) straight cable on a level of bottom flange of steel beam and no deviators. In all three cases, the axis of the cable coincides with the axis of bottom flange of steel beam in a midspan. Additionally the fourth case has been considered, it is like the first arrangement, but here an axis of the cable lays above bottom flange of steel beam in a midspan (smaller eccentricity).

There have been considered three cases of studs' distribution along the beam. The first one is a uniform distribution along the whole length of the beam; the stiffness of shear connection per unit length is similar to that reported in [6]. The second case is like the first one but near to anchorages the stiffness of shear connection is four times larger along length of L/8 from each end of the beam, according to [5]. In the third case, we deal with linear distribution, stiffness equal to zero at midspan and two times larger at the ends than in the first case.

The computer program PRESTCOMP v.1.1.3 written in MATHEMATICA environment has been used for analysis. The program is based on the method described in this paper. Results of calculations and application of the program in the analysis of composite beams under external load with nonlinear constitutive laws included have been presented in [11]. Because there is no necessity to consider nonlinear constitutive laws in the current analysis, the linear dependences have been considered. Displacement functions have been approximated with four terms of sinusoidal series and six terms of Legendre series for vertical and horizontal displacements, respectively. Post-tensioning was modelled as an axial strain in the cable with the value of 0.006, then cable was anchored and released, which came the forces in composite beam into being. Such a sequence is imposed by the program.

6. The results of analysis

The results are presented in the following graphs. There is shown a changeability of slip s between steel beam and slab along the beam and the force Q in the shear connection. Because of symmetry (simply supported beam) there is shown a half of span only, the value $x = 0$ represents the support of the beam. Positive slip corresponds with a situation, where the end of slab is moving beyond the end of top flange of the beam. Graphs with the results have been collected according to the type of shear connection (Figures 2, 3, 4 and 5). Different cable profiles are distinguished in each graph; profiles 1, 2 and 3 in Figures 2, 3 and 4 and profiles 1 and 4 in Figure 5. Discontinuities in Figures 3 and 5 appear, because the stiffness of shear connection has changed in these points (the second case of studs' distribution).

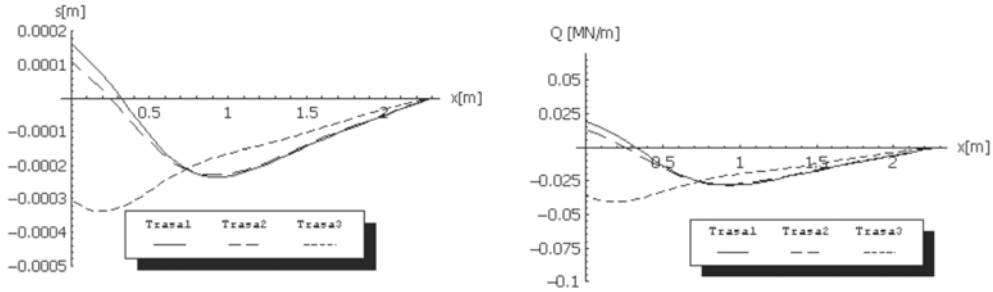

Fig. 2. Results for uniform studs' distribution

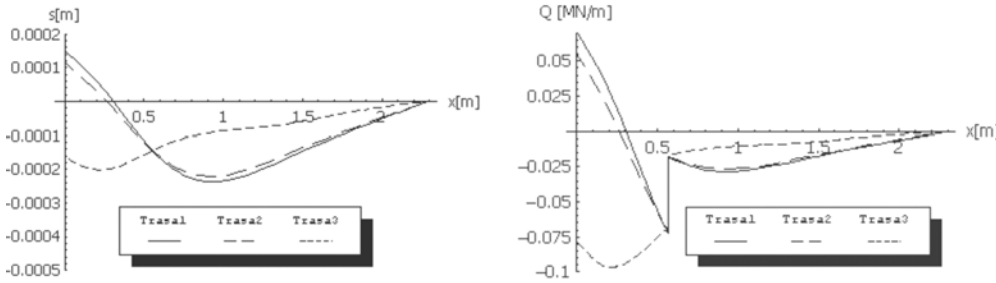

Fig. 3. Results for uniform studs' distribution with concentration of studs near to anchorages

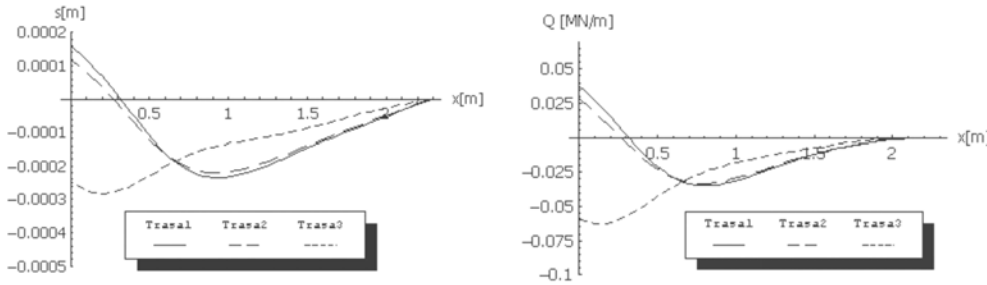

Fig. 4. Results for linear studs' distribution

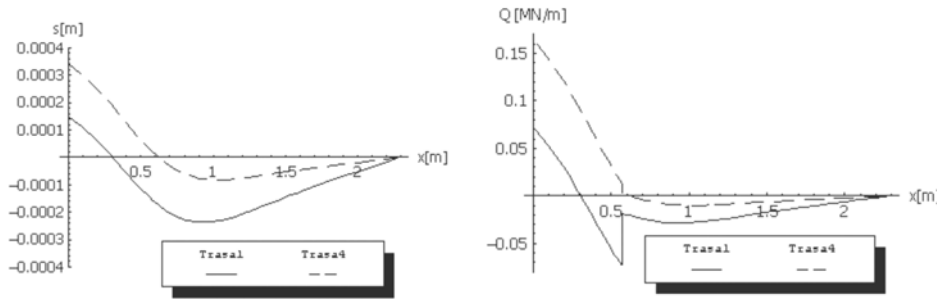

Fig. 5. Results for uniform studs' distribution with concentration of studs near to anchorages, when cable is anchored near to top flange of steel beam and different eccentricity of cable in a midspan is considered

7. Interpretation of the results

On the basis of the results of analysis it can be stated that cable profile has significant influence on the arrangement of forces in shear connection which is confirmed by a shape of curves. Depending on the cable profile (straight cable or "king-post" arrangement), the forces in shear connection near to anchorages can be both positive and negative. The influence of the stiffness of shear connection can be seen as well. The results can be interesting in the context of the results of experiments carried out on push-out specimens and composite beams under cyclic loading [9, 10]. A nonlinear changeability of the stiffness of shear connection in time due to cyclic loading is presented in the mentioned papers (such a situation takes place in the bridge structures). It is remarked that the phenomenon intensifies, if the force in shear connection changes its sign. The comparison of the forces in graphs with the forces induced in shear connection due to external load allows a conclusion that exactly such a situation takes place. The results of the most extensive research program [3], consisting of the experiments on both composite beams and entire composite bridges, seem to confirm the conclusions drawn above.

External prestressing becomes the way of strengthening the existing bridges and is used often and often for composite bridges. Therefore the problem should be verified by the experiments run on composite beams posttensioned with external cables. Such a research program has already begun at the Technical University of Wrocław. It has been aimed at both theoretical analysis and experiments carried out on six composite beams, each 5.50 m in length.

8. Summary

An approach to the analysis of the capacity and behaviour of composite beams prestressed with external tendons has been presented. It enables modelling the struc-

ture by nonlinear constitutive laws for steel, concrete and shear connection in a manner similar to that of nonlinear studs' distribution along the beam. The computer program based on the approach presented was created. A problem of forces in shear connection due to prestressing was formulated and numerical solutions were performed taking advantage of the program. The influence of the cable profile and the stiffness of shear connection on shear forces in connection during prestressing stage was presented. The problem of decreasing the stiffness of shear connection due to cyclic external loading was identified.

References

[1] Dall'Asta A., Dezi L.: *Nonlinear behaviour of externally pre-stressed composite beams: analytical model,* J. of Structural Engineering, 1998, pp. 588–597.

[2] Dall'Asta A., Dezi L. & Leoni G.: *Failure mechanisms of externally pre-stressed composite beams with partial shear connection,* Steel & Composite Structures, 2002, Vol. 2, pp. 315–330.

[3] Klaiber F.W., Dedic D.J., Dunker K.F., Sanders W.W. Jr: *Strengthening of existing single span steel beam and concrete deck bridges. Final Report – part I, ERI Project 1536, ISU-ERI-Ames 83185*, Engineering Research Institute, Iowa State University, 1983.

[4] ENV 1994-1-1:1992. *Projektowanie zespolonych konstrukcji stalowo-betonowych.* Część 1-1: *Zasady ogólne i reguły dla budynków*.

[5] ENV 1994-2:1997. *Projektowanie konstrukcji zespolonych stalowo-betonowych.* Część 2*: Mosty zespolone.*

[6] Saadatmanesh H., Albrecht P., Ayyub B.M.: *Experimental study of pre-stressed composite beams,* Journal of Structural Engineering, 1989, Vol. 115, pp. 2348–2363.

[7] Machelski C., Biliszczuk J.: *Raport serii SPR nr 21/96. Nadzór naukowy nad remontem mostu w miejscowości Ścibórz w ciągu drogi krajowej nr 408 Kłodzko–Gliwice. Badania efektywności sprężenia dźwigarów głównych przy pomocy prostoliniowych kabli odcinkowych,* Instytut Inżynierii Lądowej Politechniki Wrocławskiej, 1996.

[8] Machelski C., Kamiński L., Onysyk J.: *Raport serii SPR nr 97/97. Ocena efektywności wzmocnienia mostu przez Widawę w ciągu ul. Kamieńskiego we Wrocławiu oraz ocena stanu technicznego czterech obiektów inżynieryjnych w ciągu ul. Kamieńskiego we Wrocławiu,* Instytut Inżynierii Lądowej Politechniki Wrocławskiej, 1997.

[9] Taplin G., Grundy P.: *Steel–concrete composite beams under repeated load*, Sixteenth Australian Conference on the Mechanics of Structures and Materials, Sydney, 1999.

[10] Taplin G., Grundy P.: *Incremental slip of stud shear connectors under repeated loading*, Proceedings of the International Conference on Composite Construction, Innsbruck, Austria, 1997.

[11] Lorenc W., Kubica E., Adrjan P.: *Analiza zachowania się belek zespolonych sprężonych kablami zewnętrznymi*, Problemy Naukowo-Badawcze Budownictwa, XLIX Konferencja Naukowa Komitetu Inżynierii Lądowej i Wodnej PAN i Komitetu Nauki PZITB, Warszawa–Krynica, 2003.

Nieliniowe modelowanie belek zespolonych sprężanych kablami zewnętrznymi

Przedstawiono metodę umożliwiającą analizę zarówno nośności zespolonych belek stalowo-betonowych sprężanych kablami zewnętrznymi, jak i ich zachowania się pod wpływem obciążenia. Umożliwia ona uwzględnienie nieliniowych zależności materiałowych dla stali konstrukcyjnej i zbrojeniowej oraz betonu, a także nieliniowej charakterystyki zespolenia oraz nieliniowego rozkładu łączników wzdłuż belki. Artykuł dotyczy konstrukcji mostowych, jako że zewnętrzne sprężanie zespolonych belek stalowo-betonowych, będące jednym ze sposobów wzmacniania tego typu konstrukcji, znajduje zastosowanie przede wszystkim w budownictwie mostowym [3, 7, 8]. Na zachowanie się tego typu belek zarówno w fazie sprężania, jak i po sprężeniu pod obciążeniem użytkowym istotny wpływ ma sztywność i układ zespolenia [11]. Na podstawie prezentowanej metody stworzono program komputerowy i wykorzystano go do rozwiązania konkretnego problemu, dotyczącego układu sił w zespoleniu podczas sprężania belek. Przedstawiono wpływ kształtu trasy cięgna oraz zmiennej wzdłuż belki sztywności zespolenia na układ sił ścinających w zespoleniu w fazie sprężania. Zwrócono uwagę na możliwość zwiększenia się podatności zespolenia pod wpływem cyklicznego obciążenia zewnętrznego, gdyż powoduje ono w zespoleniu belki sprężonej powstawanie sił ścinających o różnym zwrocie.

ARCHIVES OF CIVIL AND MECHANICAL ENGINEERING

Vol. IV 2004 No. 1

Information about PhD thesis at the Civil Engineering Faculty and the Mechanical Engineering Faculty of Wrocław University of Technology

Title: ***Analysis of identification process of flexible elements of mechanical systems under complex nonharmonic dynamic loading using nonlinear models*** **(in Polish)**
Analiza procesu identyfikacji podatnych elementów układów mechanicznych poddanych złożonym wzburzeniom dynamicznym z zastosowaniem modeli nieliniowych

Author: Mirosław Bocian
Supervisor: Professor Maciej Kulisiewicz
Promoting Council: Council of Mechanical Engineering Faculty
Reviewers:
Professor Wacław Kasprzak, Wrocław University of Technology
Professor Andrzej Buchacz, Silesian University of Technology
Date of PhD thesis presentation: January 15th, 2003
PhD thesis is available in Main Library and Scientific Information Centre of WUT
The paper contains: 127 pages, 221 figs, bibliography, 66 items
Keywords: *identification, nonlinear dynamic system, modelling*

Abstract: The analysis of some identification of mechanical elements with nonlinear description was presented. In order to make this identification, non-conventional models with flexible elements (the so called degenerated elements) mixed with non-linear elements (for instance, of dry friction type) were proposed. Results of Experimental Modal Analysis for nonlinear structures and structures with the so-called one half a degree of freedom were given. The aim of this work was to prepare a proper research methods taking into consideration not only the value of vibration damping, but first of all its type (for example friction, clearance at the kinetic junctions, etc.). The author proves that using energy balance and power balance method for nonlinear structure with appropriate dynamic characteristics it is possible to solve these problems. Verification test on simulated computer model to prove algorithm correctness is provided.

Title: *Free-edge effect in spatial elements made of composite laminates* **(in Polish)** *Efekt brzegowy w przestrzennych elementach wykonanych z laminatów kompozytowych*

Author: Karol Kaczmarek
Supervisor: Professor Leszek Gołaski
Promoting Council: Council of Metal Science and Technica Mechanics Institute
Reviewers:
Professor Tomasz Topoliński, Technical University of Opole
Professor Marek Rybaczuk, Wrocław University of Technology
Date of PhD thesis presentation: December 10th, 2003
PhD thesis is available in Main Library and Scientific Information Centre of WUT
The paper contains: 177 pages, 74 figs, bibliography, 134 items
Keywords: *free-edge effect, delamination, acoustic emission, MES, fracture mechanics*

Abstract: Free-edge effect in composite laminates resulting in spatial stress state at the laminate free edge creates a serious barrier to a wide application of composite laminates to mass products. There are a number of literature data related to the free-edge effect, but majority of them treat the effect itself and do not take into account the impact of that effect on the engineering practices. As far as author knows there is no methods that deal with failure mechanism explanation and failure load prediction related to the free-edge delamination problems. The main assumption of the thesis is that the free edge-effect in curved composite laminate beams increases their susceptibility to delamination, and therefore has an impact on the strength of the elements made of composite materials.

The results of the experimental and numerical analyses of a number of specimen types, varying in shape and dimensions and made of glass/fibre composite laminates with $(0_n/\pm 45_m)$ stacking sequence, confirm that the free-edge effect in curved composite laminate beams makes the structural elements more susceptible to delamination at the laminate free edge. This has the impact on the strength of the elements made of composite materials. It was shown that the free-edge effect could be successfully described in the quantitative manner. The size effect as well as the effects of the laminate curvature on the delamination were successfully described in an quantitative way. The method and procedure for evaluating a delamination onset using acoustic emission analysis was proposed. The conditions of the onset of the delamination failure process were determined. In addition, the hypothesis explaining the failure mechanism and proposing the failure criteria was derived and confirmed by the results of experimental and numerical investigations. Finally, the failure load prediction methods were derived based on the linear elastic fracture mechanics giving very good agreement with experiments.

Title: *Trade-off studies of mechanical and radiological properties of bone tissues* (in Polish)
Badania porównawcze właściwości mechanicznych i radiologicznych struktur kostnych

Author: Elżbieta Gawin
Supervisor: Professor Romuald Będziński
Promoting Council: Council of Mechanical Engineering Faculty
Reviewers:
Professor Lech Dietrich, Polish Academy of Science, Warsaw
Professor Jerzy Kaleta, Wrocław University of Technology
Professor Jan Kuryszko, Wrocław Agriculture Academy
Date of PhD thesis presentation: April 23th, 2003
PhD thesis is available in Main Library and Scientific Information Centre of WUT
The thesis contains: 119 pages, 98 figs, bibliography, 111 items
Keywords: *hip joint, remodelling, implantation*

Abstract: Body skeleton is made up of bones which are the most amazing material in science. Diversity and number of existing remodelling theories as well as substantial discrepancy between mechanical and physical properties prove that there is no common view on this topic and that investigation of mechanical properties of bone structures is justified. Many different techniques were applied in the dissertation in order to examine a bone structure. They can be itimized as follows: computer topography, scanning microscopy, histology and physical density measurement. Bone mechanical parameters were determined using electronic speckle pattern interferometry (ESPI) as well as speckle photography. Different kinds of loads were measured using MTS machine (compression, three- and four-point bending) and microbreak machine (stretching). Investigation of structure carried out using scanning microscopy allows us to explain some relationships observed during investigation. Mechanical properties measured on opposite sides were the same, whereas for adjacent sides differences amounted to 15%. This could be explained by the decomposition of the Haversian canal, which was heterogeneous.

Title: *Evaluation of anisotropic properties of the bone tissues measured by quantitative computerized tomography* (in Polish) *Ocena anizotropowych właściwości mechanicznych struktur kostnych badanych metodą tomografii komputerowej*

Author: Piotr Mielecki
Supervisor: Professor Romuald Będziński
Promoting Council: Council of Mechanical Engineering Faculty
Reviewers:
Professor Tadeusz Burczyński, Silesian University of Technology
Professor Marek Sąsiadek, Wrocław Medical Academy
Professor Zbigniew Huzar, Wrocław University of Technology
Date of PhD thesis presentation: June 27th, 2003
PhD thesis is available in Main Library and Scientific Information Centre of WUT
The paper contains: 124 pages, 46 figs, bibliography, 102 items
Keywords: *biomechanics, mechanical strength of bone tissues, models*

Abstract: The aim of the work was to introduce computer imaging technique (QCT) and medical image-data management standards (DICOM) into computer-aided design of human bone prostheses and routine research on mechanical properties of the bone tissues. The standard X-ray QCT technique has been employed in experimental study to determine the distribution of the bovine cancellous bone and cortical bone optical density for X-rays (CT density) in 108 specimens of cortical bone and 36 specimens of cancellous bone extracted from trochanter minor region. The values being measured were correlated with mechanical parameters (physical density for cortical bone, apparent density for cancellous bone and Young's modulus) determined by mechanical testing. The attempts were made to observe and measure mechanical anisotropy of the bone tissue in the QCT examinations relative to the direction of X-ray energy propagation (projection). Significant anisotropy of the CT density ($p<0.001$) was observed for both cancellous and cortical bone specimens examined using two orthogonal projections. Young's modulus of the cortical bone correlated directly with CT density with power-law regression model gave the good correlation (r^2 up to 0.68). Structural Young's modulus of the cancellous bone correlated with the mean CT density specimen gave worse correlation ($r^2 = 0.51$). The sensitivity of the QCT to anisotropy was compared for next 48 specimens of cortical bone with the sensitivity of mechanical measurements with ESPI camera, giving comparable results of difference between planes measured ($p<0.001$).

Title: *The effect of cyclic loads on the torsional vibration damping model for selected structural elements using nonlinear identification methods* (in Polish)
Wpływ obciążeń cyklicznych na model tłumienia drgań skrętnych wybranych elementów konstrukcyjnych z wykorzystaniem nieliniowych metod identyfikacji

Author: Mariusz Wajda
Supervisor: Professor Maciej Kulisiewicz, Wrocław University of Technology
Promoting Council: Council of Mechanical Engineering Faculty
Reviewers:
Professor Ewald Macha, Technical University of Opole
Professor Mieczysław Szata, Wrocław University of Technology
Date of PhD thesis presentation: December 1th, 2003
PhD thesis is available in Main Library and Scientific Information Centre of WUT
The paper contains: 146 pages, 144 figs, bibliography, 102 items
Keywords: *material damping, nonlinear identifications, material fatigue, cyclic loading, torsional vibration*

Abstract: The monograph is an attempt at practical applying nonlinear identification methods to analysis of spring–dissipative properties of pipes made of different kinds of materials under cyclic loads. The basic aim was to specify the forms of models which can be used for describing the spring–dissipative properties of the pipes tested; however, the main aim was to evaluate the influence of long-term cyclic loads on parameters of accepted models. Therefore, the dissertation was divided into two parts. The first, devoted to evaluation of spring–dissipative models, deals with a detailed discussion of research aims, description of searching methods for adequate forms of models and analysis of rheological models and procedures of nonlinear identification methods. This part includes also description of research system and presens the software package using the FFT algorithm. The most important in this part are the results of experiments carried out by author. They inclined him to search for optimal forms of models of spring–dissipative properties of tested pipes. Some methods for identification and verification of selected models using computer simulations were presented. In the second part, dealing with the influence of long-term cyclic loads on parameters of spring–dissipative models, basic information about fatigue material cracks is given and the range of cyclic testing is defined. The results of experiments on the changes of model parameters under cyclic loads are discussed. Author has revealed and proved that the changes of damping in the elements tested were connected with the number of cyclic loads applied. Therefore he was able to determine wearing of tested elements based on the changes of the damping value before their destruction.

Information about habilitations at the Civil Engineering Faculty and the Mechanical Engineering Faculty of Wrocław University of Technology

Title: ***Methods for vibration and noise reduction in fluid power pumps and systems. Procedures, measures and potential for noise reduction*** **(in Polish)**
Metodyka zmniejszania drgań i emisji hałasu pomp wyporowych i układów hydraulicznych. Sposoby, zmiany konstrukcyjne i możliwości zmniejszenia hałasu

Author: Wiesław Fiebig
Promoting Council: Concil of Mechanical Engineering Faculty
Reviewers:
Professor Andrzej Balawender, Gdańsk University of Technology
Professor Edward Lisowski, Kraków University of Technology
Professor Edward Palczak, Wrocław University of Technology
Date of habilitation colloquium: March 19th, 2003
Habilitation monograph is available in Main Library and Scientific Information Centre of WUT
The monograph contains: 208 pages, 136 figs, bibliography, 157 items
Keywords: *machine dynamics, fluid power drive and control, vibrations, noise*

Title: ***Some problems of mechanics in pipeline bending processes*** **(in Polish)**
Wybrane zagadnienia mechaniki gięcia łuków gładkich rurociagów

Author: Zdzisław Śloderbach
Promoting Council: Concil of Mechanical Engineering Faculty
Reviewers:
Professor Michał Życzkowski, Kraków University of Technology
Professor Piotr Perzyna, Polish Academy of Science, Warsaw
Professor Jerzy Okrajni, Silesian University of Technology
Date of habilitation colloquium: September 29th, 2003
Habilitation monograph is available in Main Library and Scientific Information Centre of WUT
The monograph contains: 218 pages, 41 figs, bibliography, 192 items
Keywords: *pipe bending, deformations, bending angle, plastic localisation of deformation, free energy, enthalpy, dissipation*

Information for Authors

Send to: *Archives of Civil and Mechanical Engineering*
Polish Academy of Sciences, Wrocław Branch
Podwale 75, 50-414 Wrocław, Poland

Archives of Civil and Mechanical Engineering (ACME) publishes both theoretical and experimental papers which explore or exploit new ideas and techniques in the following areas: structural engineering (structures, machines and mechanical systems), mechanics of materials (elasticity, plasticity, rheology, fatigue, fracture mechanics), materials science (metals, composites, ceramics, plastics, wood, concrete, etc., their structures and properties, methods of evaluation), manufacturing engineering (process design, simulation, diagnostics, maintenance, durability, reliability). In addition to research papers, the Editorial Board welcome: state-of-the-art reviews of specialized topics, letters to the Editor for quick publication, brief work-in-progress reports, brief accounts of completed doctoral thesis (one page is maximum), and bibliographical note on habilitation theses (maximum 250 words). All papers are subject to a referee procedure, except for letters, work-in-progress reports and doctoral and habilitation theses, which are briefly reviewed by the Editorial Board.

The papers submitted have to be unpublished works and should not be considered for publication elsewhere.

The Editorial Board would be grateful for all comments on the idea of the journal.

Submit three copies, each complete with abstract, tables, and figures.
Detailed information about the Journal on web:

http://www.pan.wroc.pl
www.ib.pwr.wroc.pl/wydzial/czasopismoACME.html
http://www.wmech.pwr.wroc.pl

Price 12 zł
(0% VAT)